Enterobacterial type three secretion system effectors and their interference with host innate immunity

by

Miaomiao Wu

B.S., Southwest University, 2011
M.S., University of Chinese Academy of Sciences, 2014

AN ABSTRACT OF A DISSERTATION

submitted in partial fulfillment of the requirements for the degree

DOCTOR OF PHILOSOPHY

Department of Diagnostic Medicine/Pathobiology
College of Veterinary Medicine

KANSAS STATE UNIVERSITY
Manhattan, Kansas

2019

Abstract

Microbial pathogens have evolved secretion systems to deliver arsenals of virulence proteins (effectors) to disrupt host homeostasis and manipulate host immune defenses. The best-characterized system mediating effector delivery into host cells is type III secretion system (T3SS) expressed by Gram-negative bacteria, including enteric pathogens enteropathogenic/enterohemorrhagic *Escherichia* coli (EPEC/EHEC), *Shigella, Yersinia, and Salmonella*. Pathogen-host cell protein interactions within the host cell alter host cell signaling and ultimately subvert pathogen-induced inflammatory response.

In the first project, we identified the *Salmonella* Secreted Effector L (SseL) that deubiquitinated ribosomal protein S3 (RPS3) to inhibit its nuclear translocation. RPS3 guides the nuclear factor kappa-light-chain-enhancer of activated B cells (NF-κB) subunits to specific κB sites and plays an important role in the innate response to bacterial infection. Two *E. coli* effectors block RPS3 nuclear translocation. Non-locus-of-enterocyte-effacement (non-LEE) encoded effector NleH1 inhibits RPS3 phosphorylation by IKK-β, an essential aspect of the RPS3 nuclear translocation process. NleC proteolysis of p65 generates an N-terminal p65 fragment that competes for full-length p65 binding to RPS3, thus also inhibiting RPS3 nuclear translocation. Thus, *E. coli* has multiple mechanisms by which to block RPS3-mediated transcriptional activation. With this in mind, we considered whether other enteric pathogens also encode T3SS effectors that impact this important host regulatory pathway. In this study, we report that SseL, which was previously shown to function as a deubiquitinase and inhibit NF-κB signaling, also inhibits RPS3 nuclear translocation by deubiquitinating this important host transcriptional co-factor. RPS3 deubiquitination by SseL was restricted to K63-linkages and mutating the active-site cysteine of SseL abolished its ability to deubiquitinate and subsequently inhibit RPS3 nuclear translocation. Thus, *Salmonella* also encodes at least one T3SS effector that impacts RPS3 activities in the host nucleus.

In the second project, we attempted to identify a cofactor involved in the interaction between *E. coli* effector NleH1 and host kinase the IκB kinase-β (IKKβ). The EHEC NleH1 effector inhibits NF-κB pathway by reducing the nuclear translocation of RPS3. NleH1 prevents RPS3 phosphorylation by

IKKβ. IKKβ is a central kinase in the NF-κB signaling pathway, yet the EHEC NleH1 effector only restricts the phosphorylation of a subset of the IKKβ substrates. We hypothesized that a protein cofactor might dictate the inhibitory specificity of NleH1 on IKKβ. We used mass spectrometry and determined that heat shock protein 90 (Hsp90) interacts with both NleH1 and IKKβ, and that inhibiting Hsp90 activity reduces RPS3 nuclear translocation.

In the third project, we focused on the crystal structures of *Salmonella* secreted effector SseK1 and SseK2 from *Salmonella typhimurium SL1344*, and non-LEE encoded effector NleB2 from *E. coli* O145:H28 and propose catalytic residues for arginine glycosylation. *Salmonella* SseK1 and SseK2 are *E. coli* NleB1 orthologs that behave as NleB1-like glycosyltransferases, although they differ in protein substrate specificity. The bacterial effectors SseK and NleB1 glycosylate host cell death domain target proteins on arginine residues that inhibits death receptor signaling. We report crystal structures of SseK1, SseK2, and NleB2 and found they are highly similar to each other and comprises three domains including helix-loop-helix (HLH), lid, and catalytic domain. His-Glu-Asn (HEN) motif in the active site is essential for enzyme catalysis. We observe differences between SseK1 and SseK2 in interactions with substrates and identify substrate residues that are important for enzyme recognition.

Enterobacterial type three secretion system effectors and interference with host innate immunity

by

Miaomiao Wu

B.S., Southwest University, 2011
M.S., University of Chinese Academy of Sciences, 2014

A DISSERTATION

submitted in partial fulfillment of the requirements for the degree

DOCTOR OF PHILOSOPHY

Department of Diagnostic Medicine/Pathobiology
College of Veterinary Medicine

KANSAS STATE UNIVERSITY
Manhattan, Kansas

2019

Approved by:

Major Professor
Dr. Philip Hardwidge

Copyright

Abstract

Microbial pathogens have evolved secretion systems to deliver arsenals of virulence proteins (effectors) to disrupt host homeostasis and manipulate host immune defenses. The best-characterized system mediating effector delivery into host cells is type III secretion system (T3SS) expressed by Gram-negative bacteria, including enteric pathogens enteropathogenic/enterohemorrhagic *Escherichia* coli (EPEC/EHEC), *Shigella, Yersinia, and Salmonella*. Pathogen-host cell protein interactions within the host cell alter host cell signaling and ultimately subvert pathogen-induced inflammatory response.

In the first project, we identified the *Salmonella* Secreted Effector L (SseL) that deubiquitinated ribosomal protein S3 (RPS3) to inhibit its nuclear translocation. RPS3 guides the nuclear factor kappa-light-chain-enhancer of activated B cells (NF-κB) subunits to specific κB sites and plays an important role in the innate response to bacterial infection. Two *E. coli* effectors block RPS3 nuclear translocation. Non-locus-of-enterocyte-effacement (non-LEE) encoded effector NleH1 inhibits RPS3 phosphorylation by IKK-β, an essential aspect of the RPS3 nuclear translocation process. NleC proteolysis of p65 generates an N-terminal p65 fragment that competes for full-length p65 binding to RPS3, thus also inhibiting RPS3 nuclear translocation. Thus, *E. coli* has multiple mechanisms by which to block RPS3-mediated transcriptional activation. With this in mind, we considered whether other enteric pathogens also encode T3SS effectors that impact this important host regulatory pathway. In this study, we report that SseL, which was previously shown to function as a deubiquitinase and inhibit NF-κB signaling, also inhibits RPS3 nuclear translocation by deubiquitinating this important host transcriptional co-factor. RPS3 deubiquitination by SseL was restricted to K63-linkages and mutating the active-site cysteine of SseL abolished its ability to deubiquitinate and subsequently inhibit RPS3 nuclear translocation. Thus, *Salmonella* also encodes at least one T3SS effector that impacts RPS3 activities in the host nucleus.

In the second project, we attempted to identify a cofactor involved in the interaction between *E. coli* effector NleH1 and host kinase the IκB kinase-β (IKKβ). The EHEC NleH1 effector inhibits NF-κB pathway by reducing the nuclear translocation of RPS3. NleH1 prevents RPS3 phosphorylation by

IKKβ. IKKβ is a central kinase in the NF-κB signaling pathway, yet the EHEC NleH1 effector only restricts the phosphorylation of a subset of the IKKβ substrates. We hypothesized that a protein cofactor might dictate the inhibitory specificity of NleH1 on IKKβ. We used mass spectrometry and determined that heat shock protein 90 (Hsp90) interacts with both NleH1 and IKKβ, and that inhibiting Hsp90 activity reduces RPS3 nuclear translocation.

In the third project, we focused on the crystal structures of *Salmonella* secreted effector SseK1 and SseK2 from *Salmonella typhimurium SL1344*, and non-LEE encoded effector NleB2 from *E. coli* O145:H28 and propose catalytic residues for arginine glycosylation. *Salmonella* SseK1 and SseK2 are *E. coli* NleB1 orthologs that behave as NleB1-like glycosyltransferases, although they differ in protein substrate specificity. The bacterial effectors SseK and NleB1 glycosylate host cell death domain target proteins on arginine residues that inhibits death receptor signaling. We report crystal structures of SseK1, SseK2, and NleB2 and found they are highly similar to each other and comprises three domains including helix-loop-helix (HLH), lid, and catalytic domain. His-Glu-Asn (HEN) motif in the active site is essential for enzyme catalysis. We observe differences between SseK1 and SseK2 in interactions with substrates and identify substrate residues that are important for enzyme recognition.

Table of Contents

List of Figures

List of Tables

Acknowledgements

First of all, I would like to express my special appreciation and thanks to my advisor Prof. Philip Hardwidge for the continuous support of my Ph.D. study and related researches, for his patience, advice, and immense knowledge. His guidance and motivation helped me in all the time of the research and the writing of this thesis.

Besides my advisor, I would also like to express my sincere gratitude to the rest of my committee members, Prof. Sherry Fleming, Prof. T. G. Nagaraja, Prof. Elizabeth Davis, Prof. Wenjun Ma, and Prof. Valentina Trinetta for serving as my committee members, for their kind assistance, brilliant comments and suggestions on completing this research and thesis. I also want to say thanks for letting my defense be an enjoyable moment.

Thirdly, I also thank my fellow labmates, Mike Hays, Dr. Samir El Qaidi, Dr. Gaochan Wang, Yang Yang, and Congrui Zhu for the stimulating discussions and for all the fun we have had in the last four years. I really appreciate their help and assistance.

Fourthly, I want to express my gratitude to all my friends, Kangming Chen, Guan Yang, David George, Shiqiang Jin, and Mac Wenbo Mao, who gave me encouraged me to strive towards my goal. A special gratitude goes out to my friends, Leigh Ann George, Zhiping Xu, Zhenzhen Shi, Nannan Shan, and Zijun Wu. It was fantastic to have them in my life. I would also like to express appreciation to my dear cousin, Jiahui Xue, who spent so much time in cooking for me and was always my support in the moments when I felt frustrated.

Finally, a special thanks to my brother, my sister, and my parents. The conviction with which to pursue and realize my doctorate was made a reality only through the unwavering love and support of my mom and dad.

Chapter 1 - Literature Review

I contributed to all the figures and tables, except for Figure 3a, 4a, and 5a, and part of Figure 3b, 4b, and 5b in Chapter 1. A modified version of this chapter is published in Protein Reviews (El Qaidi, Wu, Zhu, & Hardwidge, 2018).

El Qaidi, S., Wu, M., Zhu, C., & Hardwidge, P. R. (2018). Salmonella, E. coli, and Citrobacter Type III Secretion System Effector Proteins that Alter Host Innate Immunity. Adv Exp Med Biol. doi:10.1007/5584_2018_289

Bacterial pathogens must circumvent both the host immune system and competition from commensal bacteria to establish an infection. Innate immunity is a primary stage of defense required for elimination of the invading pathogens (Medzhitov & Janeway, 1997). In addition to physical and chemical barriers, the innate immune system also consists of surface proteins classified as pattern recognition receptors (PRRs) that sense components of pathogens known as pathogen-associated molecular patterns (PAMPs) (Suresh & Mosser, 2013). These receptor-ligand associations lead to the induction of the NF-κB signaling pathway that ultimately culminates in the production of pro-inflammatory cytokines (T. Liu, Zhang, Joo, & Sun, 2017). In turn, bacterial pathogens have evolved various strategies to target and inhibit NF-κB signaling pathway to promote their colonization (Le Negrate, 2012).

Bacteria have evolved multiple secretion systems to deliver arsenals of virulence proteins termed ‘effectors’ to counteract host innate immunity. The best-characterized secretion system mediating bacterial effector delivery into target eukaryotic cells is the type III secretion system (T3SS) expressed by Gram-negative bacteria, including the human enteric pathogens enterohemorrhagic *Escherichia coli* (EHEC), enteropathogenic *E. coli* (EPEC), *Citrobacter rodentium*, and *Salmonella enterica.* Type three secretion system (T3SS) is a syringe-like secretion apparatus that injects effectors that bind host proteins. These interactions ultimately

subvert the generation of an inflammatory response to the infecting pathogen (Daniell et al., 2001).

Human enteric pathogens

EPEC and EHEC

Enteric bacterial human pathogens are important endemic health threats and major sources of food borne disease. In the United States, at least 75 million food borne illnesses result in 5,200 deaths annually (Centers for Disease Control and Prevention). Diarrheagenic *E. coli* contribute greatly to the enormous economic and health burden of food borne disease. EPEC and EHEC are attaching/effacing (A/E) pathogens that cause severe gastroenteritis.

EPEC colonizes the small intestinal mucosa. Specifically it colonizes in the duodenum, terminal ileum and Peyer's Patches (Fitzhenry et al., 2002). It is considered one of the predominant causative agents of infantile diarrhea primarily in the developing countries (Clarke, Haigh, Freestone, & Williams, 2002), which was first described in the 1940s and 1950s (J. Hu & Torres, 2015).

EHEC have been of particular concern because of the low infectious dose (<100 organisms) and serious nature of disease, especially in the immunocompromised, the elderly, and young children (Karmali, 1989). EHEC mainly colonizes the Peyer's Patches and the large intestine (Phillips et al., 2000). It is a human pathogen that causes of severe hemorrhagic colitis, in the worst case, hemolytic uremic (HUS), following transmission to humans through ingestion contaminated food and water, or through contact with contaminated animals (Newell & La Ragione, 2018). One characteristic feature of EHEC and EPEC infection in common is the colonization in the intestinal mucosa via the formation of A/E lesions in the intestinal epithelial cells, characterized by effacement (destruction) of the intestinal brush border microvilli, intimate bacterial

attachment to the residual apical enterocyte membrane, and formation of a pedestal underneath the adherence site. Take EPEC as an example, EPEC adherence is mediated by an interaction between the bacterial translocated intimin receptor (Tir) and intimin proteins to create intimate contact with host intestinal cells (Kenny et al., 1997). Briefly, the bacteria inject their receptor protein Tir into host cells through T3SS (Frankel et al., 2001), where it inserts in the host cell membrane and binds to a bacterial outer membrane proteins called intimin, initiating a cascade of signaling events, leading to actin polymerization and pedestal-like structure formation, and ultimately resulting in intimate attachment on the microvilli, in other words, formation of A/E lesion (Batchelor et al., 2000). The EPEC chromosome harbors the locus of enterocyte effacement (LEE), a pathogenicity island (PAI) encoding a T3SS and multiple effectors . The genome of EPEC contains several LEE encoded effectors associated with intimated attachment of EPEC to intestinal epithelium, which are designated by the term 'Esp'. Seven effectors including Tir, Map, EspF, EspG, EspH, EspZ, and EspB are known encoded in the LEE pathogenic island (Garmendia, Frankel, & Crepin, 2005; Mills, Baruch, Charpentier, Kobi, & Rosenshine, 2008; N. A. Thomas, Deng, Baker, Puente, & Finlay, 2007). It also contains several non-LEE encoded effectors (designated as 'Nles') that have been demonstrated to subvert host immunity. Nle effectors, such as NleA(EspI), NleB, NleC, NleD, NleE, NleF, NleG, NleH, EspJ, and EspL, are encoded on prophages (Petty et al., 2010), of which NleB, NleC, NleE, NleE, and NleH have been reported to block NF-kB signaling via different mechanisms (H. Yen, Karino, & Tobe, 2016). EHEC also contains the LEE and Nles, but also encodes Shiga-like toxins that are responsible for causing more serious disease.

C. rodentium

C. rodentium is a natural pathogen of mice that was discovered during a collapse of mouse colonies due to transmissible murine colonic hyperplasia (TMCH) (Luperchio et al., 2000; Mundy, MacDonald, Dougan, Frankel, & Wiles, 2005). Mice infected with *C. rodentium* develop TMCH that can then turn into diarrhea (Mundy et al., 2005). Both EPEC and EHEC are strictly human pathogens, they are poorly pathogenic in mice (Mundy et al., 2005). It requires pretreatment with antibiotics for colonization of mice with EPEC and EHEC. The genomic and mechanistic similarities between *C. rodentium* and EPEC have made *C. rodentium* become a principal rodent model system with which to study infections with A/E enteropathogens *in vivo* (Collins et al., 2014; Silberger, Zindl, & Weaver, 2017).

Salmonella enterica

Salmonella enterica (*S. enterica*, formerly *Salmonella choleraesuis*), serovars of which cause a wide range of gastrointestinal and extraintestinal diseases and remains one of the most frequently reported causes of foodborne illness (Yombi, Martins, Vandercam, Rodriguez-Villalobos, & Robert, 2015). It is estimated to cause 1.2 million illnesses annually in the United States (Jackson, Griffin, Cole, Walsh, & Chai, 2013; Scallan et al., 2011). Ingestion of contaminated animal-derived foods, especially poultry, is the primary source of infection, although contaminated water, plant products, and direct contact with animals are also risk factors. *S. enterica* colonizes the gastrointestinal tract, and infections by *S. enterica* causes gastroenteritis, bacteremia, enteric fever, and an asymptomatic carrier state. The infection is more common in children younger than 5 years old, adults 20 to 30 years old, and patients 70 years old or older (Zanetti M, 2015). *Salmonella* encodes multiple virulence-related T3SSs. T3SS1, encoded by the *Salmonella* pathogenicity island (SPI)-1, has many functions, including the invasion of epithelial

cells and the induction of an inflammatory response at the intestinal surface (Marcus, Brumell, Pfeifer, & Finlay, 2000). T3SS2 is encoded by SPI-2 and is a key virulence determinant for systemic disease in mice (Ochman, Soncini, Solomon, & Groisman, 1996). T3SS2 is induced intracellularly and is required for Salmonella-containing vacuole (SCV) biogenesis. Some T3SS effectors are encoded inside SPI-1 or SPI-2, but many of them are encoded outside the two main islands, usually within large DNA segments acquired by independent events of horizontal gene transfer.

Gram-negative bacterial secretion systems

Bacterial adaptation to ecological niches depends not only on evolving specific regulatory strategies to adapt their metabolism to the extracellular environments, but also secreting virulence. The past few decades have seen the discovery of diverse systems that enable bacteria to transport virulence proteins from the cytosol into host cell or host environment across one or two membranes. Bacterial pathogens have developed multiple ways to export proteins to specific locations, among which dedicated protein secretion systems are essential for subverting the antibacterial response and promoting infection. There are several different types of bacterial secretion systems, their structures differ based on whether their secreted protein substrates are transported through a single phospholipid membrane, two or three membranes, bacterial and host membranes included. To date, six major secretion systems have been found in Gram-negative bacteria, including Type I, II, III, IV, and VI secretion system (T1SS, T2SS, T3SS, T4SS, and T6SS) (Desvaux, Hebraud, Talon, & Henderson, 2009).

Type I secretion system

T1SS was first discovered by identifying two membrane proteins of *E. coli*, HlyB and HlyD, which are important for transporting cytotoxin hemolysin A (HlyA) (Nicaud, Mackman, Gray, &

Holland, 1985). T1SS, also known as ATP-binding cassette (ABC) dependent transporter, represent a wide-spread mode of protein secretion across phospholipid membranes in pathogenic Gram-negative bacteria, where they transport their substrates in a single-step process across the inner and outer bacterial membranes without a stable periplasmic intermediate (Koronakis, Hughes, & Koronakis, 1991). The Hly translocator is a simple, tripartite system, including HlyB, which is an ABC transporter localized in the inner membrane and is also known as a periplasmic adaptor protein (M. Lee et al., 2012), and TolC, which localized in the outer membrane and is often the final portal in the pathways of protein toxin transport (Koronakis, Sharff, Koronakis, Luisi, & Hughes, 2000). HlyD forms a continuous, solvent-accessible channel by anchoring in the inner membrane that bridges HlyB to TolC. T1SS is involved in translocating cytotoxins belongings to the repeats in toxin (RTX) protein family, cell surface layer proteins, proteases, lipases, bacteriocins, and hae-acquisition proteins. One of the characterized T1SS substrates is the cell-lysing toxin HlyA of uropathogenic *E. coli* (Lenders et al., 2015), which belongs to RTX protein family. The transport process occur unfolded with substrates size vary greatly between 78 (uncharacterized protein from *Sinorhizobium meliloti*) and 8682 amino acids (Delepelaire, 2004). These indicate that T1SS operate by a special mechanism with the unfolded polypeptide being moved through a transporter formed by the translocator's TM domains (S. Thomas, Holland, & Schmitt, 2014).

Type II secretion system

T2SS has been identified and studied in many pathogens and non-pathogens, such as *Vibrio cholera*, EHEC, and enterotoxigenic *Escherichia coli* (ETEC). T2SS, also known as secreton, is a sophisticated multiprotein nanomachine containing 40-70 proteins of 12-15 different proteins spans the inner and outer membranes, which are encoded in the single operon gspC (Sandkvist,

2001). Compared to T1SS, T3SS, T4SS, and T6SS, T2SS is the only transporter that secretes protein substrates in the native folded form from periplasm into extracellular environment. The reason is that T2SS is only found in the outer membrane of bacteria and uses a two-step mechanism for translocation. Precursor effector substrates transported through this machinery must first be translocated through the inner membrane by the Sec translocon or Tat pathway, then the effector proteins are transported by the T2SS via the outer membrane (Voulhoux et al., 2001). The transporter plays a key role in bacterial pathogenesis as the substrates secreted through T2SS are vital toxins of many bacterial pathogens, such as heat-labile enterotoxin of EHEC and ETEC (Tauschek, Gorrell, Strugnell, & Robins-Browne, 2002). T2SS has four substructures, a secretion ATPase GspE, an inner membrane platform, a pseudopilus, and an outer membrane complex which is a GspD channel for secretion. This secretion system generates mechanical energy through ATP hydrolysis in the cytoplasm to promote assembly of filamentous structures anchored in the inner membrane. The inner-membrane platform is composed of multiple copies of four core membrane proteins. The pseudopilus is a periplasmic filamentous structure formed by five different pseudopilins, including Gsp-H-I-J-K, with multiple copies of the major pseudopilin (Korotkov, Sandkvist, & Hol, 2012). GspD is one of the members in secretin superfamily, which also occur in T3SS, type 4 pilus biogenesis system (T4PS), and filamentous phage secretion system (Campos, Cisneros, Nivaskumar, & Francetic, 2013). T2SS is the best adapted to releasing a large number of effector proteins in the outer environment, compared to the other 4 systems, which transport limited number of substrates. This broad specificity enables one T2SS translocator to transport multiple proteins. T2SS is highly similar to T4PS as well as to archaeal flagella and pili, indicating their early common origins. The two systems have similar secretins in outer membrane, filamentous structures (the pseudopilus in

T2SS and pilus in T4SS), prepilin peptidases and cytoplasmic ATPases, and homologous membrane proteins (the GspF in T2SS and PilC in T4SS) (Korotkov et al., 2012).

Type III secretion system

The bacteria inject their own receptor protein Tir into host cells through T3SS, where it inserts in the host cell membrane and binds to a bacterial outer membrane protein, intimin, initiating a cascade of signaling events, leading to polymerization and pedestal formation, and ultimately resulting in formation of A/E lesion (Batchelor et al., 2000). Activation of T3SS plays a crucial role in formation of A/E lesions and secretion of effectors in the pathogenesis of pathogenic bacterial that contains T3SS. The structure of T3SS, known as injectisome, is a complex molecular nanomachine assembled from more than 20 structural proteins and is composed of a syringe shaped structure, and truly behaves as a "molecular syringe". The components of this syringe can be categorized into four parts according to the functions and substructures they form, listed from inside and out: export apparatus, basal body, needle complex, and translocators. The structure of T3SS in EPEC and EHEC is shown in **Figure 1** and **Table 1**.

Figure 1 Type III secretion system.

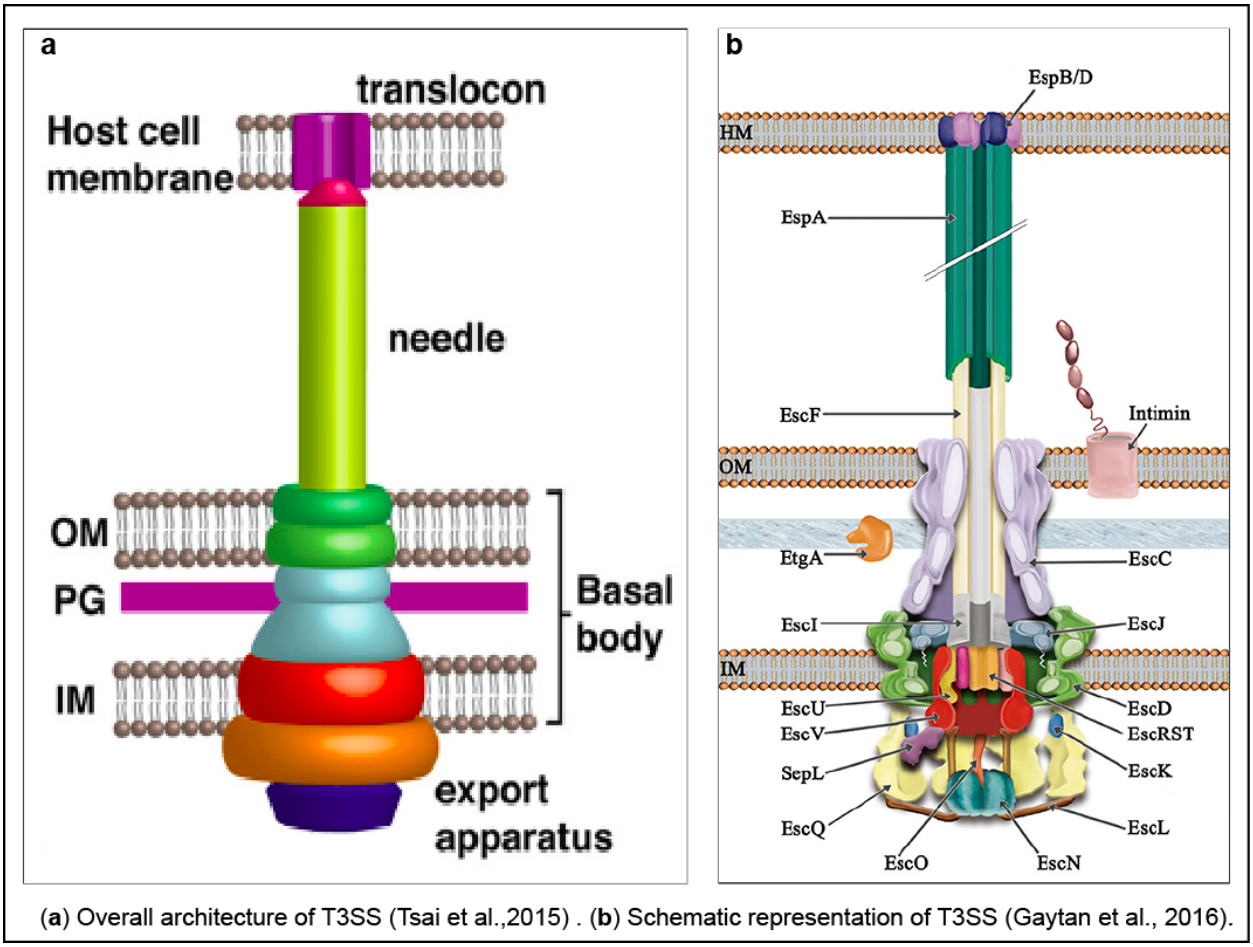

(**a**) Overall architecture of T3SS (Tsai et al.,2015) . (**b**) Schematic representation of T3SS (Gaytan et al., 2016).

a Overall architecture of T3SS (Tsai et al., 2015). **b** Schematic representation of the T3SS (Gaytan et al., 2016).

Export apparatus and ATPase

The export apparatus is one of the most conserved components of T3SS, which is composed of five different proteins, including EscR, EscS, EscT, EscU, and EscV, also known as EscRSTUV (Portaliou, Tsolis, Loos, Zorzini, & Economou, 2016), as well as a soluble ATPase complex. The ATPase complex is formed by EscN in EPEC and EHEC with its positive and negative regulators, EscO and EscL, respectively (Biemans-Oldehinkel, Sal-Man, Deng, Foster, & Finlay, 2011; Romo-Castillo et al., 2014). The 5 components localized to the inner membrane, enclosed by the two inner membrane rings of the basal body, and associate with the base of the needle complex (Diepold, Wiesand, & Cornelis, 2011). EscL functions as an inner rod protein and is

also secreted as an early effector. It interacts with EspP and EscU, and both interactions are implicated in the substrate – switching event (Thomassin, He, & Thomas, 2011). EscU is an important inner membrane ring protein of the injectisome, and its auto-cleavage forms a secretion-dependent state, and promotes translocon and effectors secretion (Sal-Man, Deng, & Finlay, 2012). EscRSTUV play a crucial role in the recruitment and regulation of substrates insertion into the syringe (Minamino et al., 2010).

EscN is one of the best characterized injectisome ATPase. EscN is like FliI in the flagellar FliI/FliH/FliJ ATPase complex (Minamino & MacNab, 2000), and shows structural similarity to the α and β subunits of F1-ATPase (Zarivach, Vuckovic, Deng, Finlay, & Strynadka, 2007). EscN forms a complex with EscL, which is similar to FliH, and has been linked to the β subunit of the F1-ATPase and implicated as a component of the sorting platform in *Shigella* (B. Hu et al., 2015). EscO is functionally related to FliJ (Romo-Castillo et al., 2014). EscL acts as a putative ATPase negative regulator, and EscO acts as a positive regulator (Biemans-Oldehinkel et al., 2011).

Basal body

The part of the needle complex embedded in the inner and outer membrane of pathogens is named the basal body, which is composed of three membrane rings connected directly to the inner rod structure (Schraidt & Marlovits, 2011). There are two inner membrane rings, named inner membrane ring 1 (IR1) and inner membrane 2 (IR2). IR1 locates in the periplasm and is composed of EscD and EscJ proteins. IR2 locates in the cytoplasm and is formed by EscC protein. The outer membrane protein EscC is associated with EscD and the needle protein EscF, but no interaction with EscJ was detected (Creasey, Delahay, Daniell, & Frankel, 2003). The EscC plays an important role in T3 secretion and needle complex formation and functions as a

channel for effectors secretion across the outer membrane (Deng et al., 2004). EscC protein interacts with EscO, which is an ATPase complex component (Romo-Castillo et al., 2014), instead of EscA (Sal-Man, Biemans-Oldehinkel, et al., 2012). EscC, EscD, and EscJ are all required for the formation of functional injectisome apparatus (Ogino et al., 2006).

Needle complex

The core architecture of the needle complex has high similarity in bacteria. The needle is assembled from multiple copies of the EscF protein, which functions as a projection channel required for the T3SS dependent protein secretion of all substrates (Deng et al., 2004). The structure of EPEC needle is one of the smallest, which is 23 nm in length and 8-9 nm in width (Monjaras Feria et al., 2012), compared to the needle in *Salmonella enterica,* which is 30 nm in length and 25 nm in width (Schraidt et al., 2010). The length of EPEC needle appears to be tightly regulated (Wilson, Shaw, Daniell, Knutton, & Frankel, 2001). The inner diameter of the channel in A/E pathogens is unknown, which was estimated to be 2-3 nm in other T3SS (Blocker et al., 2001; Hodgkinson et al., 2009; Loquet et al., 2012). Folded proteins cannot accommodate in this channel. Therefore, it is hypothesized that before being injected into host cells, effectors should be kept unfolded (Fujii et al., 2012), which was confirmed by Dohlich et al (Dohlich, Zumsteg, Goosmann, & Kolbe, 2014) and Radics et al(Radics, Konigsmaier, & Marlovits, 2014). The characteristic feature of EPEC and EHEC T3SS is the presence of EspA filament, which functions as an adaptor between the needle and the tip. The length of EspA filament is flexible up to 600 nm (Crepin, Shaw, Abe, Knutton, & Frankel, 2005).

Translocator

The Translocator is formed of EspB and EspD, which delivers the effectors to the host cell cytoplasm from needle filament EspA (Ide et al., 2001). EspD protein is necessary for EspA

synthesis, which indicates that EspD functions both as an anchor to connect EspA filament to the host cytoplasma and as a capping protein of EspA protein (Delahay et al., 1999). EspD interacts with itself (Creasey, Delahay, Bishop, et al., 2003) and EspB (Ide et al., 2001). The translocator can mediate hemolysis of red blood cells (Hakansson et al., 1996; Warawa, Finlay, & Kenny, 1999), which indicates EspD is the major protein of translocator and EspB is also necessary for full hemolytic activity (Shaw, Daniell, Ebel, Frankel, & Knutton, 2001).

Table 1 Summary of structure of T3SS in EPEC/EHEC

STRUCTURE	**COMPONENT**	**EPEC/EHEC**
Export apparatus	APTase	EscN
	Central stalk	Orf15
	Peripheral stalk	EscL
	C-ring homolog	SepQ
	Gate	EscV
	Gate-keeper	SepL/SepD
	Autoprotease	EscU
	IM component	EscR
	IM component	EscT
	IM component	EscS
Basal body	IM ring	EscD
	IM ring	EscJ
	OM ring	EscC
	Pilotin	N/A

	Inner rod	EscI
Needle	Filament	EscF
Translocator	Tip	EspA
	Minor subunit	EspD
	Minor subunit	EspB

Type IV secretion system

T4SS spans the periplasm and both bacterial membranes, and is a macromolecular nanomachine utilized for a variety of processes, ranging from the translocation of virulence proteins to conjugative transport of genetic material and uptake or release of DNA through the Gram-negative bacteria membranes. T4SS can secrete a variety of substrates, including single proteins, protein complexes, and DNA and nucleoprotein complexes, thus the systems can serve multiple functions, including conjugative transfer of DNA, DNA uptake and release, and transport of virulence proteins or protein/DNA complexes into target cells (Campos et al., 2013). Although diversity in the substrates and functions of this apparatus exist, all T4SS are evolutionarily related, sharing common components and operating in a similar manner, and are similar to the *Agrobacterium. tumefaciens* VirB/D T4SS. VirB/D T4SS comprises 12 proteins named VirB1 to VirB11, and VIrD4, which are membrane associated, have multiple copies, and interact with themselves and each other. T4SS includes three parts, including three ATPases, secretion channel, and extracellular pilus. The polytopic membrane protein VirB6, and bitopic membrane proteins VirV8 and VirB10 proteins are located in the periplasm, inner and outer membranes, and form the secretion channel and its accessory proteins. VirB4, VirB11, and VirD4 are found in the inner membrane and serve as ATPase that power the substrates secretion and assist in the

assembly of transporter. VirD4 also functions as a coupling protein, and binding proteins through the channel. Generally, but not always, T4SS also includes an extracellular pilus composed of a major (VirB2) and a minor (VirB5) subunit (Fronzes, Remaut, & Waksman, 2008). T4SS are divided into three groups according to their functions, including conjugation systems, pilus-based effector protein translocation systems, and contact independent systems. Conjugation systems transfer DNA from one cell to another, which increases bacterial genome plasticity and plays an essential role in human care as a major vehicle of antibiotic resistance among pathogens. Pilus-based effector protein translocation systems transfer proteins, and is dependent on direct cell contact. Contact independent systems secrete complex protein toxin across bacterial membranes. A major focus in the T4SS recently is on understanding the functions of these effector proteins affecting mammalian cells.

Type VI secretion system

T6SS is the most recently identified example of these transporters to be discovered and plays an essential role in delivery of toxins into eukaryotic and, more commonly, prokaryotic cells. It is a proteinaceous injection apparatus that transports virulence effectors directly into the target cell in a one-step process, which is different to injectisome T3SS in a two-step process. This machinery is encoded within large and multiple gene clusters which all include 13 conserved Type six subunits (Tss) ‘core’ genes important for functions, encoding the components forming the basic structure of the secretion system (Shneider et al., 2013). Though the assembly and the mechanism are conserved across bacterial species, the repertoire of secreted virulence effectors and the diversity of the regulatory mechanisms and of recipient cells make the T6SS a highly versatile translocator. Unlike other Gran-negative secretion systems, T6SS delivers virulence effectors into other cells in a contact-dependent manner, which is crucial in bacterial

communication and interactions in the host environment. T6SS core components collectively assemble a structure resembling an upside-down bacteriophage-like structure anchored to bacterial membranes, including sub-complexes, the needle hub, the needle sheath, and the needle tail and syringe. The needle hub includes the baseplate (TssE, and TssK) and membrane complex, which is composed of three membrane-associated subunits: TssL, TssM and TssJ. It has been discovered T6SS TssE subunit has about 40% sequence similarity with bacteriophage T4gp25 component. The contractile sheath of T6SS is composed of TssB and TssC, which could form tubular structures with the appearance of cogwheels in vitro spontaneously (Lossi et al., 2013). TssE displays detectable homology with the bacteriophage baseplate protein gp25 and is necessary for TssBC assembly. TssK is a cytoplasmic protein which can form higher order oligomers. The interactions of TssK with TssC, TssL and Hcp in *E. coli*, indicating that it may play an essential role in connecting T6SS bacteriophage tail-like and membrane components. VgrG and PAAR proteins form a complex similar to phage spike acts as a syringe to disrupt the target cell membrane. VgrG is structurally related to gp27/gp5 hub complex forming the spike of bacteriophage T4. The hallmark of T6SS secretion is Hcp protein together with VgrG. It is hypothesized that T6SSs play a key role in secreting virulence effectors from bacterial pathogens both into host cells, and into neighboring bacteria that may compete with that bacteria to exploit a specific host niche.

Summary

Here we summarize the basic structure, feature, and character of 5 important secretion systems (**Figure 2**). T6SS is the most recently identified. To date, five different protein secretion apparatuses have been identified in detail. T1SS, T3SS, T4SS and T6SS catalyze one-step secretion process direct to the medium, while T2SS and T4SS utilize a two-step procedure to

shuttle the virulence effectors to the environment. T4SS interestingly possesses a dual role. The components that form the transport systems are the intrinsic difference between these machineries. Secretion system is one of the invading strategies that bacteria pathogens use to infect host cells, damage tissue sites, and fight with host immune systems. These secretory systems play an important role in release of virulence proteins into target cells, conjugation and horizontal gene transfer, antigenic variation, and peptidoglycan and LPS synthesis and modification.

Figure 2 Major protein secretion systems in Gram negative bacteria

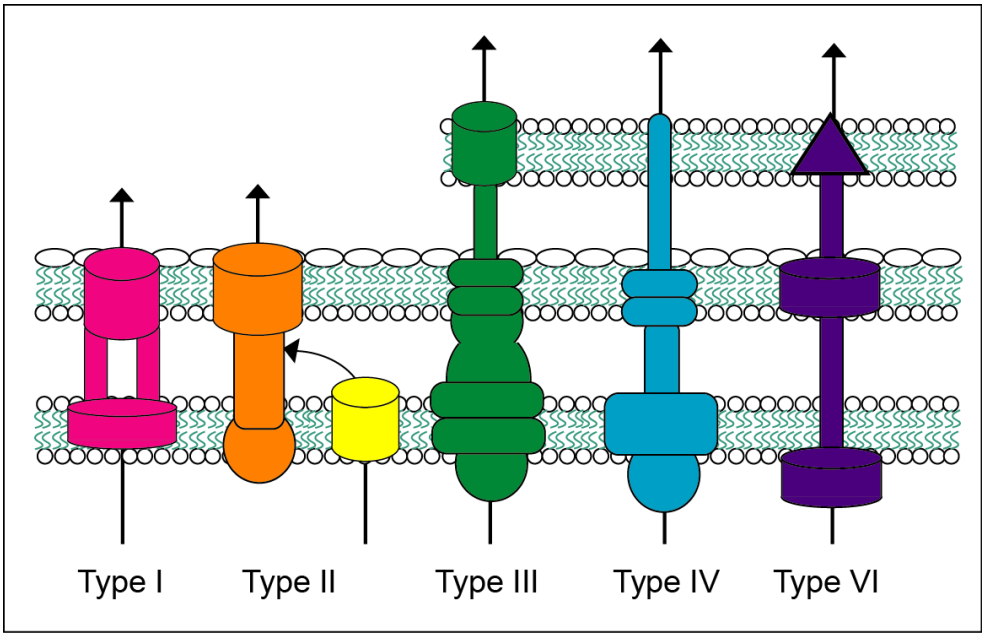

T3SS effectors

E. coli and *Citrobacter* effectors

NleA inhibits Nod-like Receptor 3 (NLRP3)-mediated inflammasome activation via a direct association with NLRP3. NleA binding to NLRP3 prevents its deubiquitination, which is required for inflammasome assembly and activation (H. Yen, Sugimoto, & Tobe, 2015). As a consequence, interleukin 1 beta (IL-1β) secretion decreases due to caspase 1 inhibition (H. Yen

et al., 2015). NleA also binds the Sec24 subunit of the mammalian coatamer protein II complex (COPII) to inhibit vesicle trafficking (J. Kim et al., 2007).

NleB is a glycosyltransferase that glycosylates host proteins with N-acetylglucosamine (GlcNAc) on arginine residues (El Qaidi et al., 2017; S. Li et al., 2013; Pearson et al., 2013). Deleting *nleB* significantly attenuates *C. rodentium* virulence (Kelly et al., 2006). While a single *nleB* gene is found in *C. rodentium*, two *nleB* genes, *nleB1* and *nleB2*, are found in most EPEC and EHEC strains. EPEC NleB1 glycosylates the tumor necrosis factor receptor (TNFR) type 1-associated DEATH domain protein (TRADD) and the FAS-associated death domain-containing protein (FADD) (S. Li et al., 2013; Pearson et al., 2013), with preferential affinity for FADD (Scott et al., 2017). Glycosylation of TRADD inhibits its dimerization, thus preventing the proper assembly of the TNFR complex and the activation of the NF-κB pathway (S. Li et al., 2013; Pearson et al., 2013). EHEC NleB1 and *C. rodentium* NleB also glycosylate glyceraldehyde-3-phosphate dehydrogenase (GAPDH) (El Qaidi et al., 2017; X. F. Gao et al., 2013), which reduces GAPDH binding to TRAF2, subsequently limiting the extent of TRAF2 ubiquitination, leading to reduced NF-κB activity (X. F. Gao et al., 2013).

NleC is a zinc metalloprotease that cleaves the NF-κB p65 subunit, leading to NF-κB pathway inhibition (Baruch et al., 2011; Giogha, Lung, Muhlen, Pearson, & Hartland, 2015; H. L. Yen et al., 2010). NleC-mediated cleavage of p65 occurs between C38 and E39, generating a $p65^{1-38}$ fragment that also competes with full-length p65 for binding to the ribosomal protein RPS3, an NF-κB subunit (Hodgson et al., 2015). This competition reduces the extent of RPS3 nuclear translocation, thus additionally inhibiting NF-κB pathway activation (Hodgson et al., 2015).

NleD is also a zinc metalloprotease that cleaves and inactivates the mitogen-activated protein kinase signaling proteins c-Jun N-terminal kinase (JNK) and p38 (Baruch et al., 2011). JNK

cleavage by NleD occurs before Y185 in the TPY (T183-P184-Y185) motif within the kinase activation loop of JNK, whereas p38 cleavage occurs at residue M213 (Creuzburg et al., 2017). As p38/JNK activation influences pro-inflammatory cytokine gene expression, their cleavage by NleD contributes downregulated inflammatory responses. In a random mutagenesis study of NleD, R203 was found to be critical for protease activity against p38 but not JNK (Creuzburg et al., 2017). In another study, mutation of E143 within the metalloprotease motif ($H^{142}ELLH^{146}$) abrogated JNK cleavage (Baruch et al., 2011).

NleE was originally described to inhibit the nuclear translocation of the p65 NF-κB subunit by preventing IκBα phosphorylation (Newton et al., 2010). The C terminal IDSY(M/I)K motif was found to be critical for NleE-mediated inhibition of p65 translocation (Newton et al., 2010). It was later shown that NleE is an S-adenosylmethionine (SAM)-dependent methyltransferase that modifies a zinc-coordinating cysteine in the Npl4 zinc finger (NZF) domains in TAB2 and TAB3, which are two ubiquitin-chain sensory proteins involved in NF-κB signaling (L. Zhang et al., 2012). Upon NleE mediated methylation of C673 and C692 in TAB2 and TAB3 respectively, the two proteins lose their ability to bind zinc and ubiquitin chains (L. Zhang et al., 2012). The NleE crystal structure displays a SAM pocket that particularly involves two critical residues, R107 and Y212 (Yao et al., 2014).

NleF is important to EHEC colonization of germ-free piglets (Echtenkamp et al., 2008). NleF is a pro-inflammatory effector because it induces NF-κB activation during the early stages of the infection (Pallett, Berger, Pearson, Hartland, & Frankel, 2014; Pollock et al., 2017). The C-terminal region of NleF is essential for its interaction with caspase 4, 8, and 9 (Blasche et al., 2013). NleF counteracts the host inflammatory response by preventing the heteromerization of caspase-4-p19 and caspase-4-p10, which is essential for caspase-4 activation and the eventual

expression of IL-1β (Blasche et al., 2013; Song et al., 2017). The transient pro-inflammatory activity of NleF is later overcome by the anti-inflammatory functions of other effectors such as NleE, NleH, and NleB.

NleH1 and **NleH2** are two paralog effectors (with 84 % homology) that contain a C-terminal kinase domain (Grishin et al., 2014). Both proteins bind RPS3, but only NleH1 inhibits RPS3 translocation to the nucleus (X. Gao et al., 2009). NleH1 interaction with RPS3 prevents its phosphorylation on S209 by IKKβ (F. Y. Wan et al., 2011). NleH1 phosphorylates the v-crk sarcoma virus CT10 oncogene-like protein (CRKL), which may play an important scaffolding role between NleH1 and IKKβ (Pham, Gao, Singh, & Hardwidge, 2013). K159 in NleH1 and K169 in NleH2 are critical residues for the kinase activity of these effectors (X. Gao et al., 2009).

EspL is a cysteine protease that directly cleaves the receptor interacting protein (RIP) homotypic interaction motif (RHIM) domain-containing proteins RIPK1, RIPK3, TRIF, and ZBP1/DAI, leading to their rapid inactivation, with subsequent inhibition of necroptosis and inflammatory signaling (Pearson et al., 2017). EspL-mediated cleavage of these host proteins is both proteasome- and caspase-independent. A conserved cysteine protease motif with catalytic residues C47, H131, and D153 was defined (Pearson et al., 2017). The proteolytic activity of EspL is essential for *Citrobacter rodentium* intestinal colonization of mice (Pearson et al., 2017).

Tir. In addition to its well-studied role in bacterial adhesion, Tir also inhibits NF-κB pathway activation by interacting with TNFR-associated factor (TRAF) adaptor proteins leading to their proteasomal-independent degradation (Ruchaud-Sparagano, Muhlen, Dean, & Kenny, 2011).

Salmonella effectors

GogB is the first ORF in the Gifsy-1 prophage in *Salmonella enterica* serovar Typhimurium (McClelland et al., 2001). GogB is a leucine-rich repeat protein that is secreted by both type three secretion systems encoded in Salmonella Pathogenicity Island-1 (SPI-1) and SPI-2 (Coombes et al., 2005). GogB is regulated by its transcriptional regulator SsrB through SPI-2 induction, and then localizes to the host cell cytoplasm (Xu & Hensel, 2010). GogB alters the function of the host SKP, cullin, F-box containing complex (SCF) E3 type ubiquitin ligase by interacting with the human F-box only 22 (FBXO22) protein and S-phase kinase associated protein 1 (Skp1) (Pilar, Reid-Yu, Cooper, Mulder, & Coombes, 2012). GogB-deficient *Salmonella* fail to limit NF-κB activation in RAW264.7 cells, indicating that GogB is an anti-inflammatory factor (Pilar et al., 2012).

PipA, **GtgA**, and **GogA** comprise a family of proteases that cleave both the RelA (p65) and RelB NF-κB transcription factors, thus limiting host inflammatory responses (H. Sun, Kamanova, Lara-Tejero, & Galan, 2016). *Salmonella* mutants in the *pipA*, *gogA*, or *gtgA* genes show increased NF-κB pathway stimulation and virulence in C57/BL6 mice, as compared to wild-type *Salmonella* (H. Sun et al., 2016), indicating that this family of effectors inhibits host immune responses.

Salmonella encodes three members of the novel E3 Ligase (NEL) family, **SlrP**, **SspH1**, and **SspH2**. SlrP functions as an E3 ubiquitin ligase for mammalian thioredoxin (Bernal-Bayard & Ramos-Morales, 2009), which may affect the redox state and activity of transcription factors. SlrP also binds to the chaperone ERdj3 in the endoplasmic reticulum (Bernal-Bayard, Cardenal-Munoz, & Ramos-Morales, 2010), possible impacting the unfolded protein response and apoptosis. SspH1 and SspH2 have 39 % and 38 % identity to SlrP (E. A. Miao & Miller, 2000).

Both SspH1 and SspH2 contains a leucine-rich repeat (LRR) domain, which can block the catalytic domain without the presence of substrate (Keszei et al., 2014). SspH1 inhibits NF-κB signaling (Haraga & Miller, 2006). The catalytic domain from the LRR domain of SspH1 interacts with and ubiquitinates human protein kinase N1 (PKN1), to activate its catalytic function, mutating SspH1 C492 abolised its ability to ubiquitinating PKN1 (Keszei et al., 2014). Mutating SspH1 C492 abolishes its ability to ubiquitinate PKN1 (Keszei et al., 2014). However, the inhibition of NF-κB signaling is not due to the ubiquitination and proteasome-dependent degradation of PKN1 (Keszei et al., 2014). SspH2 increases Nod1-mediated IL-8 secretion by ubiquitinating Nod1 (Bhavsar et al., 2013). Mutating SspH2 C580 abolishes its ubiquitination activity (Quezada, Hicks, Galan, & Stebbins, 2009).

SpvB is encoded by the *spv* operon in the *Salmonella* virulence plasmid (Caldwell & Gulig, 1991). SpvB ADP-ribosylates actin on R177 (Hochmann, Pust, von Figura, Aktories, & Barth, 2006), causing both actin depolymerization and apoptosis (Guiney & Lesnick, 2005). P-bodies are enzymes involved in mRNA turnover and post-transcriptional regulation. SpvB is also an important regulator of P-body disassembly (Eulalio, Frohlich, Mano, Giacca, & Vogel, 2011).

SpvC is also encoded by the *spv* operon (Coynault, Robbesaule, Popoff, & Norel, 1992) and is translocated by both T3SS-1 and T3SS-2 (Heiskanen, Taira, & Rhen, 1994). SpvC has a phosphothreonine lyase activity that targets ERK, p38, and JNK mitogen-activated protein kinases (MAPKs) (Mazurkiewicz et al., 2008). SpvC limits host inflammatory responses by reducing pro-inflammatory cytokine gene transcription (Haneda et al., 2012).

SpvD functions as a cysteine hydrolase with a papain-like fold and a catalytic triad consisting of C73, H162, and D182 (Grabe et al., 2016). SpvD interacts with the exportin Xpo2m, which mediates nuclear-cytoplasmic protein recycling (Rolhion et al., 2016). The disruption of

importin-alpha recycling from the nucleus results in p65 translocation deficiency and NF-κB inhibition (Rolhion et al., 2016).

SteC is encoded within SPI-2 and has amino acid similarity to human kinase Raf-1, a proto-oncogene serine/threonine-protein kinase (Poh et al., 2008). An *steC* mutant showed no decrease for bacterial replication and virulence, but was defective for SPI-2 dependent F-Actin meshwork formation (Poh et al., 2008). SteC phosphorylates MEK and activates a signaling pathway involving MEK and ERK, MLCK, and Myosin IIB (Odendall et al., 2012). An *steC* mutant shows greater replication in HeLa cells, as compared to wild-type Salmonella, indicating that SteC may limit bacterial replication by regulating F-Actin meshwork formation (Odendall et al., 2012).

SteD stimulates MARCH8, a member of the MARCH family E3 integral membrane ubiquitin ligases (Bayer-Santos et al., 2016). SteD causes ubiquitination and depletion of surface-localized mature MHC class II (mMHCII), thus helping to reduce T cell activation (Bayer-Santos et al., 2016).

Salmonella Secreted Effector L (**SseL**) is encoded within SPI-2 and is transported into the cytosol from the SCV via the T3SS-2. SseL functions as a deubiquitinase (DUB) to induce a delayed cytotoxic effect in *Salmonella*-infected macrophages (Rytkonen et al., 2007). NF-κB signaling in macrophages is significantly activated after infection with an *sseL* mutant, as compared to its activation by wild-type Salmonella (Le Negrate et al., 2008). Expression of SseL in mammalian cells impairs IκBα ubiquitination and degradation, and mutating C285 abolished this effect (Le Negrate et al., 2008).

AvrA is encoded on SPI-1 and is a member of the YopJ/Avr protein family (Hardt & Galan, 1997). AvrA is a multifunctional effector that influences eukaryotic cell pathways by regulating

the ubiquitination (J. Sun, Hobert, Rao, Neish, & Madara, 2004) and acetylation (S. P. Wu et al., 2010) of target proteins to modulate proliferation (X. Y. Liu, Lu, Wu, & Sun, 2010), inflammation (Du & Galan, 2009), and apoptosis (Collier-Hyams et al., 2002). AvrA acetylates p53 (S. P. Wu et al., 2010) and also inhibits JNK signaling by acetylating MKK4 (Jones et al., 2008) and MKK7 (Du & Galan, 2009). AvrA also has a deubiquitinase activity that targets β-catenin, resulting in stabilization of β-catenin and increasing intestinal epithelial cell proliferation (S. P. Wu et al., 2010). Mutating E142, I179, and C186 reduces AvrA acetyltransferase activity (S. P. Wu et al., 2010); C186 also appears to be critical for AvrA deubiquitinase activity (Ye, Petrof, Boone, Claud, & Sun, 2007). As one member of YopJ family effectors, AvrA may also have protease activities, as YopJ family effectors share a conserved cysteine protease-like catalytic triad (Cheong et al., 2014; Ye et al., 2007). However, accumulating evidence shows that many YopJ family effectors modify their target molecules by acetylating specific serine, threonine, and/or lysine residues (Ma & Ma, 2016).

Salmonella encodes up to three NleB orthologs named **SseK1**, **SseK2**, and **SseK3** (Brown et al., 2011). The NleB and SseK effectors contain a conserved DXD motif, which is required for enzymatic function of glycosyltransferases of the GT-A family (X. F. Gao et al., 2013). SseK1 and SseK2 inhibit TNF-induced NF-κB activation and cell death during infection in macrophages (Gunster, Matthews, Holden, & Thurston, 2017). SseK3 binds, but does not glycosylate TRIM32, an E3 ubiquitin ligase involved in TNF and interferon signaling (Yang et al., 2015). SseK1 and SseK3 inhibit TNF-mediated NF-κB pathway activation. SseK1 glycosylates GAPDH, while SseK2 glycosylates FADD (El Qaidi et al., 2017). SseK3 glycosylates TRADD and has an overall fold that is similar to other glycosyltransferase type-A (GT-A) family members . Mutating E258 impairs the ability of SseK3 to glycosylate TRADD .

Salmonella protein tyrosine phosphatase (**SptP**) shares significant homology in its C-terminal domain to the catalytic domains of eukaryotic tyrosine phosphatases (PTPases) and the *Yersinia* protein tyrosine phosphatases YopH (Kaniga, Uralil, Bliska, & Galan, 1996). SptP inhibits ERK activation by interfering with Raf1 activation, a MAPKKK (Murli, Watson, & Galan, 2001). Inhibition is dependent on SptP-phosphatase activity, as a SptP C481S mutation no longer inhibits ERK activation (Lin, Le, & Cowen, 2003). SptP phosphatase activity is also important for inhibiting TNF-α induction during *Salmonella* infection of macrophages (Lin et al., 2003). *Salmonella* outer protein B (**SopB**, also known as **SigD**) has sequence homology to mammalian inositol polyphosphate 4-phosphatases and recombinant SopB functions as an inositol phosphate phosphatase (Norris, Wilson, Wallis, Galyov, & Majerus, 1998). It is encoded within SPI-5 but delivered into cells via T3SS SPI-1 (Knodler et al., 2002). **SopE** is 69% identical to **SopE2** (Bakshi et al., 2000). SopB, SopE, and SopE2, cooperate in a functionally redundant manner to activate Rho-family GTPases during *Salmonella* infection (Patel & Galan, 2006), resulting in activation of MAPK and NF-κB signaling pathways (Bruno et al., 2009). SopB functions as a phosphoinositide phosphatase to activate the RhoG exchange factor (Patel & Galan, 2006), while SopE and SopE2 act as exchange factors for Cdc42, Rac1, and RhoG (Stender et al., 2000). *Salmonella* invasion protein A (**SipA**) is encoded within SPI-1 (Kaniga, Trollinger, & Galan, 1995) and is transported into mammalian cells via the T3SS-1 (D. G. Zhou, 2001). SipA binds F-actin, contributing to *Salmonella* internalization and mediates the downstream activation of Rho GTPases (D. Zhou, Mooseker, & Galan, 1999). SipA induces NF-κB activation and intestinal inflammation by activating the NOD1/NOD2 signaling pathway (Keestra et al., 2011). SipA also induces IL-8 expression by inducing Jun and p38 MAPK phosphorylation (Figueiredo et al., 2009).

Here we have described many of the *E. coli* and *Salmonella* T3SS effectors that target host innate immunity. Many of these effectors apply their inhibitory effect in a cumulative or synergistic manner by blocking multiple steps within a signaling pathway. Effector translocation cell is not random but rather is temporally controlled by the pathogen (Lara-Tejero, Kato, Wagner, Liu, & Galan, 2011), allowing the pathogen to adjust the host inflammatory response not only to evade inflammation but also to alter the relative abundance of commensal flora. Microbial genomes provide information about how co-evolution has shaped pathogen targeting of host immunity. Characterizing anti-inflammatory microbial proteins offers opportunities both to identify natural modulators of inflammation and to engineer these proteins for use as effective immunotherapeutics (Ruter & Hardwidge, 2014). T3SS effectors represent a major pool of pathogen-derived immunomodulatory molecules that may have future utility in treating autoimmune disorders associated with perturbations in NF-κB signaling (S. C. Sun, Chang, & Jin, 2013).

Figure 3 EHEC and *Salmonella* genomes

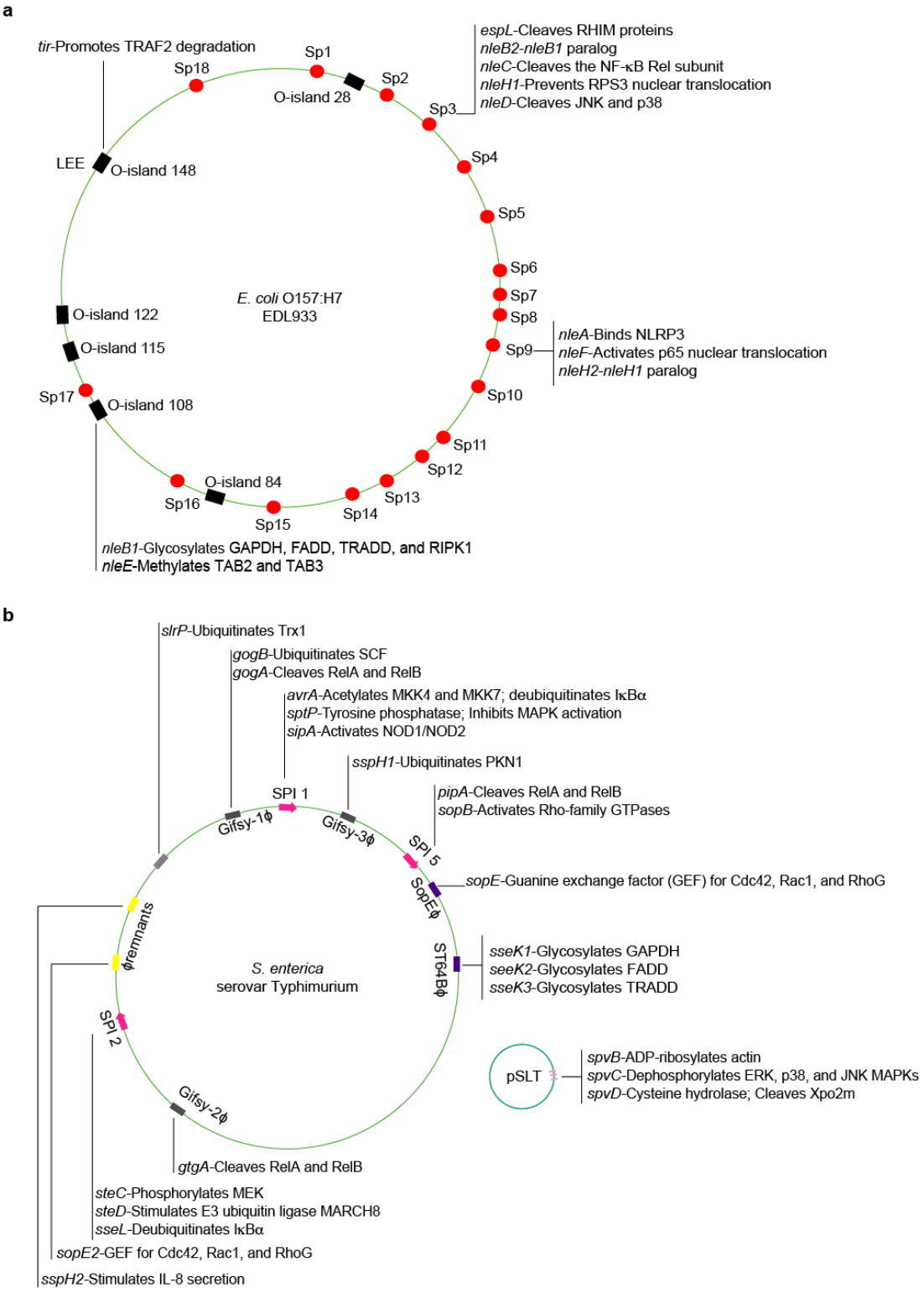

a Schematic of the EHEC O157:H7 EDL933 genome. Black rectangles, O-islands; red dots, prophage elements. **b** Schematic of the *S.* Typhimurium genome. Red arrows, *Salmonella* pathogenicity islands (SPIs); Grey and yellow rectangles, prophage elements.

Figure 4 Effector amino acids and functional domains

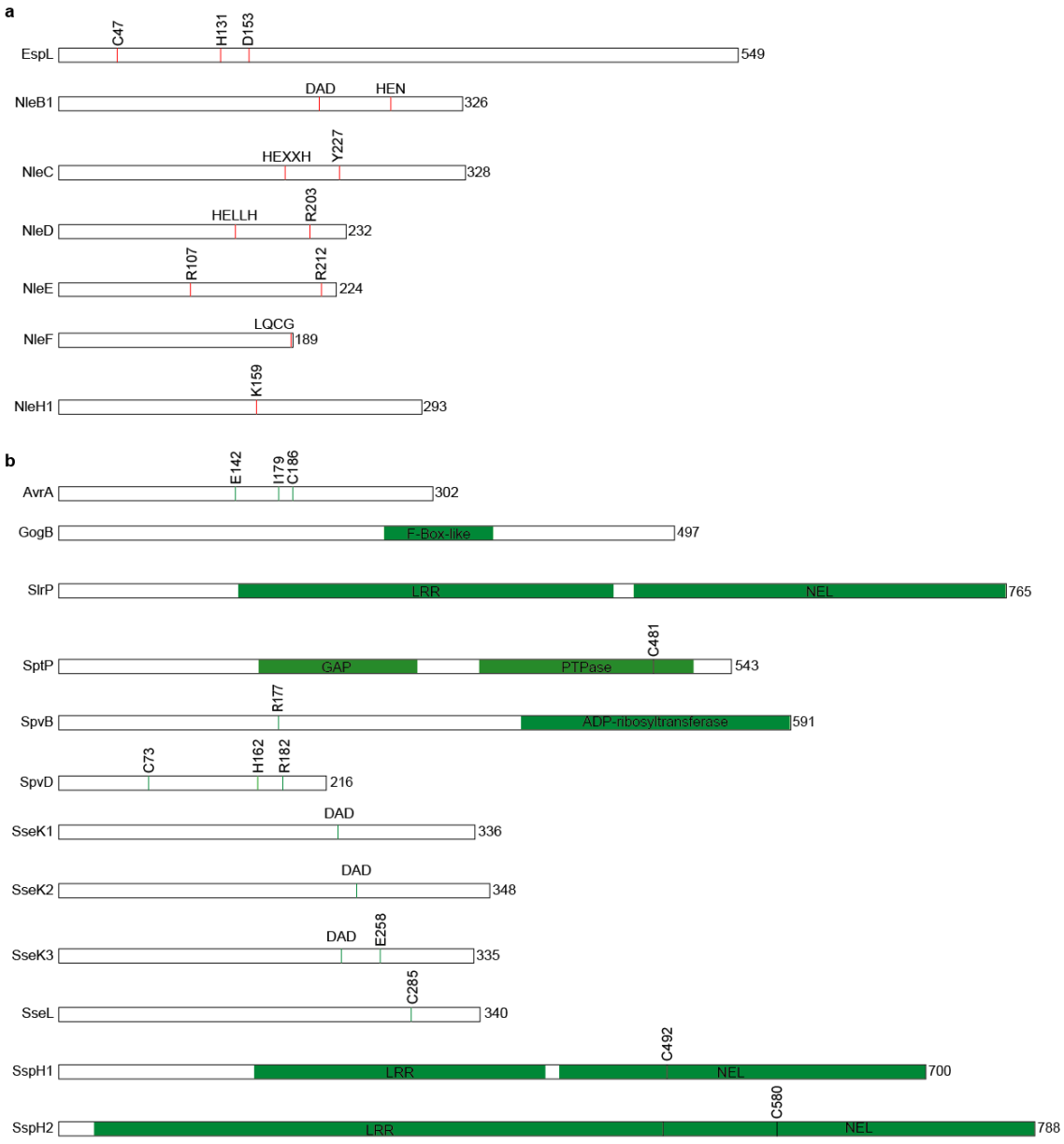

Schematic representation of T3SS effectors targeting host innate immunity. Critical amino acids and secondary structures are highlighted. **a** EHEC/EPEC/*C. rodentium* effectors. **b** *S.* Typhimurium effectors.

Figure 5 Host inflammatory pathways and their targeting by T3SS effectors

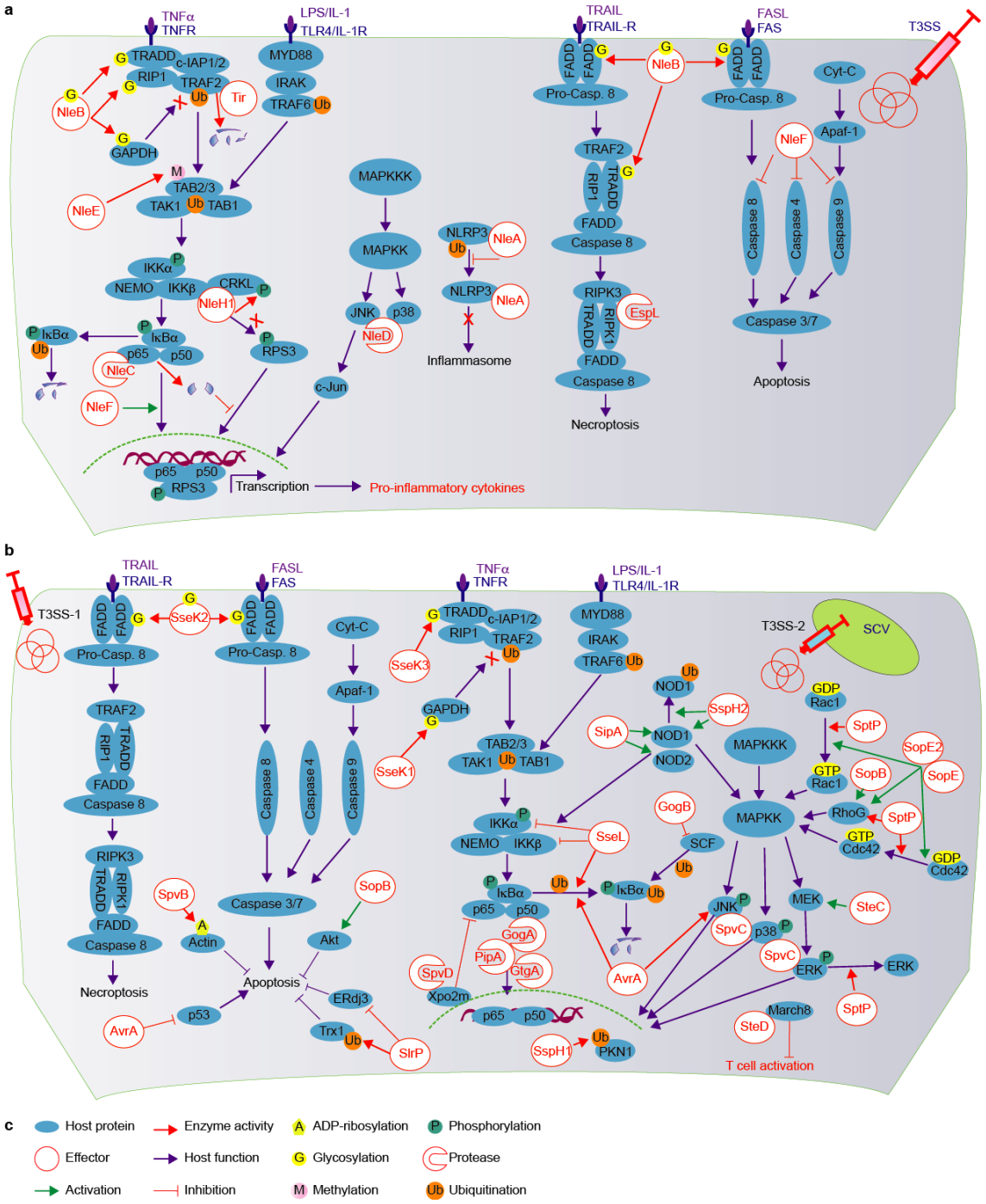

Upon TNFα stimulation, TRADD forms a complex with TRAF2, leading to RIP1 and TRAF polyubiquitination followed by recruitment of TAK1. TAK1 activation results in activation of the IKK complex and phosphorylation of IκBα, which is then ubiquitinated and degraded, releasing NF-κB for nuclear translocation and pro-inflammatory gene transcription. Stimulation of TLR4 or IL-1R by LPS or IL-1β initiates a signaling cascade that leads to TAK1 activation. Stimulation with FASL results in FADD oligomerization and activation of caspase 8, leading to caspase

3/7 maturation and apoptosis. Stimulation with TRAIL initiates necroptosis through a pathway involving the formation of a complex among RIP1, RIP3, TRADD, FADD, and caspase 8. Upon extracellular stimulation, mitogen activated protein kinases (MAPKs) pathway activation begins with the binding of Ras/Rho family proteins to a mitogen activated protein kinase kinase kinase (MAPKKK), which in turn leads to the phosphorylation and activation of a mitogen activated protein kinase kinase (MAPKK), followed by the phosphorylation of the mitogen activated protein kinases (MAPKs) ERK, p38, and JNK. NOD1 and NOD2 recruit receptor-interacting serine/threonine-protein kinase 2 (RIPK2), which further activates MAPKs and the IKK complex. **a** Strategies used by EHEC/EPEC/*C. rodentium* to counteract inflammation. **b** Strategies used by *Salmonella enterica* Serovar Typhimurium to counteract inflammation.

Chapter 2 - SseL deubiquitinates RPS3 to inhibit its nuclear translocation

I contributed to all the figures and tables except for Figure 7b and 9b in Chapter 2. A modified version of Chapter 2 is published in Pathogens (M. Wu, El Qaidi, & Hardwidge, 2018).

Wu, M., El Qaidi, S., & Hardwidge, P. R. (2018). SseL Deubiquitinates RPS3 to Inhibit Its Nuclear Translocation. Pathogens, 7(4). doi:10.3390/pathogens7040086

Introduction

Gram-negative bacteria export virulence proteins (effectors) into host cells using a type three secretion system (T3SS) (Galan, Lara-Tejero, Marlovits, & Wagner, 2014). Effectors bind and/or post-translationally modify host proteins, preventing the host from generating inflammatory responses to the pathogen. Enterohemorrhagic *E. coli* (EHEC) is an attaching/effacing (A/E) pathogen that causes hemorrhagic colitis and pediatric renal failure in humans (Newell & La Ragione, 2018). The EHEC T3SS and some effectors are encoded on a pathogenicity island termed the locus of enterocyte effacement (LEE) (McDaniel, Jarvis, Donnenberg, & Kaper, 1995). Most of the effectors encoded within the LEE are referred to as *E. coli* secreted proteins (Esps), while effectors encoded outside the LEE are referred to as non-LEE encoded effectors (Nles). *Salmonella enterica* serovars encode multiple T3SSs; T3SS-1 is encoded on *Salmonella* pathogenicity island (SPI-1) and delivers effectors across the host cell plasma membrane to trigger actin rearrangements that contribute to bacterial invasion (Patel & Galan, 2005). T3SS-2 is encoded on SPI-2 and translocates virulence proteins from the *Salmonella* containing vacuole (SCV) into the host cell cytoplasm (Ochman et al., 1996).

The recognition of bacterial pathogens by host cells triggers multiple signaling pathways to induce host inflammatory responses (Le Negrate et al., 2008), many of which are regulated by

the nuclear factor kappa-light-chain-enhancer of activated B cells (NF-κB). The ribosomal protein S3 (RPS3) is a component of the eukaryotic 40S small ribosomal subunit, which is responsible for the regulation of ribosome maturation and also plays multifunctional roles in DNA repair, apoptosis, survival, and radioresistance via interaction with various binding partners (W. Kim et al., 2018). RPS3 possesses endonuclease activity functioning in DNA repair (S. B. Lee et al., 2010). Knockdown of RPS3 results in significant cell survival after hydrogen peroxide treatment (Hegde, Yadavilli, & Deutsch, 2007). RPS3 can be phosphorylated by PKCδ, leading to its mobilization in the nucleus to repair damaged DNA (T. S. Kim, Kim, & Kim, 2009). Besides, RPS3 was previously identified as a "specifier" component in NF-κB complexes (F. Wan & Lenardo, 2009). RPS3 guides NF-κB to specific κB sites by increasing the affinity of the NF-κB p65 subunit for target gene promoters (F. Wan et al., 2007). RPS3 associates with p65 in the inhibitory p65-p50-IκBα complex in the cytoplasm of resting cells (F. Wan et al., 2007). Activation of NF-κB is initiated by external stimuli that activate the IκB kinase (IKK) complex. Activated IKKβ phosphorylates IκBα, leading to its subsequent ubiquitination and degradation, which allows for p65 and p50 nuclear translocation (Alkalay et al., 1995). IKKβ also phosphorylates RPS3 on Ser209, enhancing its association with importin-α and mediating RPS3 nuclear translocation (F. Y. Wan et al., 2011).

Two EHEC effectors disrupt the activation of the innate immune system of intestinal epithelial cells by impact RPS3 nuclear translocation. NleH1 binds to RPS3 (X. Gao et al., 2009) and inhibits its phosphorylation by IKKβ (F. Y. Wan et al., 2011). NleC proteolysis of p65 generates an N-terminal p65 fragment that competes for full-length p65 binding to RPS3, thus inhibiting RPS3 nuclear translocation (Wier, Neighoff, Sun, Fu, & Wan, 2012). Thus, EHEC has multiple mechanisms by which to block RPS3-mediated transcriptional activation. With this in mind, we

considered whether other enteric pathogens also encode T3SS effectors that affect this important host regulatory pathway. Here we report that the *Salmonella* Secreted Effector L (SseL), which has been previously shown to inhibit NF-κB signaling (Le Negrate et al., 2008) and function as a deubiquitinase (Rytkonen et al., 2007), also inhibits RPS3 nuclear translocation.

Materials and methods

Cloning, Chemicals, and Antibodies. The strains and plasmids used in this study are listed in Table 2. Primers used in this study are listed in Table 3. Chemicals were used according to manufacturers' recommendations and were obtained from Sigma, except for the following: Polyjet DNA In Vitro Transfection Reagent (SignaGen Laboratories), Glutathione sepharose 4B (GE healthcare Life Sciences), Nickel-nitrilotriacetic acid (Ni-NTA) agarose beads (Qiagen), TNF-α (Cell Signaling). Antibodies were obtained from the following sources: anti-HA, anti-FLAG, Sigma; anti-RPS3, Proteintech Group; anti-β-tubulin, anti-β-actin, anti-His, Santa Cruz Biotechnology; anti-IκBα, anti-ubiquitin, Cell Signaling; anti-PARP, BD Transduction Laboratories.

Table 2 Strains and plasmids used in Chapter 2.

Strain/plasmid	Description	Source
Strain		
E. coli BL21(DE3)	*E. coli* F$^-$*omp*T *hsd*SB (r_B^-_m_B^-) *gal dcm* (DE3)	Novagen
BL21(DE3)/NleH1-pET42a	GST-EHEC NleH1	(X. Gao et al., 2009)
BL21(DE3)/SseL-pET42a	GST-*S. Typhimurium* SseL	This study
BL21(DE3)/RPS3-pET28a	His-RPS3	This study
BL21(DE3)NleB1-pET42a	GST-EHEC NleB1	(El Qaidi et al., 2017)
BL21(DE3)/SseL(C262A)-pET42a	GST-*S. Typhimurium* SseL(C262A)	This study
Plasmid		
HA	HA fusion expression	Clontech
NleH1-HA	HA fused to *E. coli* EDL933 NleH1	(X. Gao et al., 2009)
SseL-HA	HA fused to *S. Typhimurium* SseL	This study

SseL(C262A)-HA	HA fused to *S. Typhimurium* SseL(C262A)	This study
FliC-HA	HA fused to ETEC FliC	(G. Wang, Geisbrecht, Rueter, & Hardwidge, 2017)
3×FLAG	FLAG expression	Sigma
3×FLAG-RPS3	FLAG-RPS3	(F. Wan et al., 2007)
pET42a	Bacterial GST fusion expression	Novagen
NleH1-pET42a	GST-EHEC NleH1	(X. Gao et al., 2009)
NleB1-pET42a	GST-EHEC NleB1	(El Qaidi et al., 2017)
SseL-pET42a	GST-*S. Typhimurium* SseL	This study
SseL(C262A)-pET42a	GST-*S. Typhimurium* SseL(C262A)	This study

Cell culture and transient DNA transfection. HEK293 cells were maintained at 37 °C, 5% CO_2 in DMEM supplemented with 10% fetal bovine serum (FBS) and penicillin-streptomycin (100 U/mL). Cells were seeded in a 6-well plates 18-24 h prior to transfection. Media was replaced with 1 ml fresh complete DMEM per well 0.5-1 h before transfection. DNA was transfected into cells using Polyjet transfection reagent (SignaGen Laboratories). After 24 h of incubation at 37 °C, the cells were harvested.

Table 3 Oligonulceotides used in Chapter 2.

Description	Sequence
Salmonella sseL XhoI forward	ATGCCTCGAGAGCGATGAGGCGCTTACATT
Salmonella sseL NotI reverse	GCGGCGGCCGCTTACTGGAGACTGTATTCATA
Salmonella sseL BamHI forward	ATGCGGATCCAGCGATGAGGCGCTTACATTGT
Salmonella sseL XhoI reverse	GCGCTCGAGCTGGAGACTGTATTCATATAT
Salmonella sseL(C262A) forward	CAGAACAATGTACCCAACGGCGCTGGTCTATTTTGTTACC ATACAATTC
Salmonella sseL(C262A) reverse	GAATTGTATGGTAACAAAATAGACCAGCGCCGTTGGGTA CATTGTTCTG
RPS3 NdeI forward	ATATCATATGGCAGTGCAAATATCCAAG
RPS3 SalI reverse	ACGCGTCGACTGCTGTGGGGACTGGCTGGGG

Cell fractionation. Nuclear and cytosolic protein extracts were obtained as described previously (El Qaidi et al., 2017). Briefly, HEK293 cells were transfected and 48 h later, TNF-α was added at 50 ng/ml for 30 min. Nuclear and cytosolic protein extracts were prepared using the NE-PER nuclear and cytoplasmic extraction reagents (Thermo Fisher). Data were analyzed by Western blotting for nuclear RPS3. Poly(ADP-ribose) polymerase and β-tubulin or β-actin were used to normalize the protein concentrations of nuclear and cytoplasmic fractions, respectively.

Co-immunoprecipitation Assay. Transfected HEK293 cells were washed using pre-chilled PBS, scraped into ice-cold PBS, and centrifuged at 16,000 × g for 5 min. Supernatants were removed, and cells were lysed in 50 mM Tris-HCl, pH 7.4, 0.15 mM NaCl, 1 mM EDTA, 1 % Triton X-100, supplemented with 1 × halt protease inhibitor cocktail (Thermo Fisher). Samples were incubated on ice for 30 min, with occasional shaking, and cell lysates were collected by centrifugation at 12,000 × g for 10 min at 4 °C. Anti-FLAG M2 Gel (Sigma) was centrifuged at 7,000 × g for 30 s at 4 °C, supernatants were removed, and beads were washed twice using 50 mM Tris-HCl, 250 mM NaCl, pH 7.4 (TBS). Prepared beads were incubated with lysates for 45 min at 4 °C. The mixture was pelleted by centrifugation at 7,000 × g for 1 min at 4 °C, and washed 3 times with pre-chilled TBS. The beads were resuspended in 2 × SDS loading dye, incubated for 5 min at 95 °C, and analyzed using 10% SDS-PAGE.

Protein purification. RPS3 was cloned into pET28a, and SseL was cloned into pET42a. They were expressed in *E. coli* BL21(DE3) cells. Bacterial cultures were grown to A_{600}=0.5 and isopropyl β-$_D$-thiogalactopyranoside (IPTG) was added to a final concentration of 0.5 mM. After 3 h of additional growth, cells were pelleted using centrifugation, and lysed in 50 mM sodium phosphate, pH 8.0, 0.5 mg/ml lysozyme. Lysates were incubated on ice for 30 min with occasional shaking, after which an equal volume of 50 mM sodium phosphate, pH 8.0, 1 M

NaCl, 8 mM imidazole, 20 % glycerol, 1 % sarkosyl was added, followed by further incubation on ice for 30 additional min. The bacterial lysate was sonicated and then clarified by centrifugation. The supernatant was incubated with nickel-nitrilotriacetic acid beads (Qiagen) with end-to-end rotation for 1 h at 4 °C, and slurries were loaded on a Poly-Prep Chromatography Column (BioRad), and washed twice with 5-7 bead volumes of 50 mM sodium phosphate, pH 8.0, 600 mM NaCl, 60 mM imidazole, 10 % glycerol. Proteins were eluted in 50 mM sodium phosphate, pH 8.0, 600 mM NaCl, 250 mM imidazole, 20 % glycerol. Proteins were analyzed using 10% SDS-PAGE.

Pulldown assays. Glutathione S-transferase (GST) pulldown experiments were performed as described (Tuan Nguyen and James Goodrich, 2006). GST-tagged bait proteins (10 μM) were immobilized on glutathione sepharose 4B beads (GE Healthcare) in 20 mM Tris-HCl, pH7.9, 0.1 M NaCl, 5 mM $MgCl_2$, 1 mM EDTA, 1 mM DTT, 0.2 mM PMSF, 20% glycerol, 0.1% Nonidet P-40, supplemented with 0.33 unit/μl of DNase I and RNase A. After overnight incubation at 4 °C, the beads were incubated with His-tagged proteins (10 μM) for 1 h at 4 °C. The beads were then washed 3-4 times with 20 mM Tris-HCl, pH 7.9, 1 M NaCl, 1 mM EDTA, 1 mM DTT, 0.2 mM PMSF, 20 % glycerol, 0.1 % Nonidet P-40. Proteins were eluted with 10 mM reduced glutathione and analyzed using 10 % SDS-PAGE.

Deubiquitination assays. HEK293 cells were transfected with FLAG-RPS3, Ubiquitin-HA, and either SseL or SseL(C262A). The cells were washed with pre-chilled 1 × PBS, and cell pellets were lysed in 50 mM Tris-HCl, pH7.4, 0.15 mM NaCl, 1 mM EDTA, 1% Triton X-100, supplemented with 1 × halt protease inhibitor cocktail (Thermo Fisher) on ice for 30 min and then mixed with anti-FLAG M2 affinity resin and rotated at 4 °C for 2 h. The resins were centrifuged at 7,000 × g for 30 s at 4 °C and then washed three times with pre-chilled TBS. The

resins were resuspended in 2 × SDS loading dye, boiled for 5 min at 95 °C, and immunoblotted with appropriate antibodies.

RT-PCR. Total RNA was isolated from cells using the RNeasy Plus Mini kit (QIAGEN). RNA was first reverse-transcribed using a first-strand cDNA synthesis kits (QIAGEN) and quantitative PCR was then carried out using a Rotor-Gene SYBR Green kit (QIAGEN). The comparative Ct method was used to calculate the relative abundance of IL-8 transcripts with normalization to beta-actin expression.

Statistical analyses. Protein abundance was quantified using Li-COR Image Studio software. RPS3 nuclear translocation and ubiquitination were analyzed statistically using either one-way analysis of variance (ANOVA) or t-tests. p values < 0.05 were considered significant.

Results

SseL Reduces the Nuclear Abundance of RPS3. RPS3 translocates to the nucleus after stimulation with human tumor necrosis factor-α (TNF-α) in HEK293 cells (F. Wan et al., 2007). The *Salmonella* T3SS effector protein SseL impairs IκBα ubiquitination and degradation (Le Negrate et al., 2008). To determine whether SseL also inhibits RPS3 nuclear translocation, we quantified the relative abundance of nuclear vs. cytoplasmic RPS3 in HEK293 cells in the presence or absence of transfected SseL-HA after TNF stimulation. As expected, the nuclear abundance of RPS3 significantly increased after TNF treatment. EHEC NleH1, a positive control, significantly decreased RPS3 nuclear translocation. The nuclear abundance of RPS3 was reduced in nuclear fractions containing SseL, while cytoplasmic RPS3 concentrations were unchanged. SseL was detected only in the cytoplasm. Quantitative analysis of RPS3 abundance revealed that SseL significantly reduced the relative abundance of nuclear RPS3 after TNF stimulus (**Figure 6**).

Figure 6 SseL inhibits RPS3 nuclear translocation.

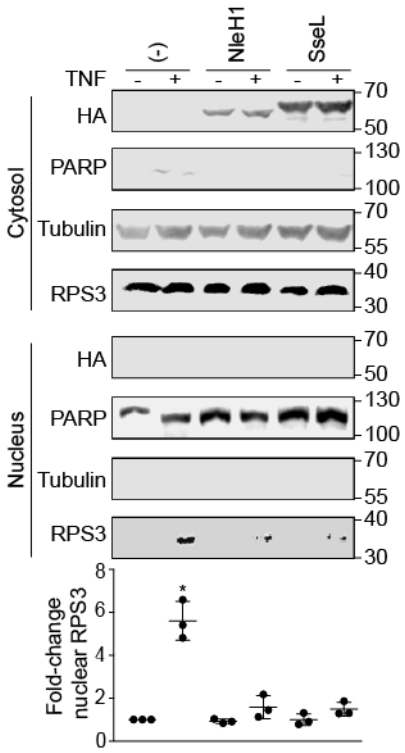

HEK293 cells were transfected with the indicated plasmids and treated with TNF-α (50 ng/ml, 30 min) 24 h later. The cells were lysed, separated into nuclear and cytosolic extracts, and subjected to immunoblotting using the indicated antibodies. Poly(ADP-ribose) polymerase (PARP) and tubulin were used to normalize nuclear and cytosolic protein concentrations, respectively. RPS3 quantification data (n = 3) are shown as means ± S.E after normalization to nuclear PARP abundance. Asterisk indicate significantly different protein abundance as compared with the TNF-α control ($p < 0.05$, ANOVA).

SseL Binds to RPS3. To determine whether SseL interacts with RPS3 in mammalian cells, we performed co-immunoprecipitation experiments. After co-transfecting either FliC-HA (as a negative control), NleH1-HA (as a positive control), or SseL-HA with FLAG-RPS3, cell lysates were immunoprecipitated with anti-FLAG M2 beads and subsequently immunoblotted. NleH1-HA and SseL-HA, but not FliC-HA, interacted with FLAG-RPS3 (**Figure 7a**). To determine whether SseL binds directly to RPS3, we conducted GST pulldown assays. Purified GST-NleH1 (positive control), GST-NleB1 (negative control), and GST-SseL were immobilized on GST

beads and incubated with RPS3-His. RPS3 was enriched in the NleH1 and SseL pulldown samples, as compared to the negative control (**Figure 7b**). Thus, SseL interacts with RPS3 in mammalian cells and binds directly to RPS3 in vitro.

Figure 7 SseL binds to the host ribosomal protein S3 (RPS3).

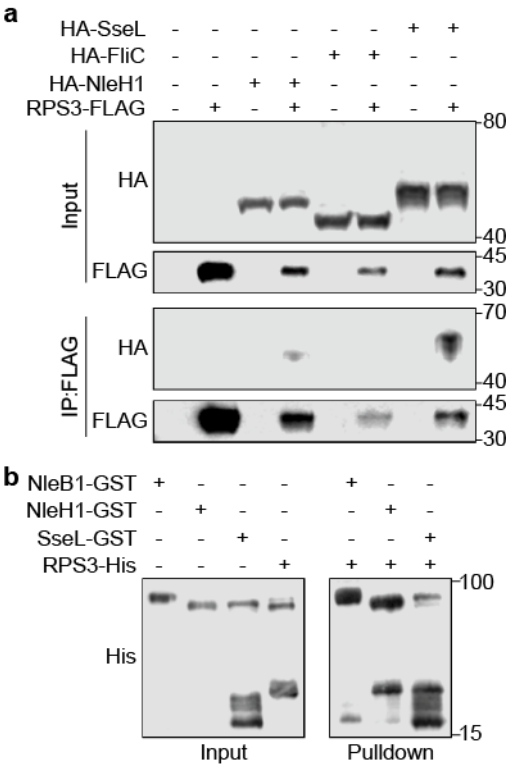

a Co-immunoprecipitation of SseL-HA from HEK293 cells with FLAG-RPS3. HEK293 cells were transfected with the indicated plasmids. Cell lysates were immunoprecipitated using anti-FLAG M2 gel and immunoblotted for FLAG and HA. **b** Pulldown assay to detect binding between SseL and RPS3. His-RPS3 was incubated with GST-SseL and subjected to GST pulldown assay using glutathione-sepharose beads (GE Healthcare). Protein complexes were eluted with 10 mM reduced glutathione followed by 10 % SDS-PAGE analysis. GST-NleB was used as a negative control, and GST-NleH1 was used as positive control.

SseL Deubiquitinates RPS3. SseL is a deubiquitinase (DUB) that induces a delayed cytotoxic effect in *Salmonella*-infected macrophages (Rytkonen et al., 2007) by impairing IκBα ubiquitination and degradation (Le Negrate et al., 2008). IKKβ-mediated phosphorylation of RPS3 S209 is a prerequisite for RPS3 nuclear translocation (F. Y. Wan et al., 2011). We hypothesized that the deubiquitinase activity of SseL might be required for its ability to inhibit RPS3 nuclear translocation. Ubiquitination of RPS3 has been recently demonstrated to be important for ribosome quality control (Jung et al., 2017; Simms, Yan, & Zaher, 2017), but the role of ubiquitination in potentially regulating RPS3 nuclear translocation has been less extensively studied. We first determined that RPS3 is ubiquitinated and such ubiquitination can occur using both K48 and K63 isopeptide linkages (**Figure 8a**). Ubiquitinated RPS3 was detected in the nucleus as well as the cytoplasm, as shown by performing nuclear fractionation assays (**Figure 8b**). Co-transfecting SseL significantly decreased the extent of RPS3 ubiquitination (**Figure 8c**).

Figure 8 SseL deubiquitinates RPS3.

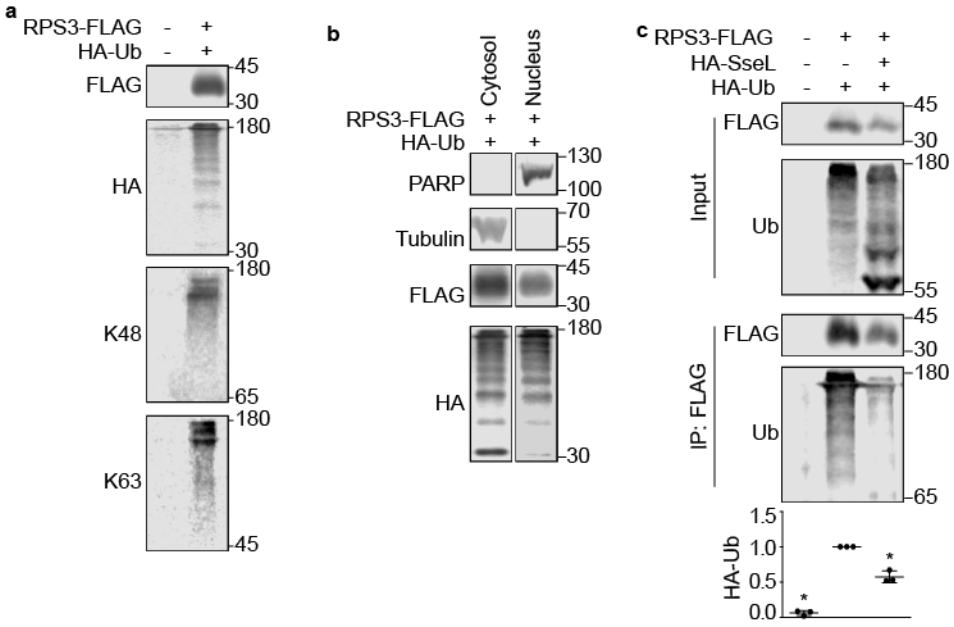

a RPS3 ubiquitination. HEK293 cells were co-transfected with FLAG-RPS3 and HA-ubiquitin plasmids. After 24 h, cell lysates were immunoprecipitated using anti-FLAG M2 gel and immunoblotted for FLAG, HA, K48-Ub, and K63-Ub. **b** Nuclear RPS3 is ubiquitinated. HEK293 cells were co-transfected with FLAG-RPS3 and HA-ubiquitin plasmids. After 24 h, cells were stimulated with TNF-α (50 ng/ml, 30 min) and then lysed, separated into nuclear and cytosolic extracts, and used in immunoblotting experiments, which were then immunoprecipitated (*IP*) using anti-FLAG M2 gel and subjected to immunoblotting using indicated antibodies. **c** SseL deubiquitinates RPS3. HEK293 cells were transfected with the indicated plasmids. After 24 h, cell lysates were immunoprecipitated using anti-FLAG M2 gel and immunoblotted. Quantification (n = 3) of the fold-change in ubiquitin signal intensity after normalization with FLAG-RPS3 intensity is shown as mean ± S.E. Asterisk indicate significantly different protein abundance as compared with ubiquitinated RPS3 control group ($p < 0.05$, ANOVA).

SseL DUB activity is important to inhibiting RPS3 nuclear translocation. Mutating SseL C262 abolishes its ability to hydrolyze ubiquitin (Rytkonen et al., 2007). To determine whether the SseL C262 residue is required for SseL interaction with RPS3, we mutated C262 into alanine and performed co-immunoprecipitation and GST pulldown assays. We observed that both SseL wild-type and SseL C262A interacted with RPS3 (**Figure 9a**), and they both bound directly to RPS3 (**Figure 9b**), indicating that this residue is not essential for SseL binding to RPS3. The SseL C262A mutant, in contrast to SseL wild-type, showed a reduced ability to deubiquitinate RPS3 after co-transfection (**Figure 9c**). RPS3 deubiquitination by SseL was restricted to K63 linkages (**Figure 9d**).

Figure 9 SseL DUB activity blocks RPS3 nuclear translocation.

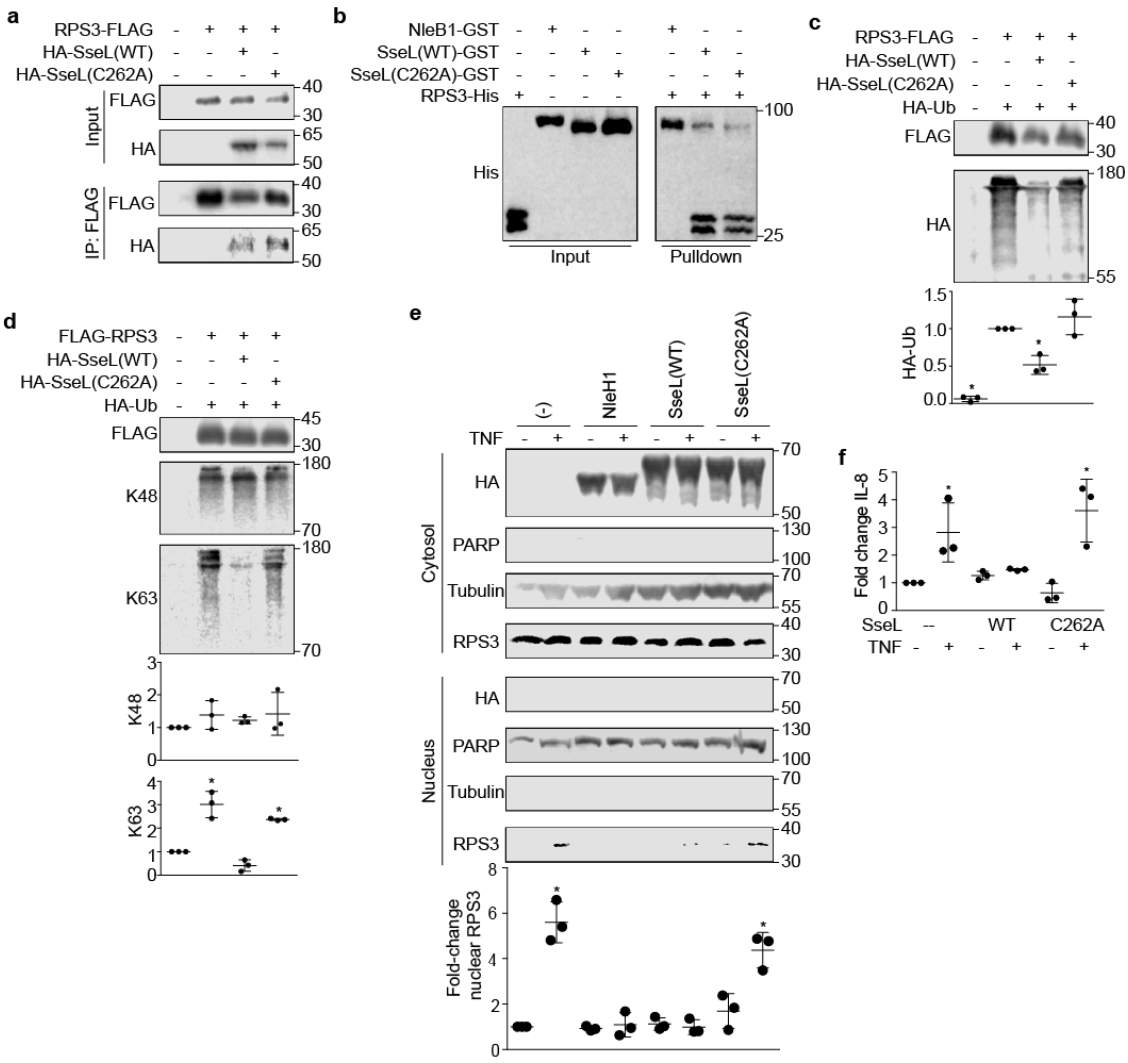

a Co-immunoprecipitation of SseL WT-HA and SseL(C262A)-HA with FLAG-RPS3. HEK293 cells were transfected with the indicated plasmids, immunoprecipitated using anti-FLAG M2 gel, and immunoblotted for FLAG and HA. **b** Pulldown assay to detect binding between SseL(C262A) and RPS3. His-RPS3 was incubated with GST-SseLWT or GST-SseL(C262A) and subjected to GST pulldown assay using glutathione-sepharose beads. Protein complexes were eluted with 10 mM reduced glutathione followed by 10 % SDS-PAGE analysis. GST-NleB1 was used as a negative control. **c** SseL(C262A) fails to deubiquitinate RPS3. HEK293 cells were transfected with the indicated plasmids, immunoprecipitated using anti-FLAG M2 gel, and immunoblotted for FLAG and HA. Quantification (n = 3) of the fold-change in ubiquitin signal intensity after normalization with FLAG-RPS3 intensity is shown as mean ± S.E. Asterisk indicates significantly different protein abundance as compared with ubiquitinated RPS3 control group ($p < 0.05$, ANOVA). **d** SseL DUB activity on RPS3 is specific to K63 linkages. HEK293 cells were transfected with the indicated plasmids, immunoprecipitated using anti-FLAG M2 gel, and immunoblotted for FLAG, HA, K48-Ub, and K63-Ub. Quantification (n = 3) of the fold-change in ubiquitin signal intensity after normalization with FLAG-RPS3 intensity is shown as mean ± S.E. Asterisk indicates significantly different protein abundance as compared with ubiquitinated RPS3 control group ($p < 0.05$, ANOVA). **e** SseL C262A fails to inhibit RPS3 nuclear translocation. HEK293 cells were transfected with the indicated plasmids. After 24 h, cells were stimulated with TNF-α (50 ng/ml, 30 min) and then lysed, separated into nuclear and cytosolic extracts, and used in immunoblotting experiments.

RPS3 quantification data (n = 3) are shown as means ± S.E after normalization to nuclear PARP abundance. Asterisk indicates significantly different protein abundance as compared with the TNF-α control ($p < 0.05$, ANOVA). **f** SseL inhibits IL-8 expression. HEK293 cells were transfected with either SseL-WT or SseL(C262A) and then stimulated with 50 ng/mL TNF-α for 30min. IL-8 expression was quantified using RT-PCR, and data were normalized to β-actin expression.

To determine whether SseL DUB activity is important to inhibiting RPS3 nuclear translocation, we transfected HEK293T cells with WT SseL-HA or SseL(C262A)-HA and evaluated the relative abundance of nuclear vs. cytoplasmic RPS3. The nuclear abundance of RPS3 was unchanged in the nuclear fraction of cells transfected with SseL(C262A), but was significantly inhibited in cells transfected with SseL wild-type (**Figure 9e**). To evaluate whether SseL alters RPS3/NF-κB-dependent gene expression, we performed quantitative RT-PCR experiments to assess whether SseL reduced the ability of TNF-α to activate the expression of IL-8, a gene that is dependent upon RPS3 for maximal expression (X. Gao et al., 2009). TNF-α induced IL-8 expression was significantly inhibited by WT SseL but not by SseL(C262A) (**Figure 9f**), showing the biological significance of how SseL-mediated reduction in RPS3 nuclear abundance affects host transcriptional responses associated with innate immunity. Taken together, our data suggest that SseL functions as a DUB that inhibits RPS3 nuclear translocation by deubiquitinating RPS3 (**Figure 10**).

Figure 10 Working model.

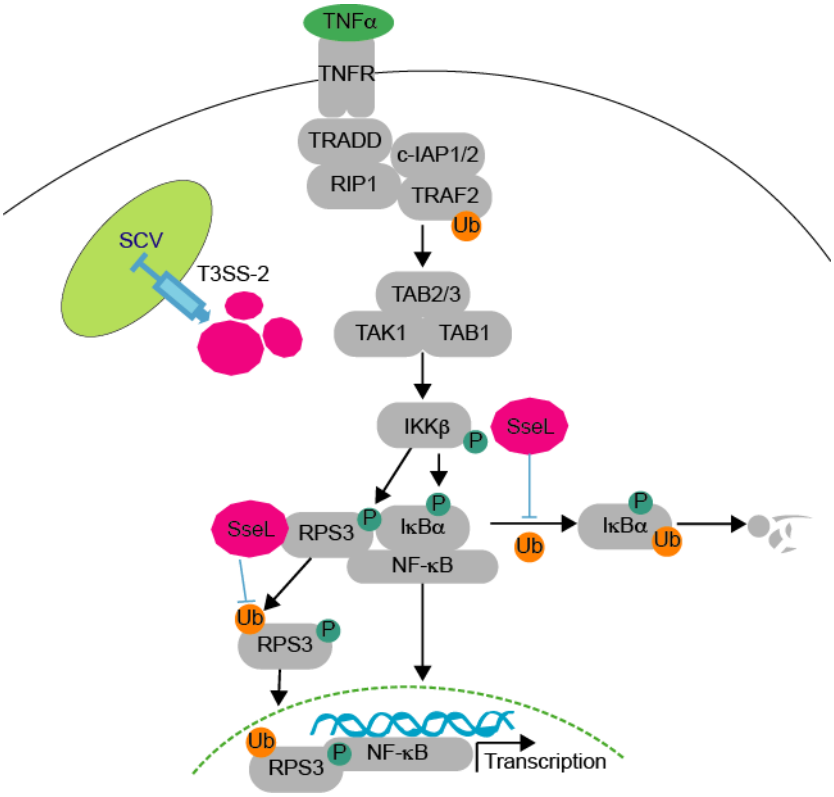

After TNF-α stimulation through the tumor necrosis factor receptor (TNFR), transforming growth factor beta-activated kinase 1 (TAK1) activation is induced, promoting IKKβ activation, which then phosphorylates both IκBα and RPS3. During *Salmonella* infection, SseL is translocated into host cells through the T3SS-2 and then interacts with both IκBα and RPS3. SseL impairs IκBα ubiquitination and degradation, thus limiting host NF-κB pathway activation and promoting bacterial pathogen colonization (Le Negrate, 2012). SseL binds and deubiquitinates RPS3, resulting in reduced RPS3 nuclear translocation.

Discussion

Here we further examined the mechanism of RPS3 nuclear translocation and gained novel insights into the importance of RPS3 ubiquitination in this process. We provide evidence that the *Salmonella* effector SseL binds to RPS3 and functions as a DUB to inhibit its nuclear translocation. RPS3 was identified as a "specifier" component in NF-κB complexes (F. Wan & Lenardo, 2009). RPS3 guides NF-κB to specific κB sites by increasing the affinity of the NF-κB p65 subunit for target gene promoters (F. Wan et al., 2007). Evidence is emerging suggesting

that some ribosomal proteins correlate with NF-κB signaling. p53 loss does not alter IκBα phosphorylation and degradation, and p65 nuclear translocation (Murphy et al., 2011). TNF induced synthesis of H_2S sulfhydrates p65 at cysteine 38 and promotes its association with RPS3 to enhance expression of cytoprotective genes (Sen et al., 2012). Ribosomal protein rpL3 stabilizes IκBα to inhibit p65 nuclear translocation in p53 mutated cells, thus reduces IL-8 production (Russo et al., 2016). Human RPS3 contains twenty lysine residues that are potential ubiquitination sites (Danielsen et al., 2011; Shi et al., 2011; Wagner et al., 2011). The unfolded protein response triggers ubiquitination of RPS3 K214 (Higgins et al., 2015). Regulatory RPS3 ubiquitination catalyzed by ZNF598 plays a pivotal role in regulating mammalian ribosome-associated quality control pathways (Jung et al., 2017; Simms et al., 2017; Sundaramoorthy et al., 2017). RPS3 was shown to interact with p53 (Yadavilli et al., 2009), but its mono-ubiquitination is independent of p53 (Jung et al., 2017). Non-ribosomal RPS3 is protected from ubiquitination and proteasome-dependent degradation by interacting with Heat shock protein 90 (Hsp90), which helps retain the function and biogenesis of the ribosome (T. S. Kim et al., 2006). There is little information available concerning the role of RPS3 ubiquitination in its nuclear translocation, although it is known that nuclear RPS3 can be ubiquitinated by ring finger protein 138 (RNF138) (W. Kim et al., 2018). This ubiquitination leads to RPS3 degradation and affects radioresistance (W. Kim et al., 2018). As no active E3 ligase that is specific to RPS3 is commercially available, we were unable to perform experiments to detect RPS3 ubiquitination and deubiquitination *in vitro*.

Two *E. coli* effectors inhibit RPS3 nuclear translocation; NleH1 inhibits RPS3 phosphorylation by IKK-β, an essential aspect of the RPS3 nuclear translocation process (X. Gao et al., 2009). NleC proteolysis of p65 generates an N-terminal p65 fragment that competes for full-length p65

binding to RPS3, thus also inhibiting RPS3 nuclear translocation (Wier et al., 2012). We examined whether *Salmonella* effectors also target this pathway, and, by using nuclear fractionation and transfection experiments, we observed a significant reduction in nuclear RPS3 abundance by expressing SseL (**Figure 6**). SseL interacted with RPS3 in mammalian cells and bound directly to RPS3 in vitro (**Figure 7**). SseL deubiquitinated RPS3 in transfected mammalian cells (**Figure 8**). However, we were unable to confirm this activity by performing *in vitro* deubiquitination assays, as no specific E3 ligase for RPS3 is available.

Ubiquitination plays an important role in regulating protein localization (Beverly, Lockwood, Shah, Erdjument-Bromage, & Varmus, 2012; Gregory, Taniguchi, & D'Andrea, 2003) and there is precedent for K63-linked polyubiquitination in regulating the relative cytoplasmic vs. nuclear abundance of proteins (P. Y. Wang, Chang, Lin, Kuo, & Wang, 2018). In the context of SseL, deubiquitination of K63-RPS3 significantly reduced the extent of RPS3 nuclear translocation (**Figure 9**). This phenotype was dependent upon SseL DUB activity, as the SseL C262A mutant had no impact on RPS3 nuclear translocation. Overall, we propose that, similarly to *E. coli*, an important aspect of *Salmonella* virulence may be that *Salmonella* injected at least one effector through their conserved T3SS into host cells where they interfere with host cell signaling cascades, particularly the RPS3 signaling, to modulate host innate immune responses to the pathogen's advantage.

Chapter 3 - Hsp90 interacts with the bacterial effector NleH1

I contributed to all the figures and tables in Chapter 3. A modified version of Chapter 3 is published in Pathogens (M. Wu & Hardwidge, 2018).

Wu, M., & Hardwidge, P. R. (2018). Hsp90 Interacts with the Bacterial Effector NleH1. Pathogens, 7(4). doi:10.3390/pathogens7040087

Introduction

The nuclear factor kappa-light-chain-enhancer of activated B cells (NF-κB) family of transcription factors regulates innate and adaptive immune responses. In addition to the well-characterized Rel family proteins (Le Negrate, 2012), ribosomal protein S3 (RPS3) is a key non-Rel subunit and was identified as a "specifier" NF-κB component. RPS3 guides NF-κB to specific κB sites by increasing the affinity of the NF-κB p65 subunit for target gene promoters (F. Wan et al., 2007). Activation of NF-κB signaling is initiated by external stimuli that activate the IκB kinase (IKK) complex. This complex consists of two catalytic components IKKα (IKK1) and IKKβ (IKK2), in addition to a regulatory subunit, the NF-κB Essential Modulator (NEMO; IKKγ). The canonical IKK complex plays a central role in regulating many cellular processes in response to a variety of physiological and pathological stimuli, among which NF-κB is the best known. Activated IKKβ phosphorylates IκBα, resulting in its subsequent ubiquitination and degradation, which allows for p65 and p50 nuclear translocation (Alkalay et al., 1995). IKKβ also phosphorylates RPS3 on Ser209, enhancing its association with importin-α and mediating RPS3 nuclear translocation (F. Y. Wan et al., 2011).

Bacteria have evolved secretion systems to transport virulence proteins termed 'effectors' to counteract host innate immunity. Enterohemorrhagic *Escherichia coli* (EHEC) encodes numerous type three secretion system (T3SS) effectors that subvert cellular processes to create an environment conductive to bacterial survival. EHEC encodes two forms of the NleH effector, NleH1 and NleH2 (X. Gao et al., 2009; Pham et al., 2013). Both effectors bind RPS3, but only NleH1 inhibits RPS3 nuclear translocation by preventing RPS3 phosphorylation on S209 by IKKβ (X. Gao et al., 2009; F. Y. Wan et al., 2011). NleH1 activity only restricts the phosphorylation of a subset of the IKKβ substrates, suggesting that an additional host co-factor might dictate this inhibitory specificity. Here we identified heat shock protein 90 (Hsp90) as an NleH1 binding partner and found that inhibiting Hsp90 activity reduced RPS3 nuclear translocation.

Materials and methods

Cloning, Chemicals, and Antibodies. The strains and plasmids used in this study are listed in **Table 4**. All chemicals were used according to manufacturers' recommendations and were obtained from Sigma, except for the following: Nickel-nitrilotriacetic acid (Ni-NTA) agarose beads (Qiagen), Glutathione sepharose 4B GST-tagged protein purification resin (GE healthcare Life Sciences), Polyjet DNA In Vitro Transfection Reagent (SignaGen Laboratories), TNF-α (Cell Signaling). Antibodies were obtained from the following resources: anti-FLAG, anti-HA, Sigma; anti- IκBα, Cell Signaling; anti-β-tubulin, anti-β-actin, anti-His, Santa Cruz Biotechnology; anti-PARP, BD Transduction Laboratories; anti-RPS3, Proteintech Group.

Table 4 Strains and plasmids used in Chapter 3**.**

Strain/plasmid	Description	Source
Strain		
E. coli BL21(DE3)	*E. coli* F$^-$ *ompT hsdSB* (r_B-m_B-) *gal dcm* (DE3)	Novagen
BL21(DE3)/NleH1-pET42a	GST-EHEC NleH1	(X. Gao et al., 2009)

BL21(DE3)/NleH2-pET42a	GST-EHEC NleH2	(X. Gao et al., 2009)
BL21(DE3)/IKKβ pET28a	His-IKKβ	This study
EHEC EDL933	wild type E. coli O157:H7 isolate	CDC
EHL933 ΔnleH1	EHEC nleH1 deletion	(X. Gao et al., 2009)
Plasmids		
HA	HA fusion expression	Clontech
NleH1-HA	HA fused to *E. coli* EDL933 NleH1	(X. Gao et al., 2009)
NleH2-HA	HA fused to *E. coli* EDL933 NleH2	(X. Gao et al., 2009)
Hsp90-HA	HA fused to Hsp90	This study
3×FLAG	FLAG expression	Sigma
3×FLAG-IKKβ	FLAG-IKKβ	(F. Y. Wan et al., 2011)
3×FLAG-NleH1	FLAG-EHEC NleH1	This study
3×FLAG-NleH2	FLAG-EHEC NleH2	This study
pET42a	Bacterial GST fusion expression	Novagen
NleH1-pET42a	GST-EHEC NleH1	(X. Gao et al., 2009)
NleH2-pET42a	GST-EHEC NleH2	(X. Gao et al., 2009)
pET28a	Bacterial His6 fusion expression	Novagen
IKKβ pET28a	His-IKKβ	This study

Protein purification. IKKβ was cloned into pET28a, and NleH1, NleH2, and NleB1 were cloned into pET42a. They were expressed in *E. coli* BL21(DE3) cells. Bacterial cultures were grown to an OD_{600} of 0.6, and isopropyl β-$_D$-thiogalactopyranoside (IPTG) was added to a final concentration of 0.6 mM. After 4 h of additional growth, cells were pelleted using centrifugation, and lysed in 50 mM sodium phosphate, pH 8.0, supplemented with 0.5 mg/ml lysozyme and halt proteinase inhibitor (Thermo Fisher). Lysates were incubated on ice for 30 min with occasional shaking, after which an equal volume of 50 mM sodium phosphate, pH 8.0, 1 M NaCl, 8 mM imidazole, 20 % glycerol, 1 % sarkosyl was added, followed by further incubation for 30 min. Lysates were sonicated, clarified by centrifugation, and the supernatants were applied to nickel-nitrilotriacetic acid beads (Qiagen) with end-to-end rotation for 2 h at 4 °C. After washing with 50 mM sodium phosphate, pH 8.0, 600 mM NaCl, 60 mM imidazole, 10 % glycerol, proteins were eluted in 50 mM sodium phosphate, pH 8.0, 600 mM NaCl, 250 mM imidazole, 20 % glycerol. Proteins were analyzed using 10 % SDS-PAGE.

Cell culture and transfection. HEK293 cells were maintained at 37 °C, 5 % CO_2 in DMEM supplemented with 10 % fetal bovine serum (FBS) and penicillin-streptomycin (100 U/mL).

Cells were seeded in a 6-well plates 18-24 h prior to transfection. Media was replaced with 1 ml complete DMEM per well 1 h prior to transfection. DNA was transfected into cells using Polyjet DNA transfection reagent (SignaGen Laboratories). After 24 h of incubation at 37 °C, the cells were harvested.

Co-immunoprecipitation assay. Transfected HEK293 cells were washed once using pre-chilled 1 × PBS. Washed cells were scraped into pre-chilled 1 × PBS, pooled, centrifuged at 12,000 × g for 5 min. Supernatants were disposed, and cells were lysed in 50 mM Tris-HCl, pH 7.4, 0.15 mM NaCl, 1 mM EDTA, 1 % Triton X-100, supplemented with halt protease inhibitor cocktail (Thermo Fisher). Samples were incubated on ice for 30 min, with occasional shaking, and lysates were collected by centrifugation at 12,000 × g for 10 min at 4 °C. Anti-FLAG M2 Affinity Gel was incubated with cell lysates for 45 min at 4 °C. The mixture was pelleted by centrifugation at 7,000 × g for 45 s at 4 °C, and washed 3 times with 50 mM Tris-HCl, 250 mM NaCl, pH7.4. The gels were resuspended in 2 × SDS sample buffer, heated for 5 min at 95 °C, and analyzed using 10 % SDS-PAGE.

Pulldown assays. GST-tagged NleH1 and NleH2 (10 μM) were immobilized on glutathione sepharose 4B beads (GE Healthcare) in 20 mM Tris-HCl, pH 7.9, 0.1 M NaCl, 5 mM $MgCl_2$, 1 mM EDTA, 1 mM DTT, 0.2 mM PMSF, 20 % glycerol, 0.1 % Nonidet P-40, supplemented with 0.33 U/μl of DNase I and RNase A. After overnight incubation at 4 °C, the beads were incubated with His-tagged purified IKK-β proteins (10 μM) for 1 h at 4 °C. The beads were then washed 3 times with 20 mM Tris-HCl, pH 7.9, 1 M NaCl, 1 mM EDTA, 1 mM DTT, 0.2 mM PMSF, 20 % glycerol, 0.1 % Nonidet P-40. Proteins were eluted with 10 mM reduced glutathione and analyzed using 10 % SDS-PAGE.

Mass Spectrometry and Protein Identification. For mass spectrometry analysis, 500 mg of HEK293T cells were collected and lysed in 50 mM Tris-HCl, pH 7.4, 0.15 mM NaCl, 1 mM EDTA, 1 % Triton X-100, supplemented with halt protease inhibitor cocktail (Thermo Fisher) for 30 min on ice, with occasional shaking. Cell lysates were collected by centrifugation at 12,000 × g for 10 min at 4 °C. Washed beads were incubated with cell lysates for 45 min at 4 °C. The mixture was pelleted by centrifugation at 7,000 × g for 45 s at 4 °C, and washed 3 times with 50 mM Tris-HCl, 250 mM NaCl, pH7.4. The beads were resuspended in 2 × SDS sample buffer, heated and subjected to SDS-PAGE and an aliquot used for Western blotting analysis. The gel was stained with GelCode Blue Stain Reagent (Pierce) overnight and destained with ddH_2O. The stained bands of the gels were cut for in-gel tryptic digestion and introduced into an LTQ-FT tandem mass spectrometer (ThermoFinnigan). Mass spectra were acquired in the positive ion mode.

RNA interference and transfection. siRNAs targeting Hsp90, as well as a negative control siRNA, were obtained from Santa Cruz Biotechnology. Transient transfection of 25 pmol siRNA into HEK293 cells was performed using Lipofectamine RNAiMAX (Life Technologies) according to the manufacturer's instructions.

Cell fractionation. Nuclear and cytosolic protein extracts were obtained as described previously (El Qaidi et al., 2017). HEK293 cells were transfected with NleH1-HA and after 36 h, TNF-α was added at 50 ng/ml for 30 min to promote RPS3 nuclear translocation. Cells were harvested and resuspended in the buffer, nuclear and cytosolic protein extracts were prepared using the NE-PER nuclear and cytoplasmic extraction reagents (Thermo Fisher). Data were analyzed by Western blotting for nuclear RPS3. Poly(ADP-ribose) polymerase and β-tubulin were used to normalize the protein concentrations of nuclear and cytoplasmic fractions, respectively.

Adhesion assay. The human colorectal adenocarcinoma cell-line Caco-2(ATCC HTB37) was grown at 37C under 5% CO2 in complete DMEM (Gibco) supplemented with 10% heat-inactivated fetal bovine serum (FBS), 100 U/ml penicillin-streptomycin. Cells were seeded in 24-well, and grown in DMEM (Gibco) supplemented with 10% FBS, and treated with 1 ¦ M GA for 20 h. All bacterial strains were incubated at 37 ˚C in LB. After three washes with PBS, Caco-2 cells were infected with bacteria at a multiplicity of infection (MOI) of 100. Non-adherent bacteria were removed from the cells by three washes with PBS at 3 h post-infection. Cells were scraped with 1% triton X-100 in PBS, and serial 10 fold dilutions were plated overnight at 37 ˚C onto LB agar plates. The number of bacteria adherent to epithelial cells was then determined.

Statistics. Protein abundance was quantified using Li-COR Image Studio software. RPS3 and p65 nuclear abundance was analyzed statistically using either one-way analysis of variance (ANOVA) or t-tests. p values < 0.05 were considered significant.

Results

NleH1 and NleH2 bind to IKKβ. To determine whether EHEC NleH1 binds directly to IKKβ we conducted GST pulldown assays. His-IKKβ, GST, GST-NleH1, and GST-NleH2 were purified using Nickel-nitrilotriacetic acid (Ni-NTA) agarose beads. Purified GST (negative control), GST-NleH1, and GST-NleH2 were immobilized on GST beads and incubated with His-IKKβ. IKKβ was enriched in the NleH1 and NleH2 pulldown samples, as compared to the negative control (**Figure 11a**). To determine whether NleH1 and NleH2 interact with IKKβ in mammalian cells, we performed co-immunoprecipitation experiments. After co-transfecting either NleB1-HA (as a negative control), NleH1-HA, or NleH2-HA with FLAG-IKKβ, cell lysates were immunoprecipitated with anti-FLAG M2 beads and subsequently immunoblotted. NleH1-HA and NleH2-HA, but not NleB1-HA, interacted with FLAG-IKKβ (**Figure 11b**).

Thus, NleH1 and NleH2 bind directly to IKKβ in vitro, and interact with IKKβ in mammalian cells.

To identify other proteins that are enriched with IKKβ as a function of co-expression of NleH1, we repeated the transfection experiments described above and then processed the immunoprecipitated proteins samples for mass spectrometry analysis. We identified Hsp90, Cdc37, and RPS3 in these samples.

Hsp90 is an important chaperone protein that regulates the folding, stability, and trafficking of many client proteins (Csermely, Schnaider, Soti, Prohaszka, & Nardai, 1998). Cell division cycle protein 37 (Cdc37) is one of the best-studied Hsp90 co-chaperones (Calderwood, 2015; Taipale et al., 2012). Hsp90 interacts with Cdc37 and the Hsp90-Cdc37 complex can form a stable complex with IKK, which plays a critical role in its activation and regulation (Chen, Cao, & Goeddel, 2002; Hinz et al., 2007). Due to the important association between Hsp90 and IKK, we focused on the potential interactions between Hsp90, IKKβ, and NleH1.

Figure 11 NleH1 and NleH2 bind to IKKβ.

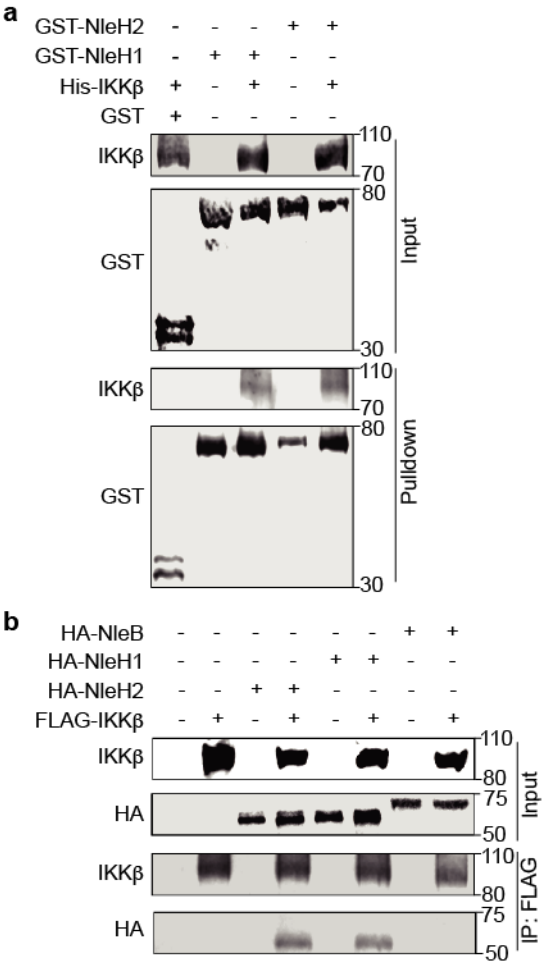

a Pulldown assay to detect binding between NleH1, NleH2, and IKKβ. His6-IKKβ was incubated with GST, GST-NleH1, and GST-NleH2 and subjected to GST pulldown assay using glutathione-sepharose beads. Protein complexes were eluted with 10 mM reduced glutathione followed by 10 % SDS-PAGE analysis. GST was used as a negative control. **b** Immunoprecipitation of NleB1-HA, NleH1-HA, and NleH2-HA with FLAG-IKKβ. HEK293 cells were transfected and cell lysates were immunoprecipitated using anti-FLAG M2 gel and immunoblotted for FLAG and HA. NleB1-HA was used as a negative control.

Hsp90 interacts with NleH1, NleH2, and IKKβ. To assess the association of Hsp90 and IKKβ in mammalian cells, we performed co-transfection and co-immunoprecipitation experiments with Hsp90-HA and FLAG-IKKβ. HEK293 cell lysates were immunoprecipitated with anti-FLAG

M2 beads and subsequently immunoblotted with anti-FLAG and anti-HA antibodies. Hsp90-HA interacted with FLAG-IKKβ (**Figure 12a**), which is consistent with a previous study showing that endogenous Hsp90 co-precipitated from HeLa cell extracts with IKKβ (Chen et al., 2002). We considered whether IKKβ might interact with both NleH1/NleH2 and Hsp90. To test this idea, we co-transfected HEK293 cells with FLAG-IKKβ, Hsp90-HA, and NleH-HA. We observed that IKKβ interacted with Hsp90, NleH1, and NleH2 (**Figure 12b**) and that Hsp90 interacted with both NleH1 and NleH2 (**Figure 12c**).

Figure 12 Interaction of NleH1, Hsp90, and IKKβ.

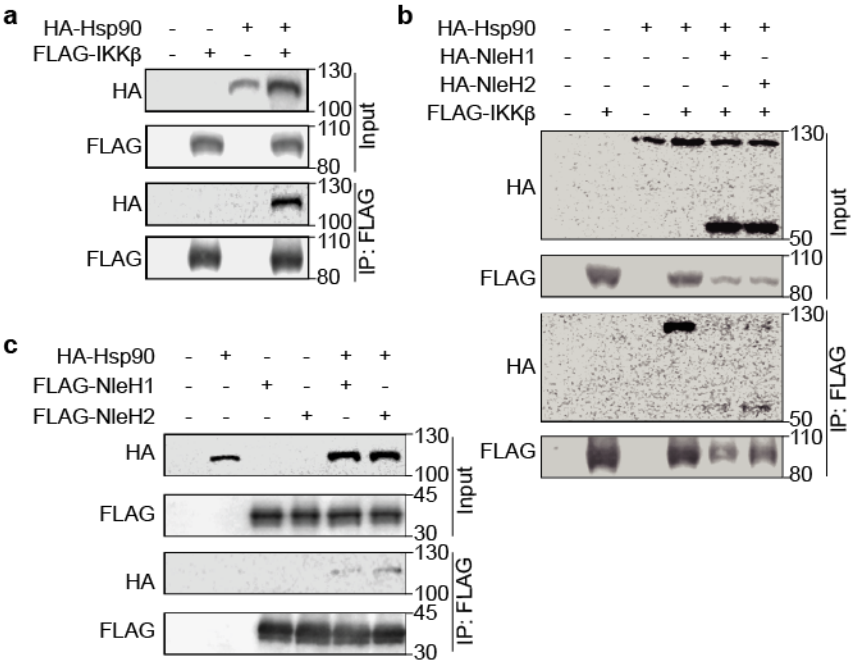

a Immunoprecipitation of Hsp90-HA with FLAG-IKKβ. HEK293 cells were transfected with FLAG-IKKβ and Hsp90-HA. Cell lysates were immunoprecipitated using anti-FLAG M2 gel and immunoblotted for FLAG and HA. **b** Immunoprecipitation of NleH1-HA/NleH2-HA and Hsp90-HA with FLAG-IKKβ. HEK293 cells were transfected with FLAG-IKKβ Hsp90-HA, NleH1-HA, and NleH2-HA. Cell lysates were immunoprecipitated using anti-FLAG M2 gel and immunoblotted for FLAG and HA. **c** Immunoprecipitation of Hsp90-HA with FLAG-NleH1 and FLAG-NleH2. HEK293 cells were

transfected with FLAG- NleH1, FLAG-NleH2, and Hsp90-HA. Cell lysates were immunoprecipitated using anti-FLAG M2 gel and immunoblotted for FLAG and HA.

Hsp90 is a cofactor of both NleH1 and IKKβ. To determine whether the interaction among Hsp90, NleH1, and IKKβ contributes to the ability of NleH1 to inhibit RPS3 nuclear translocation, we first established small interfering RNA (siRNA) knockdown conditions to reduce the steady-state levels of Hsp90 in HEK293 cells (**Figure 13a**). Hsp90 knockdown cells were transfected with either NleH1-HA or an HA epitope control plasmid. Cells were harvested after stimulation with TNF for 30 min (to induce RPS3 nuclear translocation), and then cell lysates were fractionated to separate cytosolic from nuclear proteins. RPS3 nuclear translocation induced by TNF was assessed by immunoblotting. TNF treatment induced a significant increase in RPS3 translocation to the nucleus (**Figure 13b**). NleH1-HA significantly inhibited RPS3 nuclear translocation. Knockdown of Hsp90 did not alter the ability of TNF to induce RPS3 nuclear translocation in cells (**Figure 13b**). Hsp90 knockdown also did not change the ability of NleH1-HA to inhibit RPS3 nuclear translocation with TNF stimulus (**Figure 13b**).

We then used the Hsp90 inhibitor geldanamycin (GA) to determine whether Hsp90 activity is required for RPS3 nuclear translocation. Transfecting NleH1-HA significantly inhibited RPS3 nuclear translocation, but did not affect p65 nuclear translocation (**Figure 13c**). GA inhibited the ability of TNF to induce RPS3 and p65 nuclear translocation in cells (**Figure 13c**). GA did not alter the ability of NleH1-HA to block RPS3 nuclear translocation induced by TNF (**Figure 13c**). To assess whether NleH1 is important for EHEC infection in the context of Hsp90 inhibition, we infected epithelial cells, Caco-2, with EHEC WT and EHEC nleH1 mutant, and quantified the bacterial adherence. After 3 h post-infection, a significant decrease in the amount of adhered bacteria was observed in EHEC WT infection with GA treatment, while there is no significance

between EHEC nleH1 mutant infection with and without GA treatment (**Fig. 3d**). The results indicate that Hsp90 inhibition reduces EHEC WT adherence, but when NleH1 is deleted, it does not affect the bacteria adherence ability whether Hsp90 is inhibited or not.

Figure 13 Geldanamycin (GA) inhibits RPS3 nuclear translocation.

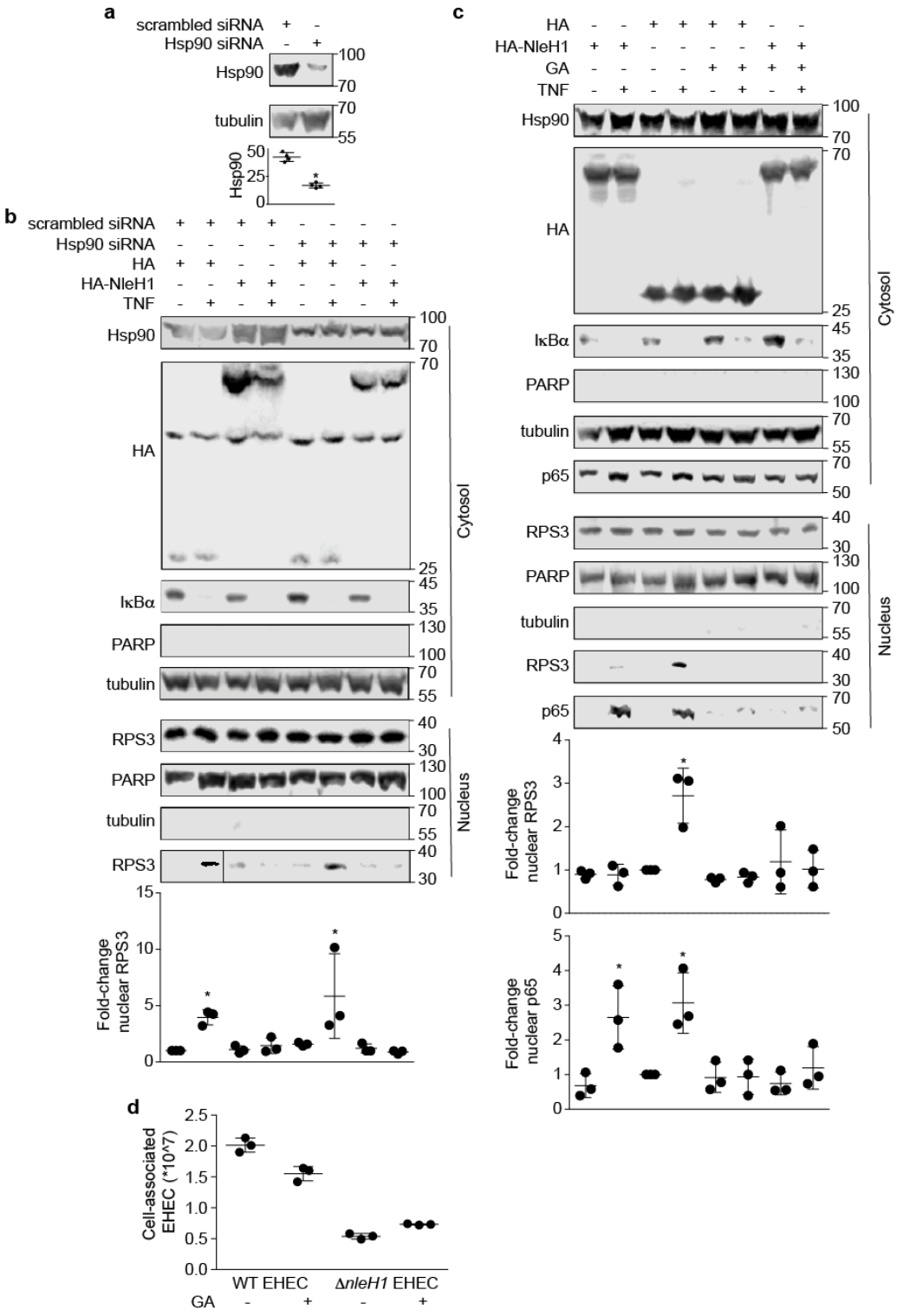

a Hsp90 knockdown with siRNAs. **b** Knockdown of Hsp90 does not alter RPS3 nuclear translocation. HEK293 cells were transfected with a pool of 4 Hsp90 siRNAs or with a nonspecific siRNA. After 24 h, cells were transfected with NleH1-HA or an HA epitope control. After 24 additional h, cells were

stimulated with TNF (50 ng/ml, 30') and then lysed, separated into nuclear and cytosolic extracts, and used in immunoblotting experiments. **c** GA inhibits RPS3 nuclear translocation. HEK293 cells were transfected with NleH1-HA or an HA epitope control. Cells were treated with 1 μM GA 5 h after transfection. After 20 h, cells were stimulated with TNF (50 ng/ml, 30') and then lysed, separated into nuclear and cytosolic extracts, and used in immunoblotting experiments. **d** Hsp90 inhibition reduces adherence of EHEC WT but not EHEC nleH1 mutant. Caco-2 cells were treated with 1 μM GA for 20h, and then were infected with bacteria at a multiplicity of infection (MOI) of 100. The number of bacteria adherent to epithelial cells was determined at 3 h post-infection by plating on LB agar plates. Results are expressed as CFU/ml.

Discussion

Hsp90 is a highly conserved and abundant heat shock protein (HSP) involved in a myriad of cellular processes. The abundance of Hsp90 accounts for ~1-3% of the total cytosolic proteins (Mazaira et al., 2018). It is required to facilitate protein folding, stabilize client proteins, and protect proteins from ubiquitin-dependent proteasomal degradation (Pearl, 2016). Geldanamycin binds to the ATP-binding site of Hsp90 to abolish the interaction between Hsp90 and its client proteins (Goetz, Toft, Ames, & Erlichman, 2003). GA abolishes TNF-induced IKKβ activation and IκBα degradation, thus blocking NF-κB activation (Lewis et al., 2000). GA treatment also causes proteasomal degradation of IKKβ , leading to altered migration of the IKK complex (Hinz et al., 2007).

NleH1 and NleH2, though share 84% amino acid sequence identity, show different ability to regulate NF-κB pathway. They both bind to RPS3. NleH1, but not NleH2, inhibits phosphorylation of RPS3 by IKKβ without affecting the kinetics of IκBα (Pham et al., 2012). However, when IKKβ is overexpressed, both NleHs were shown to attenuate NF-κB activation (Royan et al., 2010). Though our result showed that both NleH1 and NleH2 interacted with

Hsp90, only NleH1 showed inhibition of RPS3 nuclear translocation. Thus, we only focused on NleH1. Here we present evidence that Hsp90 also interacts with the bacterial effector NleH1. NleH1 only restricts a subset of the IKKβ substrates, most importantly RPS3 (F. Y. Wan et al., 2011). Hsp90 binds directly to RPS3 and the interaction of Hsp90-RPS3 protects RPS3 from proteasome-dependent degradation (T. S. Kim et al., 2006). Here we further determined that GA inhibited both TNF-mediated p65 nuclear translocation and RPS3 nuclear translocation, indicating that Hsp90 is an important cofactor in regulating host inflammatory responses to bacterial virulence proteins. We also identified a direct interaction between NleH1 and IKKβ and identified Hsp90 as a cofactor. Besides, absence of NleH1 abolished the reduction in EHEC adherence in the context of Hsp90 inhibition, which suggests interaction between nleH1 and Hsp90 is crucial for bacterial virulence.

Given that IKKβ is crucial for regulating NF-κB signaling, an emerging role of IKKβ in tumorigenesis has been supported by in increasing number of studies (Evaristo et al., 2016; Greten et al., 2004). Deletion of IKKβ, such as enterocytes, epithelial cells, and myeloid cells, leads to tumor cells apoptosis or directly decreases tumor growth (Greten et al., 2004). Induced constitutive active IKKβ in T cells enhances control of tumor growth (Evaristo et al., 2016). Hsp90 activity is shown to be required for IKK biosynthesis and activation (Broemer, Krappmann, & Scheidereit, 2004), and Cdc37-Hsp90 complex is important for stabilizing the IKK complex (Chen et al., 2002). Hsp90, as a cofactor between NleH1 and IKKβ and a binding partner of RPS3, the interaction between NleH1 and Hsp90 may be involved in the interference with IKKβ in a transient manner or strengthen the inhibition of IKKβ collaboratively. Because IKKβ has many vital roles in normal cellular function, developing multiple mechanisms that selectively target the IKKβ signaling could be a very exciting prospect.

Chapter 4 - Structural basis for arginine glycosylation of host substrates by bacterial effector proteins

I contributed to Figure 37g and 37h in Chapter 4. A modified version of Chapter 4 was published in Nature Communications (J. B. Park et al., 2018).

Park, J. B., Kim, Y. H., Yoo, Y., Kim, J., Jun, S. H., Cho, J. W., El Qaidi, S., Walpole, S., Monaco, S., Garcia-Garcia, A. A., Wu, M., Hays, M. P., Hurtado-Guerrero, R., Angulo, J., Hardwidge, P. R., Shin, J. S., Cho, H. S. (2018). Structural basis for arginine glycosylation of host substrates by bacterial effector proteins. Nat Commun, 9(1), 4283. doi:10.1038/s41467-018-06680-6

Introduction

Protein glycosylation is a post-translational modification implicated in a wide range of cellular/biological processes, including cell development, signaling cascades, and tumorigenesis (Haltiwanger & Lowe, 2004). Glycosyltransferases (GTs) catalyze the transfer of a sugar moiety to acceptor substrates and are classified according to their folding as GT-A, GT-B, GT-C (Gloster, 2014) or GT-D (H. Zhang et al., 2014). Most GT-A fold GTs are single domain proteins that contain a Rossmann-like fold though exceptions to this rule exist (Lairson, Henrissat, Davies, & Withers, 2008). GT-A GTs also have a DxD (Asp-x-Asp) motif, which is required to coordinate the divalent cation (cofactor). The donor substrates include sugar-linked nucleotide diphosphates that also interact with the cofactor. Within proteins as acceptor substrates for GTs, the most prevalent glycosylated amino acids are serine and threonine (O-linked glycosylation), and asparagine (N-linked glycosylation).

Another type of glycosylation was recently reported from studies of bacterial virulence proteins (X. F. Gao et al., 2013; S. Li et al., 2013; Pearson et al., 2013). Enteropathogenic *Escherichia coli*(EPEC) and enterohemorrhagic *Escherichia coli* (EHEC) express numerous effector proteins (Kaper, Nataro, & Mobley, 2004) which are injected into host cells via a type III secretion system (T3SS) to disrupt host cell functions (Hauser, 2009). The NF-κB transcription factor plays a central role in inducing immune responses against microbial pathogens. Some bacterial effectors suppress NF-κB itself or NF-κB-associated factors (Grishin et al., 2014; Han, Zhong, & Zhang, 2011; W. Li et al., 2014; H. H. Park et al., 2007; Pearson, Zhang, Newton, & Hartland, 2015). The T3SS and many effectors are encoded in the locus of enterocyte effacement (LEE) (Elliott et al., 1998). Effectors encoded outside this region are designed as non-LEE effectors (Nles) (Garmendia et al., 2005). The non-LEE encoded effector protein B (NleB) has GT activity and inhibits NF-κB activation by transferring *N*-acetyl glucosamine (GlcNAc) to host death domain-containing proteins and to glyceraldehyde 3-phosphate dehydrogenase (GAPDH) (X. F. Gao et al., 2013; Pearson et al., 2013; Suresh & Mosser, 2013). The glycosylation target is an arginine residue, which was unexpected because the guanidine group of arginine is nucleophilically poor at physiological pH.

NleB target proteins include the tumor necrosis factor receptor type 1-associated death domain (TRADD), Fas-associated death domain (FADD), receptor-interacting serine/threonine-protein kinase 1 death domain (RIP1-DD), tumor necrosis factor receptor death domain (TNFR-DD), and GAPDH (X. F. Gao et al., 2013; S. Li et al., 2013; Pearson et al., 2013). Most of these proteins participate in regulating the tumor necrosis factor-alpha (TNF-α) mediated apoptosis pathway via death domain mediated homo- or hetero-oligomerization (H. H. Park et al., 2007). Previous studies have reported that glycosylation of FADD Arg117 and TRADD Arg235

disrupts apoptosis and decreases NF-κB signaling in host cells (S. Li et al., 2013; Pearson et al., 2013). Glycosylation of GAPDH Arg197 and Arg200 inhibits ubiquitination of the TNF receptor-associated factors (TRAF) 2 and 3, leading to reduced NF-κB signaling and type I interferon production (El Qaidi et al., 2017; X. Gao et al., 2016).

The T3SS effectors SseK1 and SseK2 from *Salmonella typhimurium SL1344* are NleB orthologs that behave as NleB1-like GTs, although they differ in protein substrate specificity (El Qaidi et al., 2017; S. Li et al., 2013). The third member, SseK3, is inactive against FADD and GAPDH but active against TRADD (El Qaidi et al., 2017; Esposito et al., 2018). Recently, the structure of SseK3 was determined, revealing a GT-A fold (Esposito et al., 2018). However, the specific enzyme mechanism and the identification of the catalytic base remain unclear. There are also discrepancies regarding whether these enzymes are retaining or inverting GTs because this has not been experimentally probed (Esposito et al., 2018; Pan et al., 2014). In addition, details regarding substrate specificity based on structural evidence are also limited due to the lack of ternary complexes. Here, by using a combination of X-ray crystallography, STD-NMR, enzyme kinetics, molecular dynamics simulations, and in vivo experiments, we show that these enzymes are GT-A fold retaining GTs that most likely follow an S_Ni mechanism. We demonstrate that the HLH domain is relevant to protein substrate recognition and the HEN residues are critical for catalysis. We also determine differences within the SseK/NleB family on recognition of the sugar nucleotide and peptide substrates and find common features for the three peptides such as the recognition of the conserved Trp and Arg residues (WR-motif). Finally, molecular dynamics simulations reveal that the presence of GlcNAc in the donor site induces conformational changes on the side chains of the peptide substrate so that the final arginine acceptor becomes properly oriented for a front face attack to the anomeric C_1 carbon of the sugar.

Materials and methods

Protein purification. SseK (21-336) gene was generated and amplified by PCR from synthesized DNA and cloned into a modified pET28a (Novagen) in which the thrombin cleavage site was replaced with a tobacco tech virus (TEV) protease cleavage site. SseK2 (34-348) and NleB2 (1-316) gene were generated and amplified by PCR from *Salmonella typhimurium* (strain *SL1344*), *Escherichia coli* O145:H28 (strain *RM12581*) respectively and cloned into the pVFT3S vector (Korean patent 10-0690230), which has 6xHis-thioredoxin (Trx) and TEV protease cleavage site **(Table 5, Table 6).** PCR-based site-directed mutagenesis was employed to generate various point mutations. Complete amino acid sequences are shown in **Table 7**.

Table 5 Oligonulceotides used in Chapter 4.

Description	Sequence
NleB1 XhoI F	CGCGCTCGAGATGT2ATCT2CAT2A3TGTC2T2CA2TC
NleB1 KpnI F	CGCG3TAC4ATGA2CTGCAG2TATACATACTG2TAT2
NleB1 MseI F	C2AC2ATGTAC3ATACGATGT2C2AGAT2ACGCTATGT2ATCT2CAT2A3TG
NleB1 BamHI R	CTCATCA2TGTATCT2ATCATGTCTG2ATC4T2AC2ATGA2CTGCAG2TATAC
NleB1 H242A F	CTC2TGATG2TATCGCTGTG2CTGTAGAT2GTA2TG
NleB1 H242A R	CAT2ACA2TCTACAGC2ACAGCGATAC2ATCAG2AG
NleB1 E253A F	GATGAGATA5GTCT2GCA3TG2TGCGATAGT2G
NleB1 E253A R	CA2CTATCGCAC2AT3GCA2GACT5ATCTCATC
NleB1 N254A F	GAGATA5GTCT2GA2GCTG2TGCGATAGT2G
NleB1 N254A R	CA2CTATCGCAC2AGCT2CA2GACT5ATCTC
NleB1 H242A, E253A, N254A F	GATG2TATCGCTGTG2CTGTAGAT2GTA2TGATGAGATA5GTCT2GCAG CTG2TGCGATAG
NleB1 H242A, E253A, N254A R	CTATCGCAC2AGCTGCA2GACT5ATCTCATCAT2ACA2TCTACAGC2ACAG CGATAC2ATC
NleB2 H239A F	GCTC2TGATG2A2T3CA2TG2CTGTG2ATCGTCGTA2TG
NleB2 H239A R	CAT2ACGACGATC2ACAGC2AT2GA3T2C2ATCAG2AGC
NleB2 E250A F	GTA2TGATAGTGTA3TAT2GCTA2TAGTGCA2TA2T2GT2A2C
NleB2 E250A R	GT2A2CA2T2AT2GCACTAT2AGCA2TAT3ACACTATCAT2AC
NleB2 N251A F	GTA2TGATAGTGTA3TAT2GA2GCTAGTGCA2TA2T2GT2A2C
NleB2 N251A R	GT2A2CA2T2AT2GCACTAGCT2CA2TAT3ACACTATCAT2AC
NleB2 H239A, E250A, N251A F	GATG2A2T3CA2TG2CTGTG2ATCGTCGTA2TGATAGTGTA3TAT2GCTGCTA GTGCA2TA2T2G
NleB2 H239A, E250A, N251A R	CA2T2AT2GCACTAGCAGCA2TAT3ACACTATCAT2ACGACGATC2ACAGC2

	AT2GA3T2C2ATC
SseK1 XhoI F	CGCGCTCGAGATGATC3AC2AT2A3TAGATATGT2C2
SseK1 KpnI F	CGCG3TAC3TGCACATGC2TCGC3ATGA2CT3GCG
SseK1 MseI F	C2AC2ATGTAC3ATACGATGT2C2AGAT2ACGCTATGATC3AC2AT2A3TAG
SseK1 BamHI R	CTCATCA2TGTATCT2ATCATGTCTG2ATC4T2ACTGCACATGC2TCGC3ATG
SseK1 H244A F	C2G2ATG2A2TCGCTGT2GCTGTAGA3G2ATAGATG2C2
SseK1 H244A R	G2C2ATCTATC2T3CTACAGCA2CAGCGAT2C2ATC2G2
SseK1 E255A F	GATAGATG2C2GTGCT2CTATG2CTA2CG3ATA2TAGCTG
SseK1 E255A R	CAGCTAT2ATC3GT2AGC2ATAGA2GCACG2C2ATCTATC
SseK1 N265A F	GATG2C2GTGCT2CTATG2A2GC2G3ATA2TAGCTGT2GATCG
SseK1 N256A R	CGATCA2CAGCTAT2ATC3G2CT2C2ATAGA2GCACG2C2ATC
SseK1 H244A, E255A, N256A F	G2A2TCGCTGT2GCTGTAGA3G2ATAGATG2C2GTGCT2CTATG2CTGC2 G3ATA2TAGCTGT2G
SseK1 H244A, E255A, N256A R	CA2CAGCTAT2ATC3G2CAGC2ATAGA2GCACG2C2ATCTATC2T3CTAC AGCA2CAGCGAT2C2
SseK2 XhoI F	CGCGCTCGAGATG2CACGT4A2TGC2GCT4AC
SseK2 KpnI R	CGCG3TAC4TC2A2GA2CTG2CAGT2A3CTGCT2G
SseK2 H260A F	C2TGATG2TATCGCTATCGCTGTA2GTCGTA3GATA2TC
SseK2 H260A R	GAT2ATCT3ACGACT2ACAGCGATAGCGATAC2ATCAG2
SseK2 E271A F	GATA2TCATGT2AGC2T2GCA3TG3AT2AT2GCTG
SseK2 E271A R	CAGCA2TA2TC3AT3GCA2G2CTA2CATGAT2ATC
SseK2 N272A F	GATA2TCATGT2AGC2T2GA2GCTG3AT2AT2GCTGT2A2C
SseK2 N272A R	GT2A2CAGCA2TA2TC3AGCT2CA2G2CTA2CATGAT2ATC
SseK2 H260A, E271A, N272A F	G2TATCGCTATCGCTGTA2GTCGTA3GATA2TCATGT2AGC2T2GCAGCT G3AT2AT2GCTG
SseK2 H260A, E271A, N272A R	CAGCA2TA2TC3AGCTGCA2G2CTA2CATGAT2ATCT3ACGACT2ACAGC GATAGCGATAC2
SseK2 D204A F	GACA3G2TCACT2ATG2T3GC2T2CTACAGA3TCT4C
SseK2 D204A R	GA4GAT3CTGTAGA2G2CA3C2ATA2GTGAC2T3GTC
SseK2 D239A F	G2TG3TGCATATATCT2GCTGCAGATATGT2ACT2ACTG
SseK2 D239A R	CAGTA2GTA2CATATCTGCAGCA2GATATATGCAC3AC2
TRADD BamHI F	TCGCG2ATC2ATG2CAGCTG3CA4TG3C
TRADD HindIII R	C2GCA2GCT2G2C2AG2C2GC2AT2G3ATC

Each sub-cloned plasmid was transformed into *E. coli* BL21(DE3) (Novagen) and grown in high salt Luria-Broth medium. When the $O.D_{600}$ reached 0.6 ~ 0.8, the temperature was decreased to 17 °C and the culture was induced with 0.3 mM IPTG (isopropyl 1-thio-ß-D-galactopyranoside). After 16 h incubation, each protein was purified using nickel-affinity chromatography. Cell was

lysed using lysis buffer (20 mM Tris-NaCl pH 7.5, 300 mM NaCl, 30 mM imidazole, 10% glycerol) and the proteins were eluted using an elution buffer of 300 mM imidazole in lysis buffer. Thereafter, the TEV recognition site was cleaved using TEV protease. After desalting to 20 mM Tris-HCl (pH7.5), 50 mM NaCl, each protein was loaded into an anion-exchange chromatography column (Hitrap-Q, GE healthcare) and then gel-filtration chromatography (Superdex-200, GE healthcare) was carried out in SEC buffer (25 mM HEPES-NaOH 300 mM NaCl).

Selenomethionine substituted NleB2 was prepared using *E. coli* B834 (Novagen) and cultured in M9 minimal media supplemented with glucose, amino acids, and L-selenomethionine (Calbiochem). Expression condition and purification method were the same as for native NleB2. NleB/SseK genes were also cloned into pET42a and then subjected to site-directed mutagenesis. GAPDH and TRADD were cloned into pET28a. FADD was cloned into pET15b. Proteins were purified after their overexpression in *E. coli* BL21(DE3) using Ni-NTA agarose. NleB/SseK genes were sub-cloned into pCMV tag 2a, pCMV Myc or (HA tag vector) for mammalian expression. TRADD gene was cloned into pCMV tag 2a or pEGFP N1.

Table 6 Plasmids used in Chapter 4**.**

Description(Plasmids)	Source
GST-NleB1	(El Qaidi et al., 2017)
GST-NleB2	(El Qaidi et al., 2017)
GST-SseK1	(El Qaidi et al., 2017)
GST-SseK2	(El Qaidi et al., 2017)
GST-NleB1 H242A	This study
GST-NleB1 E253A	This study
GST-NleB1 N254A	This study
GST-NleB1 H242A E253A N254A	This study
GST-NleB2 H239A	This study
GST-NleB2 E250A	This study
GST-NleB2 N251A	This study
GST-NleB2 H239A E250A N251A	This study
GST-SseK1 H244A	This study
GST-SseK1 E255A	This study
GST-SseK1 N256A	This study
GST-SseK1 H244A E255A N256A	This study
GST-SseK2 H260A	This study

GST-SseK2 E271A	This study
GST-SseK2 N272A	This study
GST-SseK2 H260A E271A N272A	This study
HA-NleB1	This study
HA-NleB1 H242A	This study
HA-NleB1 E253A	This study
HA-NleB1 N254A	This study
HA-NleB1 H242A E253A N254A	This study
HA-SseK1	This study
HA-SseK1 H244A	This study
HA-SseK1 E255A	This study
HA-SseK1 N256A	This study
HA-SseK1 H244A E255A N256A	This study
FLAG-NleB1	This study
FLAG-NleB1 H242A	This study
FLAG-NleB1 E253A	This study
FLAG-NleB1 N254A	This study
FLAG-NleB1 H244A E255A N256A	This study
FLAG-NleB2	This study
FLAG-NleB2 H239A	This study
FLAG-NleB2 E250A	This study
FLAG-NleB2 N251A	This study
FLAG-NleB2 H239A E250A N251A	This study
FLAG-SseK1	This study
FLAG-SseK1 H244A	This study
FLAG-SseK1 E255A	This study
FLAG-SseK1 N256A	This study
FLAG-Ssek1 H244A E255A N256A	This study
FLAG-SseK2	This study
FLAG-SseK2 H260A	This study
FLAG-SseK2 E271A	This study
FLAG-SseK2 N272A	This study
FLAG-SseK2 H260A E271A N272A	This study
FLAG-TRADD	This study
FLAG-TRADD DD	This study
FLAG-GAPDH	This study
His-TRADD	This study
His-GAPDH	(El Qaidi et al., 2017)
His-FADD	(El Qaidi et al., 2017)
GFP-TRADD	This study
GFP-FADD	This study
Myc-SseK1	This study
Myc-SseK1 AxA	This study
Myc-SseK1 H244A	This study
Myc-SseK1 E255A	This study
Myc-SseK1 N256A	This study
His-SseK1	This study
His-SseK1 21-336	This study
His-SseK1 H244A	This study
His-SseK1 E255A	This study
His-SseK1 N256A	This study
His-SseK1 W331A	This study
His-SseK1 F187A	This study
His-SseK1 AxA	This study
His-TRX-SseK2	This study
His-TRX-SseK2 34-348	This study

His-TRX-SseK2 H260A	This study
His-TRX-SseK2 E271A	This study
His-TRX-SseK2 N272A	This study
His-TRX-SseK2 F203A	This study
His-TRX-SseK2 W347A	This study
His-TRX-SseK2 AxA	This study
His-TRX-NleB2 (1-316)	This study

Table 7 Complete amino acid sequences used in Chapter 4.

SseK1 (21-336, C39S, C210S)	MGSSHHHHHHSSGLVPRGSENLYFQSHMASMTGGQQMGRGS VTNRDIQFTSFNGKDYPL**S**FLDEKTPLLFQWFERNPARFGKNDI PIINTEKNPYLNNIIKAATIEKERLIGIFVDGDFFPGQKDAFSKLE YDYENIKVIYRNDIDFSMYDKKLSEIYMENISKQESMPEEKRD CHLLQLLKKELSDIQEGNDSLIKSYLLDKGHGWFDFYRNMAM LKAGQLFLEADKVG**S**YDLSTNSGCIYLDADMIITEKLGGIYIPD GIAVHVERIDGRASMENGIIAVDRNNHPALLAGLEIMHTKFDA DPYSDGVCNGIRKHFNYSLNEDYNSFCDFIEFKHDNIIMNTSQF TQSSWARHVQ*
SseK2 (34-348)	MGSSHHHHHHSSGLVPRGSHMSDKIIHLTDDSFDTDVLKADG AILVDFWAEWCGPCKMIAPILDEIADEYQGKLTVAKLNIDQNP GTAPKYGIRGIPTLLLFKNGEVAATKVGALSKGQLKEFLDANL ASGTTENLYFQGSTLSPPSSGHVSFAGIDYPLLPLNHQTPLVFQ WFERNPDRFGQNEIPIINTQKNPYLNNIINAAIIEKERIIGIFVDG DFSKGQRKALGKLEQNYRNIKVIYNSDLNYSMYDKKLTTIYL ENITKLEAQSASERDEVLLNGVKKSLEDVLKNNPEETLISSHN KDKGHLWFDFYRNLFLLKGSDAFLEAGKPGCHHLQPGGGCIY LDADMLLTDKLGTLYLPDGIAIHVSRKDNHVSLENGIIAVNRS EHPALIKGLEIMHSKPYGDPYNDWLSKGLRHYFDGSHIQDYD AFCDFIEFKHENIIMNTSSLTASSWR*
NleB2 (1-316, C21S, C199S)	MGSSHHHHHHSSGLVPRGSHMSDKIIHLTDDSFDTDVLKADG AILVDFWAEWCGPCKMIAPILDEIADEYQGKLTVAKLNIDQNP GTAPKYGIRGIPTLLLFKNGEVAATKVGALSKGQLKEFLDANL ASGTTENLYFQGSMLSPIRTTFHNSVNIVQSSP**S**QTVSFAGKEY ELKVIDEKTPILFQWFEPNPERYKKDEVPIVNTKQHPYLDNVT NAARIESDRMIGIFVDGDFSVNQKTAFSKLERDFENVMIIYRED VDFSMYDRKLSDIYHDIICEQRLRTEDKRDEYLLNLLEKELREI SKAQDSLISMYAKKRNHAWFDFFRNLALLKAGEIFR**S**TYNTK NHGISFGEGCIYLDMDMILTGKLGTIYAPDGISMHVDRRNDSV NIENSAIIVNRSNHPALLEGLSFMHSKVDAHPYYDGLGKGVKK YFNFTPLHNYNHFCDFIEFNHPNIIM*

Underline means vector-containing sequence and bold means point mutation site.

Crystallization and data collection. Purified SseK1 and SseK2 were concentrated to 25 mg/mL and co-crystallized with 5 mM UDP and 5 mM $MnCl_2$. Initial crystallization screening was conducted by using Mosquito robot (TTP Labtech.) and single, appropriate size of crystals appeared at 0.1 M Bis-Tris propane-HCl (pH 7.0), 1.0 M ammonium citrate tribasic and 0.1 M Bis-Tris (pH6.5), 26% (w/v) PEG3350, respectively. SseK2 apo crystals appeared 0.1 M

HEPES-NaOH (pH 7.5), 0.1 M sodium acetate, 24% (w/v) PEG4000 and for revealing UDP-GlcNAc bound SseK2 structure, 5 mM $MnCl_2$, 5 mM UDP-GlcNAc were added into SseK2 apo crystal drop. 13 mg/mL of purified NleB2 formed crystals at 0.8 M $LiCl_2$, 0.1 M Tris-HCl (pH8.5), 8% (w/v) PEG3350. The Se-Met derivative of NleB2 crystallized under the same conditions. 20 % ethylene glycol was added as a cryo-protectant to each crystal solution and flash frozen in liquid nitrogen.

All of the crystal diffraction experiments were carried out at Photon factory (KEK, Tsukuba, Japan). UDP or UDP-GlcNAc bound SseK2 and UDP bound SseK1 were diffracted at BL-5A, BL-1A beamline, respectively. Native NleB2 and Se-Met derivative NleB2 crystal was diffracted at BL-17A.

Structure determination and refinement. Diffraction data sets were processed and scaled with the programs imosfilm (Battye, Kontogiannis, Johnson, Powell, & Leslie, 2011) and Aimless from the CCP4 program suite. The phasing information was solved by SAD method from Se-Met derivative NleB2 crystal using AutoSol program and the other proteins were solved by molecular replacement using NleB2 structure. MOLREP, REFMAC5, and COOT were used for molecular replacement, structure refinement, and further modeling, respectively. All figures were prepared using PYMOL.

Peptide assignment and STD NMR. All experiments were performed at 288 K on a Bruker Avance III 800 MHz spectrometer equipped with a 5-mm TXI 800 MHz H-C/N-D-05 Z BTO probe. $FADD_{110-118}$ and $GAPDH_{195-203}$ (Genscript) samples were prepared at 1 mM in 90% H_2O/ 10% D_2O and assigned using standard COSY (cosydfesgpph), TOCSY (mlevphpr), and ^{1}H-^{13}C HSQC (hsqctgpsp) experiments. Apo-enzyme samples were prepared with 1 mM peptide and 25 μM enzyme in either 25 mM Tris-d_{11} (SseK1) or 10 mM PBS (SseK2); both at pH 7.4 in D_2O.

Holoenzyme samples were prepared in the same way, with the addition of 25 μM $MnSO_4$ and 25 μM UDP. The residual water signal was used as a reference for chemical shifts. STD NMR experiments were performed using a train of 50 ms Gaussian pulses (0.4 mW, B_1 field strength 78 Hz) applied on the f2 channel at either 0 ppm (on-resonance) or 40 ppm (off resonance). A spoil sequence (2 trim pulses of 2.5 and 5 ms followed by a 40 % z-gradient applied for 3 ms at the beginning of the experiment) was used to destroy unwanted x, y-magnetization from previous scan and a spinlock (1.55 W, 40 ms) was used to suppress protein signals (stddiff.3). The saturation time (d20) was set to 2 s and the recycle delay (d1) was set to 5 s.

Configuration of GlcNAc in the glycosylated peptide. Samples for peptide glycosylation were prepared by adding either 7.5 mM $FADD_{110-118}$ or 7.7 mM $GAPDH_{187-203}$ to 50 mM UDP-GlcNAc, 40 μM SseK1, and 2 mM $MnCl_2$ in 25 mM Tris pH 7.5, allowing the reaction to proceed for 24 h at 37 °C. The resulting glycopeptide was purified from the enzyme by using an Amicon® Ultra 10 K device. NMR experiments for the $GAPDH_{187-203}$ sample were then performed at 298 K, and consisted of a decoupled ^{1}H-^{13}C HSQC (hsqcetgpsi), and TOCSY with water suppression (mlevgpph19) at 800 MHz, and a Perfect-CLIP-HSQC (Castanar, Sistare, Virgili, Williamson, & Parella, 2015) at 500 MHz (with a digital resolution of 1.6 Hz, to determine the $^{1}J_{C,H}$ coupling of the anomeric carbon of the transferred GlcNAc residue). The HSQC recycle delay was 1.5 s. For the TOCSY, the recycle delay was 2 s and the mixing time was 80 ms. For the $FADD_{110-118}$ sample, a decoupled ^{1}H-^{13}C HSQC was recorded as above, in a Bruker Avance I 500 MHz spectrometer, equipped with a triple resonance indirect detect TXI probe with Z-gradients.

Molecular docking calculations for guanidine-SseK2. UDP-bound SseK2 structure and guanidine was loaded to Discovery Studio 4.0 and the possible binding site was set

(Radius = 10 Å, XYZ = 21.197,−9.134, 12.013). The algorithm was taken from the CHARMm protocol and the best score was selected (-CDOCKER ENERGY = 18.192, -CDOCKER INTERACTION ENERGY = 18.097)

Molecular docking calculations for FADD-SseK2. UDP-bound Crystal structures of SseK1, SseK2, and FADD (PDB 3EZQ) were imported into Schrödinger Maestro and prepared with the Protein Preparation Wizard (Sastry, Adzhigirey, Day, Annabhimoju, & Sherman, 2013). All buffer atoms and non-bridging waters were removed. Protons were then added to the model, using PROPKA to predict the protonation state of polar sidechains at pH 7 (Olsson, Sondergaard, Rostkowski, & Jensen, 2011). The hydrogen-bonding network was automatically optimized by sampling asparagine, glutamine, and histidine rotamers. The model was then minimized using OPLS3 (Harder et al., 2016) force field and a heavy atom convergence threshold of 0.3 Å.

A model of the $FADD_{110-118}$ peptide was created by truncation of the FADD crystal structure. Conformers were generated in MacroModel using torsional sampling with the OPLS3 force field, constraining all backbone atoms. Redundant conformers were eliminated using an RMSD cutoff of 0.5 Å. Any conformer with an energy 5 kcal mol^{-1} greater than the lowest energy structure was also eliminated. Resulting conformers were then minimized using the conjugate gradient method, converging on a threshold of 0.05 kcal mol^{-1}. Docking of $FADD_{110-118}$ to SseK2 was then performed using Glide (Friesner et al., 2004; Halgren et al., 2004). A cubic grid, suitable for peptide docking, was generated. It was centered on UDP-GlcNAc, with an outer box length of 45 Å and an inner box length of 40 Å. To account for flexibility, van der Waals potentials of all receptor and ligand atoms were scaled by 0.5. All ligand conformers were docked to the receptor using rigid sampling with the SP algorithm. The resulting complexes were then clustered by heavy atom RMSD to eliminate redundant poses, keeping the structure closest

to the cluster centroid from each cluster. All sidechains within 5 Å of the ligand were then optimized before minimizing using Prime (Jacobson et al., 2004). A second round of docking was performed, as described above, on the new receptor structures. The resulting complexes were clustered by heavy atom RMSD, and the lowest energy representative structure was chosen for analysis.

A model of SseK2 in complex with full length FADD was generated by aligning the backbone atoms of residues 110-118 in the full-length structure to the backbone of the docked $FADD_{110-118}$ structure. Prime optimization and minimization within 5 Å of the contact surface was used to eliminate an atomic overlap.

Molecular dynamics. UDP charges for use with UDP-GlcNAc were derived using the RESP fitting method implemented on the RED server (Vanquelef et al., 2011). The UDP fragment was generated by replacing the GlcNAc with a methyl group. In accordance with GLYCAM (Kirschner et al., 2008), the HF/6-31G* level of theory was used with a weight factor of 0.01 and all aliphatic protons were constrained to a charge of 0. The total charge of the UDP fragment was set to −2. The charge of the methyl group was set to 0.194 before removing to give a final fragment with net charge −2.194, in keeping with the modularity of GLYCAM.

Molecular dynamics simulations of SseK1, SseK2, and the SseK2: FADD complex were performed using the Amber PMEMD software. Protein atoms were parameterized using the Amber ff11SB force field and the Mn^{2+} ion was modeled using 12-6-4 LJ-type parameters (Amber ions234lm_1264_tip3p). UDP-GlcNAc was parameterized with GLYCAM 06j and GAFF. Each system was solvated in a truncated octahedral box of TIP3P water, with at least 10 Å between the solute and the edge of the box, before neutralizing with Na^+ ions. The system was minimized using the conjugate gradient algorithm, converging on a threshold of

10^{-4} kcal mol^{-1} A^{-1}, first with 20 kcal mol^{-1} A^{-2} restraints on solute atoms, before repeating with no restraints. The system was slowly heated to 310 K over 500 ps (NVT), before equilibrating the pressure to 1 atm (NPT) over a further 500 ps. In both cases with 20 kcal mol^{-1} A^{-2} restraints were used on solute atoms. These restraints were then slowly released over 800 ps before performing Gaussian accelerated molecular dynamics (GaMD) simulations (800 ns SseK1/SseK2, 500 ns SseK2: FADD complex), as implemented in AMBER, using a boost potential on both the dihedral and total potential energies. Here, the simulation was split into 4 distinct stages. First, conventional dynamics were run for 2 ns to automatically calculate an initial boost potential. The calculated boost potential was then applied and fixed for 400 ps before allowing it to adapt for a further 5.6 ns. The resulting boost potential was then fixed before performing production dynamics for 800 ns (SseK1/SseK2) or 500 ns (SseK2: FADD complex), saving coordinates every 100 ps. In all cases, the SHAKE algorithm was used to restrain all bonds involving hydrogen, allowing for a time step of 2 fs. A Langevin thermostat was used with a collision frequency of 5 ps^{-1} and the barostat used an isotropic Berendsen algorithm with a relaxation time of 1 ps. In all cases, periodic boundary conditions were used, using the particle mesh Ewald to calculate electrostatics.

Cell culture. Human embryonic kidney (HEK) 293T (ATCC, ATCC® CRL-3216™) and A549 NF-κB luciferase cells (Panomics, RC0002) were cultured in DMEM supplemented with 10% fetal bovine serum (FBS, Cellgro), 100 U/ml penicillin, 100 μg/ml streptomycin, and 2 mM L-glutamine at 37 °C in 5% CO_2.

Western blot analysis and immunoprecipitation. HEK293T cells were transfected with various combinations of plasmids using Lipofectamine 2000 (Invitrogen) as specified by the manufacturer. Cells were washed with phosphate-buffered saline (PBS) and lysed in 1 × RIPA

buffer (GenDEPOT, Barker, TX, USA) containing 150 mM NaCl, 1% Triton X-100, 1% deoxycholic acid sodium salt, 0.1 % sodium dodecyl sulfate (SDS), 50 mM Tris-HCl (pH 7.5), 2 mM EDTA, and a protease inhibitor cocktail. Whole cell lysates (WCLs) were centrifuged at 13,000 rpm for 10 min at 4 °C. To detect TRADD oligomerization, WCL were separated using a non-reducing sample buffer. About 30 μg of proteins were separated by SDS-PAGE and transferred to nitrocellulose membranes (GE Healthcare, Little Chalfont, UK). Non-specific binding was blocked, and anti-GFP (1:3000, Santa Cruz, CA, USA, SC-8334, SC-9996), anti-actin (1:5000, Cell Signaling Technology, Danvers, MA, USA, #4967), and anti-PARP (1:1000, Cell Signaling Technology, Danvers, MA, USA, #9542) anti-c-Myc (1:3000, Invitrogen, Camarillo, CA, USA, 13-2500) antibodies were used as primary antibodies. After washing, membranes were probed with the HRP-conjugated secondary antibody for 1 h. Enhanced chemiluminescent substrate (GenDEPOT, Barker, TX, USA) was used for visualization. Immunoprecipitation was performed with 15 μl of dynabeads protein G (Invitrogen, Camarillo, CA, USA). The beads were washed and incubated with 1 μg of the antibody for 1 h at RT. The beads were incubated with 300 μg WCL overnight at 4 °C after washing. Samples were separated using SDS-PAGE for immunoblotting. UDP-GlcNAc (1 mM) and $MnCl_2$ (5 mM) were added to recombinant SseK1 and incubated at 37 °C for 1 h. The same amount of wild type and auto-glycosylated SseK2 were loaded into 15% SDS-PAGE gel and anti-GlcNAc antibody (1:5000, CTD110.6, Santa Cruz, CA, USA, #sc-59623 used to detect GlcNAcylated arginine).

NF-κB luciferase assay. A549 cells (Panomics, RC0002) stably expressing NF-κB were transfected with a mixture of pNL1.1.TK(*Nluc*/TK), GFP-TRADD and various Myc-SseK1 plasmids. pNL1.1.TK(*Nluc*/TK) was used for transfection control. After 24 h, the cells were treated with 20 ng/ml TNF-α for 6 h. Luciferase assay was performed using Dual-Luciferase

Reporter Assay system (Promega, E1910). Briefly, cells were lysed with Luciferase Cell Culture Lysis Reagent and Luciferase Assay Reagent II was added to measure the luciferase activity. Stop & Glo Reagent was added into tube to quench firefly luciferase activity, and nanoLuc luciferase activity was measured using a luminometer.

Glycosytransferase kinetics assay. A549 Recombinant SseK1, SseK2 and point mutant proteins were prepared as described and GT kinetics were measured using UDP-Glo^{TM} Glycosyltransferase Assay kit (Promega, #V6961) by manufacturer's instruction. Enzyme reaction buffer (ERB) was prepared as 25 mM Tris-HCl (pH 7.5), 50 mM NaCl, 4 mM $MnCl_2$, 1 mM DTT and reaction was eliminated by using the nucleotide detection buffer. For preparing the acceptor-substrate, L-arginine (Duchefa BIOCHEMIE, > 98.5% purity) was dissolved in ERB. Synthetic peptides of GAPDH (Genscript, > 90% purify) was purchased and dissolved in ERB. White 96-well plates (ThermoScientific) were used for luminescence assay and the plate was read by using luminometer (VictorX5, PerkinElmer). Kinetics parameters were calculated using GraphPad Prism5 ver.5.03 software. The points represent an average of two samples and error bars represent mean ± S.D. The final specific activity of the transfer reaction was corrected considering the hydrolysis reaction, which was performed using SseK1/SseK2, UDP-GlcNAc, and $MnCl_2$.

Mouse infections. All animal experiments were performed according to Institutional Animal Care and Use Committee-approved protocols (Animal Welfare Assurance #3647) and conducted as previously described (X. F. Gao et al., 2013). Female BALB/c mice were obtained from the Jackson Laboratory, housed in microisolator cages, and provided with food and water ad libitum. *C. rodentium* Δ*nleB* was electroporated with pFLAG-CTC plasmids expressing EHEC *nleB1* or *nleB2* genes. Mice were challenged with $1*10^8$ CFUs of each strain and

observed twice daily for 14 days. Colon samples were dissected after euthanasia, homogenized, serially diluted in PBS, and then plated on MacConkey agar to enumerate bacteria.

pH-dependent GT activity test. Glycosylation reactions were performed as described previously (El Qaidi et al., 2017). Briefly 200 nM of enzyme was mixed with 1 μM substrate in the presence of 50 mM Tris-HCl pH 7.4, 1 mM UDP-GlcNAc, 10 mM $MnCl_2$, and 1 mM DTT for 2 h at room temperature. Samples were subjected to Western blot analysis using an anti-Arg-GlcNAc antibody (Abcam). The pH-dependence of glycosylation was assessed under similar conditions except that the Tris-HCl was replaced with McIlvaine buffers.

Isothermal titeration calorimetry. ITC experiments were conducted in a MicroCal VP-ITC (MicroCal) device. After size exclusion chromatography (SEC) in Tris-HCl (pH 7.5), 150 mM NaCl, and 1 mM $MnCl_2$, sample fractions corresponding to the single UV_{280} peak were collected and concentrated to 0.2 mM by using 10 kDa cut-off Amicon tubes. Ligands (4 mM) were dissolved in the same SEC buffer and were titrated to variant SseK proteins at 25 °C. Binding stoichiometry, enthalpy variation, entropy variation, dissociation constant and Chi-square values were calculated using MicroCal Origin software.

Results

Anomeric configuration of glycosylated peptides. To determine Recently it was proposed, though not experimentally demonstrated, that SseK3 is a retaining GT (Esposito et al., 2018). However, and in contrast to this, another NleB study synthesized Arg-*N*-GlcNAc-containing glycopeptides in a β-configuration, implying that these enzymes are inverting GTs (Pan et al., 2014). To resolve these discrepancies, we investigated by NMR spectroscopy the glycosidic bond configuration of a GlcNAc-$GAPDH_{187-203}$ glycopeptide, which was formed enzymatically by incubation with SseK1 and UDP-GlcNAc/$MnCl_2$. From 2D $^{1}H,^{13}C$-CLIP-HSQC we measured

the $^{1}J_{CH}$coupling at the anomeric position of the transferred GlcNAc to be 168 Hz, characteristic of an α-linkage (**Figure 14**). These data suggest that the transfer of GlcNAc by SseK1 follows a retaining mechanism. Considering the conserved active site residues and the structural similarity between SseK1 and SseK2/SseK3, SseK2/SseK3 also might be retaining GTs (detailed information is described below).

Figure 14 SseK1 is a retaining-glycosyltransferase.

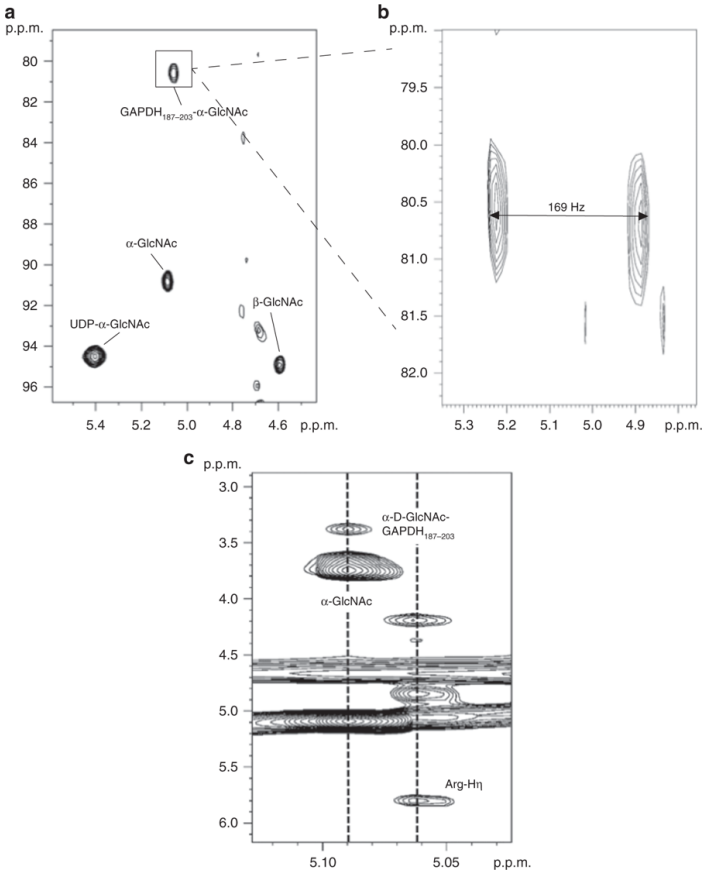

NMR spectra showing the reaction product of $GAPDH_{195-203}$ with SseK1. a Decoupled ^{1}H-^{13}C HSQC spectrum (800 MHz) showing the anomeric region, highlighting the presence of α-D-GlcNAc-$GAPDH_{187-203}$, with a large ^{13}C upfield shift relative to the free species. b Expansion of ^{1}H-^{13}C CLIP HSQC spectrum (500 MHz) with no decoupling to measure the anomeric 1JCH coupling in α-GlcNAc-$GAPDH_{187-203}$. A value of 169 Hz indicates an α-configuration. c ^{1}H-^{1}H TOCSY spectrum highlighting through-bond

correlation between the anomeric proton of α-D-GlcNAc in $GAPDH_{187-203}$-α-GlcNAc and an arginine η-proton.

Overall enzyme architecture. We solved the crystal structures of *Salmonella enterica* serovar Typhimurium SL1344 SseK1 in complex with UDP. SseK2 was solved both in its unliganded form and in complex with UDP and UDP-GlcNAc. NleB2 from *E. coli* O145:H28 was solved in its unliganded form (**Table 8**). For overexpression and crystallization, amino acids 1–20 and 1–33 at the N-terminus of SseK1 and SseK2 were truncated, respectively. This N-terminal region is predicted to be unstructured and presumably play a role in secretion and translocation into the host cell (Ghosh, 2004). Proteins containing these N-termini failed to crystallize. Point mutations (C39S, C210S) were introduced into SseK1 to prevent protein precipitation due to irregular intermolecular disulfide binding. For NleB2, amino acids 317–326 at the C-terminus were deleted for better crystal packing and Cys21 and Cys199 were also substituted to serine (**Figure 15a**). Unambiguous electron density maps for uridine 5′-diphospho-N-acetylglucosamine (UDP-GlcNAc) or uridine 5′-diphosphate (UDP) were visualized in the active sites of the crystal structures (**Figure 15b**).

Table 8 Data collection and refinement statistics.

	Seleno-Met NleB2(SAD peak)	NleB2 **(5H5Y)**	SseK1_UDP **(5H60)**	SseK2 **(5H61)**	SseK2_UDP **(5H62)**	SseK2_UDP-GlcNAc **(5H63)**
Data collection						
Space group	P21212	P21212	P6222	P21	P21	P1
Cell dimensions						
a, b, c(Å)	66.5,95.9,122.1	67.8,95.5,120.1	115.9,115.9,100.1	46.6,145.6,55.5	49.6,143.6,52.7	49.6,52.3,143.8
α, β, γ (°)	90,90,90	90,90,90	90,90,120	90,105.1,90	90,108.2,90	90,90,108
Resolution (Å)	60-3.0 (3.11-3.04)	67.8-2.1 (2.16-2.10)	70.9-3.15 (3.27-3.15)	72.8-1.9 (1.91-1.86)	47.3-1.7 (1.70-1.66)	47.9-1.9 (1.97-1.92)
Rmerge(%)	9.2(96)	11.1(94.0)	14.9(121.0)	5.6(70)	6.4(84)	7.6(36.7)
$I / \sigma I$	17.4(2.8)	15.5(3.3)	20.6(4.0)	15.8(2.1)	16.3(2.2)	9.2(3.1)
Completeness (%)	100(100)	99.7(99.9)	99.9(100)	98(95.1)	99.5(100)	94.4(94.9)
Redundancy	6.3(6.1)	13.6(14.0)	28.1(30.3)	5.5(5.5)	7.0(7.1)	2.6(2.6)
Wilson B-factor(Å2)	24.4	28.7	82.6	36.5	33.6	32.5
Refinement						
Resolution (Å)		44.4-2.1 (2.15-2.10)	70.9-3.15 (3.26-3.15)	53.6-1.9 (1.93-1.86)	41.4-1.7 (1.72-1.66)	41.1-1.9 (1.99-1.92)

No. reflections	45767 (2651)	6935 (354)	58396 (3943)	81824 (5786)	98965 (7027)
No. reflections used for Rfree	43743	6927	55555	77783	94014
Rwork/ Rfree(%)	24.3 (32.0)/29.1 (36.1)	27.4 (29.0) /35.7 (40.1)	20.2(28.6) /23.6(31.7)	19.0(28.5) /21.8(30.2)	18.4(25.3) /22.8(25.1)
No. atoms	4902	2499	5030	5516	10767
Protein	4662	2473	4765	4894	9854
Ligand/ion	-	26	-	65	162
Water	240	0	265	557	751
B-factors	45.1	89.1	37.0	29.7	28.0
Protein	45.3	92.7	35.4	28.7	28.7
Ligand/ion	-	85.5	-	24.2	21.0
Water	45.0	-	40.1	39.2	35.0
R.m.s. deviations					
Bond lengths (Å)	0.0082	0.0102	0.0211	0.0236	0.0203
Bond angles (°)	0.96	1.50	1.72	1.87	2.16
Ramachandran favored (%)	95.1	91.0	98.8	97.8	97.0
Ramachandran outliers (%)	0	0.7	0	0	0.16
Clashscore	9.0	36.0	13.1	7.26	6.46

Values in parentheses are for highest resolution shell.

The sequence identity among SseK1, SseK2, and NleB1 ranges from ~ 60-65%. The N-termini, whose function is presumably to facilitate protein translocation into host cells, differ the most among orthologs, while the rest of the sequence is highly conserved (Kujat Choy et al., 2004). Hereafter, we will focus primarily on the biochemistry for SseK1 because SseK1 is more active than SseK2. For structural analyses, we focus on SseK2 because the data-sets for this protein were obtained at a higher resolution, with three different snapshots of the active site. SseK2 possesses an overall protein fold composed of 15 α-helices and 9 β-strands that is highly similar to SseK1 and NleB2 (RMSD = 1.8 Å/1.8 Å, *Z*-score = 37.2/37.4, number of compared residues = 304/304 to SseK1/NleB2, respectively based on *DALI* pairwise comparison (Holm & Laakso, 2016)) (**Figure 15c, 15d**). These structures belong to the GT-A class, which has two abutting β/α/β Rossmann-like domains (Lairson et al., 2008) (β3-α2-β4-α3-β5) and contains an Asp-x-Asp (DxD) motif in the active site (SseK2$^{D239\text{-}x\text{-}D241}$, SseK1$^{D223\text{-}x\text{-}D225}$, and NleB2$^{D218\text{-}x\text{-}D220}$).

SseK2 can be divided into three types of sub-domains, namely the catalytic domain (40–147 and 185–336), which includes the Rossmann-like domains, the protruded helix-loop-helix (HLH) domain (148–184), and the C-terminal lid domain (337–348) (**Figure 15e**). The concave shape of the catalytic domain is composed of an α-helix and β-strand mixture, and similar to other GT-A structures, continuous central β-strands (β8, β9, β6, β3, β4, β5) form a mixture of parallel and anti-parallel strands. The C-terminal lid domain is highly flexible in the absence of a ligand. Therefore, the electron density map for this domain was not resolved. However, in the structures with UDP and UDP-GlcNAc, the substrate leads to an unambiguous electron density map for the C-terminal lid domain, implying that the domain is well ordered only in the presence of the nucleotide (detailed information is described below).

Recently, the crystal structure of EarP, an arginine rhamnosyltransferase, was solved, revealing a GT-B fold and an inverting catalytic mechanism in which a glutamate residue acts as the catalytic base (Rust, Zurita-Lopez, Clarke, & Thompson, 2011; Sengoku et al., 2018; X. Zhang, Zhou, & Cheng, 2000). Hence, SseK and EarP are likely to differ in their catalytic mechanisms (see below).

Figure 15 Overall enzyme architecture

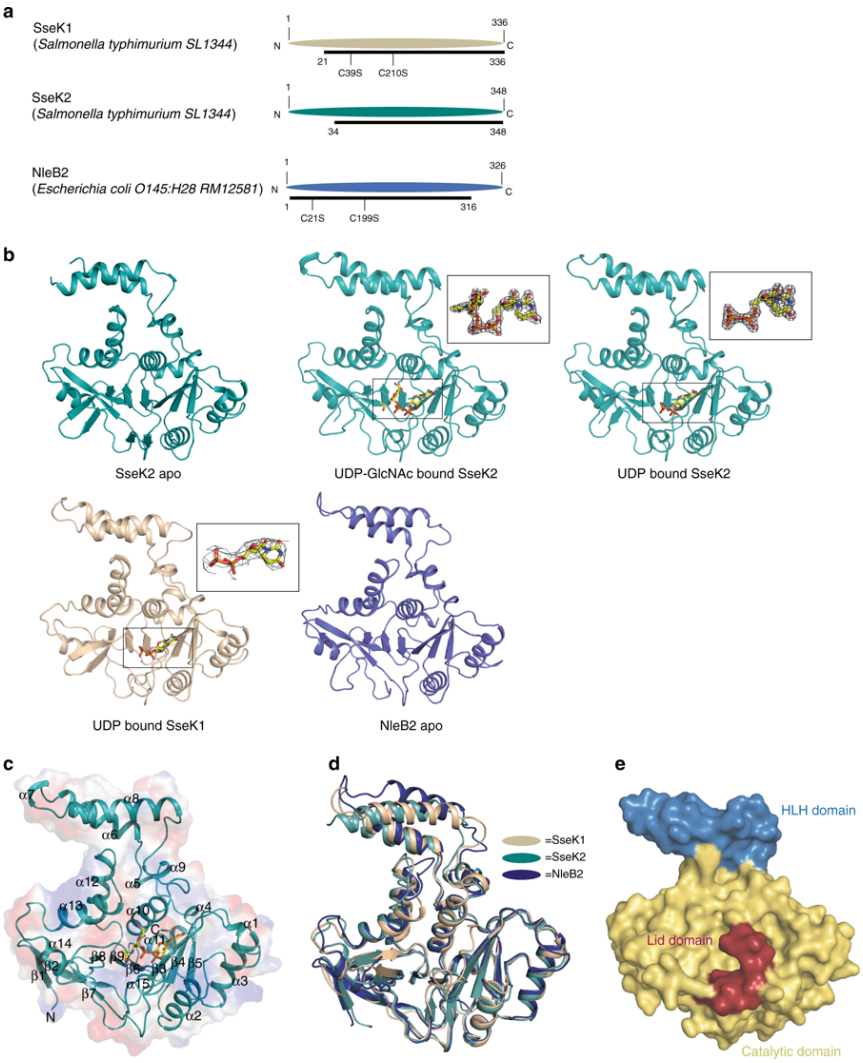

a Colored ovals show the full-length amino acid sequence and the black line under the oval shows the amino acid sequence used for overexpression and crystallization. **b** Arrange crystal structure and electron density maps of each ligands (2Fo – Fc electron density maps of UDP on SseK1 and UDP & L-arginine on SseK2 contoured at 1σ and UDP and the others are 2σ). **c** Numbering of the α-helices and β-strands of SseK2 and **d** superimposition of SseK1, SseK2, and NleB2. **e** Each sub-domain is presented in different colors (blue: HLH domain, yellow: catalytic domain, red: lid domain).

Donor substrate binding mode. Based on the complexes of SseK2 with UDP and UDP-GlcNAc, we identified the donor-substrate binding mode and substrate-mediated conformational changes.

UDP-GlcNAc consists of three groups, namely the uridine, pyrophosphate, and GlcNAc, which will be discussed independently. The uridine group has an aromatic ring tethered by Phe203 and Trp65 through π-π stacking, water-mediated indirect hydrogen bonds (backbones of Arg68 and Ser346), and hydrogen bonding with the Phe66 backbone (**Figure 16a**, upper panel). This sandwich-like π-π stacking is an unusual interaction in GTs because in most of them the sugar nucleotide uracil moiety is sandwiched between an aromatic and an apolar nonaromatic residue participating in π-π stacking and CH-π interactions, respectively (Hurtado-Guerrero et al., 2010; Lira-Navarrete et al., 2015) (**Figure 17a**), implying that this unusual interaction is not a requirement for GTs that prefer uracil-containing sugar nucleotides. However, this sandwich-like π-π stacking interaction is unique for this family of enzymes and is determinant for recognition of the uracil moiety (see below).

Both SseK1 and SseK2 share sandwich-like aromatic π-π stacking interactions and both the tryptophan and phenylalanine residues are conserved in NleB2. However, in the sandwich-like π-π stacking, the interaction modes of SseK1 and SseK2 are slightly different. In contrast to SseK2, Trp331 from the C-terminal lid of SseK1 interacts with the uracil base instead of Phe203 (**Figure 16a**, second and third panels). To confirm this structural difference, we mutated the Phe residue of SseK1 and SseK2 and measured the K_d for UDP-GlcNAc by using isothermal titration calorimetry (ITC) (**Figure 17b, c**). While the $K_d$measured for binding of UDP-GlcNAc to SseK1 F187A was similar to wild type SseK1, the K_d for binding of UDP-GlcNAc to SseK2 F203A was increased about 13-fold as compared to wild type SseK2. These data suggest that although the sandwich-like π-π stacking interactions are maintained, the uracil binding modes within SseK1 and SseK2 are slightly different. In the SseK3 structure, SseK2-like π-π stacking interaction is conserved and $Phe190^{SseK3}$ and $Trp52^{SseK3}$ (corresponding to $Phe203^{SseK2}$ and $Trp65^{SseK2}$)

participate in an interaction with the uridine group in the same orientation (Esposito et al., 2018) (**Figure 16a**, bottom panel). Mutating Trp51^{SseK1} and Trp65^{SseK2} to alanine abrogated UDP-GlcNAc binding to SseK1 and SseK2 (**Figure 17b, c**). The activity of the W51A mutant was reduced more than the W331A mutant, as measured in NF-κB activation assays, which was consistent with ITC assay data (**Figure 17d**). Overall, Trp51^{SseK1} and Trp65^{SseK2} appear to be more critical than Trp331^{SseK1} and Phe203^{SseK2} for π-π stacking interactions with UDP-GlcNAc, Note that for all sugar nucleotides the binding energy is dominated by a large negative enthalpic term and to a lesser extent by a non-favored entropic term (**Figure 17b, c**).

The GlcNAc moiety of UDP-GlcNAc establishes hydrogen bond interactions with Asp204, Arg207, Asp239, and Arg348. The acetyl group of GlcNAc stabilizes the manganese ion by water-mediated hydrogen bonds (**Figure 16b**). The importance of the acetyl moiety was confirmed by ITC data that show increased K_d of UDP-glucose (UDP-Glc) and UDP-galactose (UDP-Gal) as compared to the K_d of UDP-GlcNAc for SseK1 (**Figure 17b, c**). In comparison to UDP-GlcNAc, UDP-Glc lacks the acetyl group, leading to a decrease in the enzyme-substrate binding affinity of about 16.5-fold. Moreover, in UDP-Gal, the absence of the acetyl group and the presence of an inverted C_4 hydroxyl group may lead to steric hindrance with the enzyme, leading to the weakest K_d (69.1-fold weaker than the K_d of UDP-GlcNAc). The binding affinities of SseK1 and SseK3 for UDP-Glc and UDP-Gal are relatively different (Esposito et al., 2018); however, their binding affinities for UDP-GlcNAc are similar (2.3, 1.2, and 1.9 μM for SseK1, SseK2, and SseK3, respectively) (Esposito et al., 2018). Overall, the SseK enzymes possess an architecture that is optimized for binding UDP-GlcNAc.

Most GT-A GTs have a DxD motif that is required for enzymatic activity (Wiggins & Munro, 1998). The DxD motif in SseK2 has two significant functions, the coordination of manganese ion

and the interaction with the GlcNAc group (**Figure 16c**). The manganese ion acts as a bridge between SseK2 and the pyrophosphate of UDP-GlcNAc. In the absence of manganese, the DxD motif-mediated donor-substrate binding would not be expected to occur due to the negative charge repulsion between DxD and the pyrophosphate of UDP-GlcNAc. An octahedral molecular geometry was visualized for the manganese ion coordinated to six oxygens from the UDP pyrophosphate, Asp241, Ser340, Asn338, and a water molecule. Asp239 interacts with a water molecule and a GlcNAc moiety via hydrogen bonds. Asp241 interacts with both a manganese ion and with a water molecule that stabilizes the manganese ion. Most of the residues that interact with UDP-GlcNAc are highly conserved in the SseK and NleB families (**Figure 18**).

Figure 16 UDP-GlcNAc binding mode in SseK2.

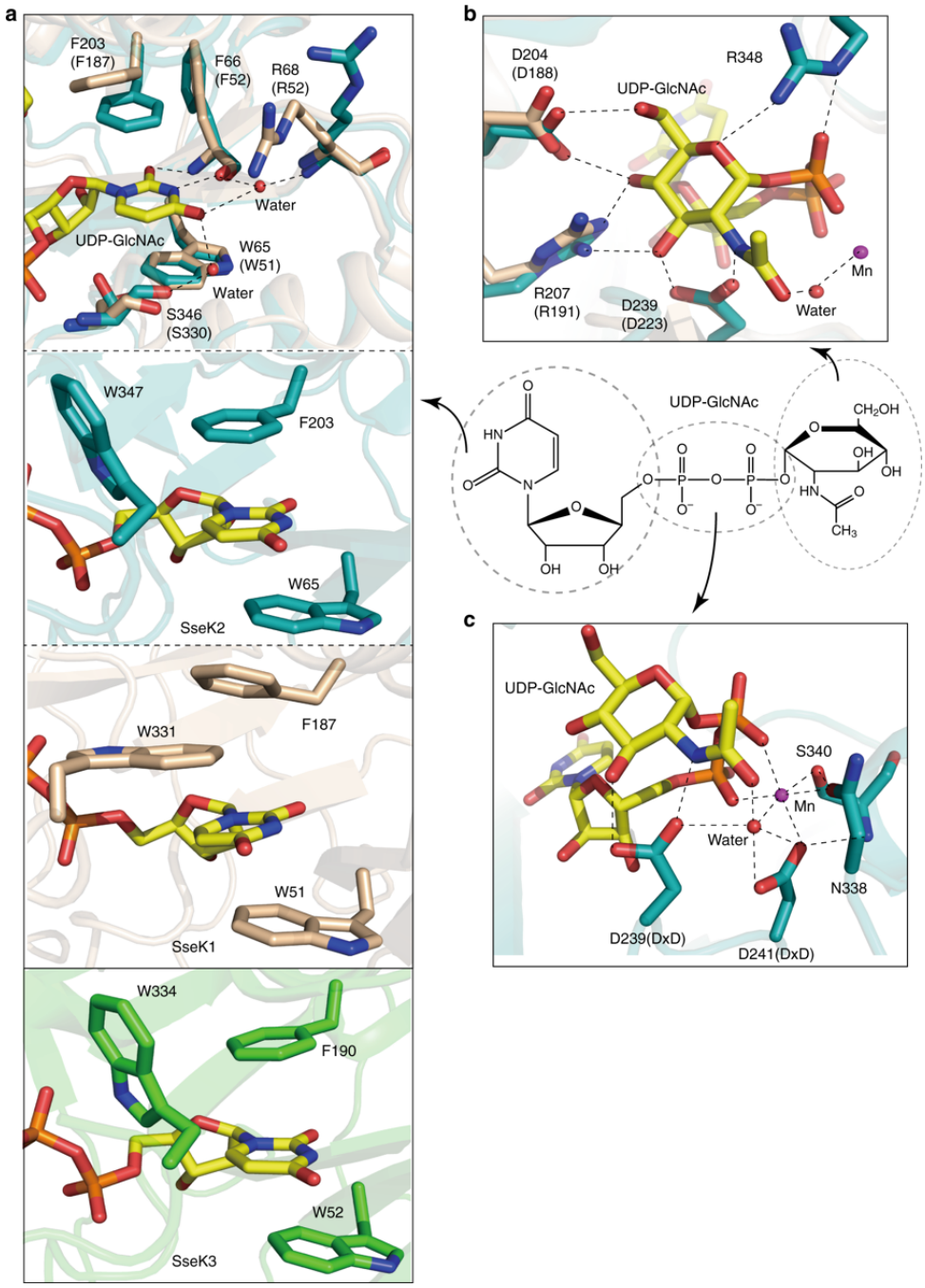

a Uracil moiety of UDP-GlcNAc interacts with SseK2 through hydrogen bonds and π-π stacking (top panel), but SseK1 uses a slightly different mechanism (second and third panel). Uracil binding mode of SseK3 is similar to SseK2 instead of SseK1 (bottom panel). **b** GlcNAc moiety of UDP-GlcNAc interacts with Asp204, Arg207, Asp239, and Arg348 by hydrogen bonds. The carbonyl group of the acetyl of GlcNAc interacts with a water molecule to stabilize the divalent metal ion. **c** Manganese ion coordinates

six oxygens from pyrophosphate, Ser340, Asn338, Asp241, and water. The DxD motif stabilizes both UDP-GlcNAc and manganese ion. *Amino acid numbering in brackets refers to conserved sequence of SseK1. Black dashed lines represent hydrogen bonds.

Figure 17 The difference in the donor substrate binding mode between SseK1 and SseK2.

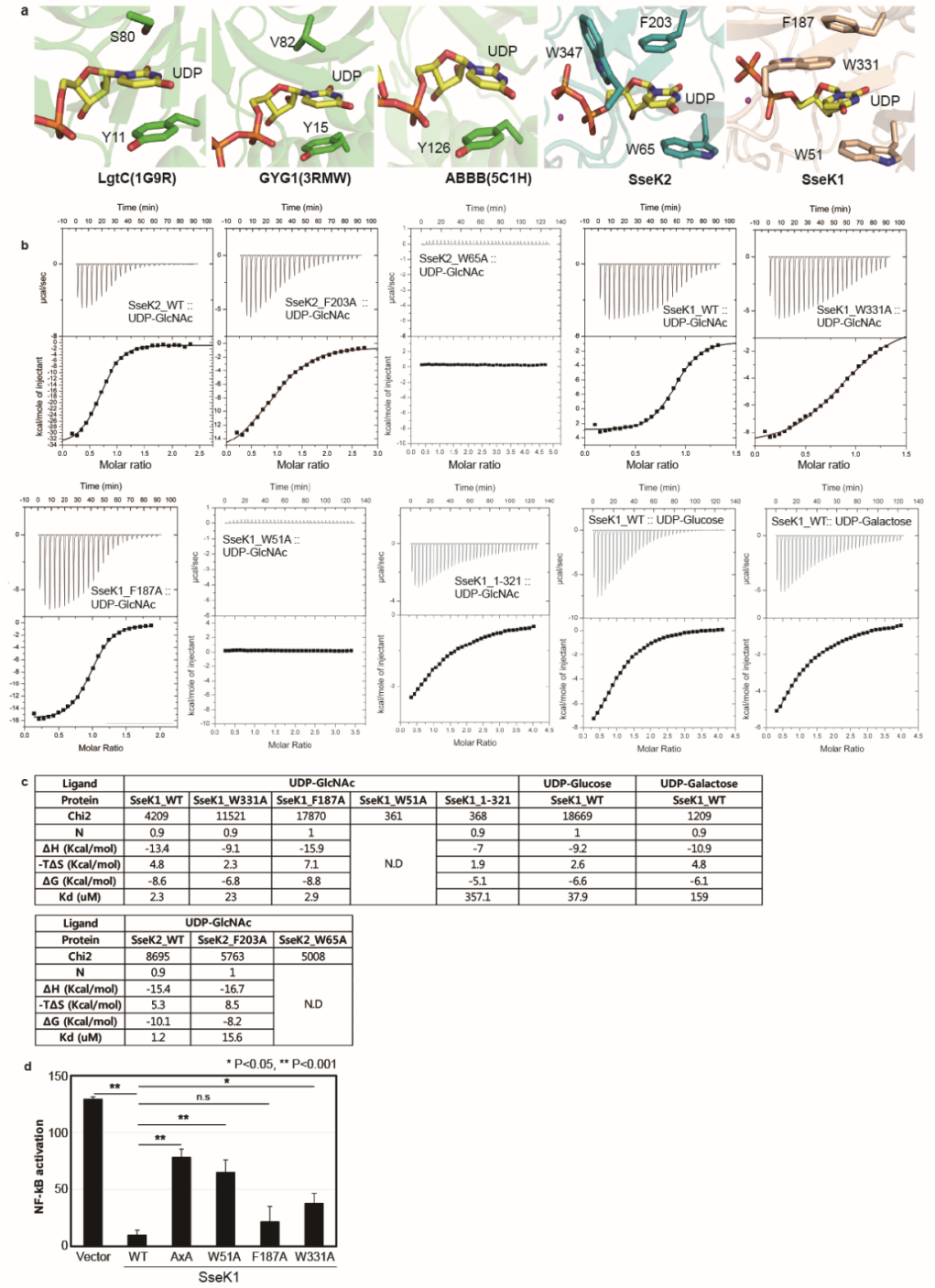

Ligand	UDP-GlcNAc					UDP-Glucose	UDP-Galactose
Protein	SseK1_WT	SseK1_W331A	SseK1_F187A	SseK1_W51A	SseK1_1-321	SseK1_WT	SseK1_WT
Chi2	4209	11521	17870	361	368	18669	1209
N	0.9	0.9	1	N.D	0.9	1	0.9
ΔH (Kcal/mol)	-13.4	-9.1	-15.9		-7	-9.2	-10.9
-TΔS (Kcal/mol)	4.8	2.3	7.1		1.9	2.6	4.8
ΔG (Kcal/mol)	-8.6	-6.8	-8.8		-5.1	-6.6	-6.1
Kd (uM)	2.3	23	2.9		357.1	37.9	159

Ligand	UDP-GlcNAc		
Protein	SseK2_WT	SseK2_F203A	SseK2_W65A
Chi2	8695	5763	5008
N	0.9	1	N.D
ΔH (Kcal/mol)	-15.4	-16.7	
-TΔS (Kcal/mol)	5.3	8.5	
ΔG (Kcal/mol)	-10.1	-8.2	
Kd (uM)	1.2	15.6	

a SseK1 and SseK2 has either a Phe-Trp pair or a Trp-Trp pair for π−π stacking interaction with the uridine of UDP-GlcNAc. Such an aromatic ring pair is an unusual structure among the GTs. The yellow stick shows a donor substrate and the four letters in the parentheses indicates the protein data bank(PDB) code number. **b** Point mutations of each Phe-Trp pair or Trp-Trp pair and lid domain truncation form were constructed and an ITC assay was performed to determine the K_d value with UDP-GlcNAc. UDP-glucose and UDP-galactose affinity of SseK1 also measured by ITC assay. ITC data were prepared by using *Origin* (Micro Cal, LLC). **c** Summary of thermodynamic parameters from ITC experiments. Data integration, correction and analysis were carried out using *Origin*7 ver. 7.0552 (MicroCal) with a single-site binding model. **d** The NF-κB level in A549-NF-κB luc cells was measured to investigate enzymatic functions. Data represent at least three repetitions.

Conformational change by the donor-substrate binding. After donor-substrate binding, several GTs undergo large local conformational changes. For example, human glycogenin1 (hGYG1) has a lid, an acceptor arm, and a C-terminal loop. Their conformational rearrangement influences the accessibility of the substrate at the active site and in turn their catalytic activity (Chaikuad et al., 2011). The SseK2 structure undergoes a dramatic conformational change induced by donor-substrate binding. In the ground state of SseK2, the C-terminal lid domain is highly flexible, impeding its visualization in the crystal structure. In this state, the donor-substrate binding site might be fully exposed to allow the access of UDP-GlcNAc (**Figure 19a,** left panel). After UDP-GlcNAc binds to the active site, the α10 helix is tilted towards the UDP-GlcNAc by ~ 3.5° and the C-terminal lid domain covers up the active site to stabilize the bound substrate and to restrict the accessibility of water molecules (**Figure 19a,** right panel and **Figure 19b**). The closure of the C-terminal lid in the presence of UDP-GlcNAc determines a closed conformation for this family of enzymes. We truncated the lid domain (SseK1 1-321) and found that the K_d of UDP-GlcNAc binding increased about 155.3-fold for the lid domain truncation, as compared to the wild type protein (**Figure 17b, c**), suggesting that the C-terminal lid domain plays a key role for donor-substrate binding.

Figure 18 Protein sequence alignment between SseK and NleB families.

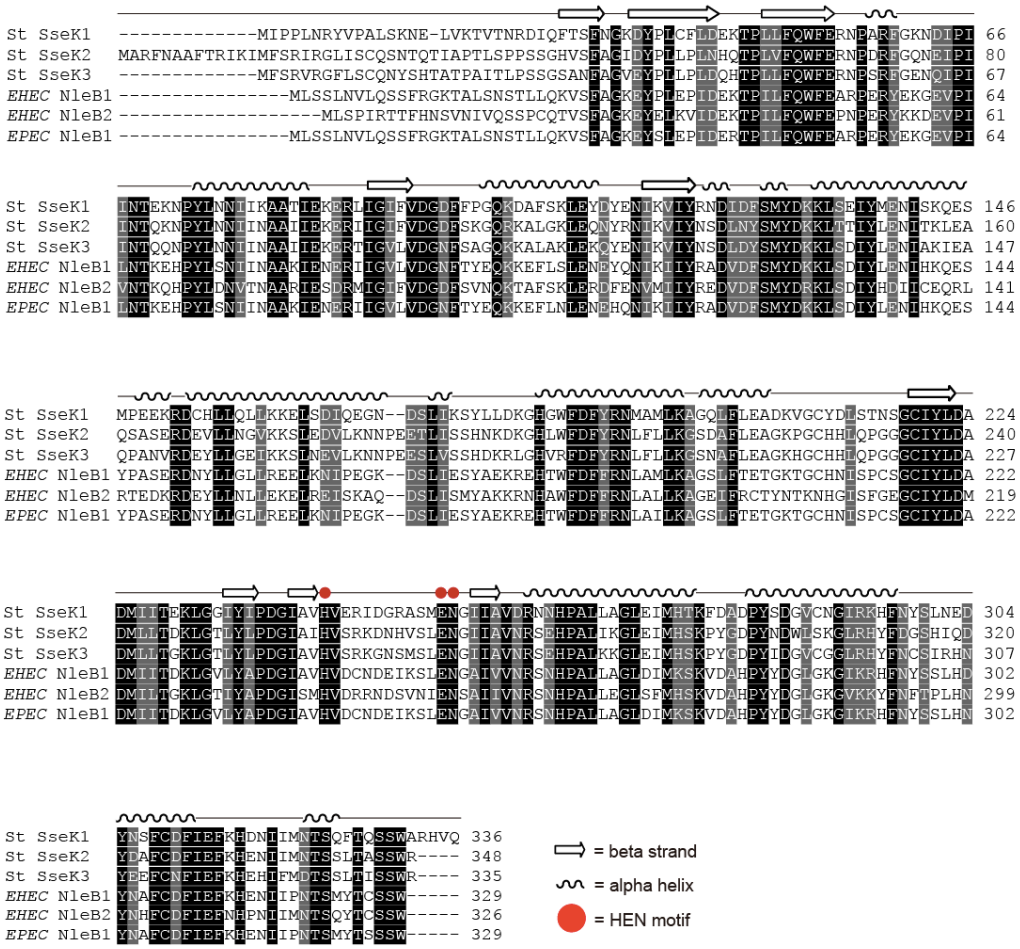

Perfectly conserved residues are highlighted in black and those that are similar among the sequences are highlighted in gray. The rest of the residues are shown in white. The figures were prepared using the Color Align Conservation in http://www.protocol-online.org/tools/sms2/color_align_cons.html website. *St= *Salmonella typhimurium SL1344*, EHEC= Enterohemorrhagic *Escherichia coli*, EPEC= Enteropathogenic *Escherichia coli*.

Both Trp334 and Arg335 in the C-terminal lid domain of SseK3 (corresponding to Trp347^{SseK2} and Arg348^{SseK2}) interact with UDP-GlcNAc (Esposito et al., 2018). This interaction is highly similar to that of SseK2. It was reported that Trp334 and Arg335 in SseK3 are essential for enzyme activity (Esposito et al., 2018). The amino acid sequence of the C-terminal lid domain of SseK1 is slightly different from SseK2 and SseK3. The conserved arginine residue in

SseK2 and SseK3 ($Arg348^{SseK2}$, $Arg335^{SseK3}$), which is located in the lid domain, is substituted to an alanine residue in SseK1 ($Ala332^{SseK1}$). In addition, an arginine residue is located next to an alanine residue ($Arg333^{SseK1}$). In the crystal structure of UDP-bound SseK1, the backbone direction of Ala332 is located at the opposite side of UDP (**Figure 19c).** This implies that the lid domain of SseK1 is likely more flexible than SseK2 and SseK3. Furthermore, the sequence alignment shows that the NleB family lacks the arginine residue, though a conserved Trp is present at the C-terminus. We would expect that both the SseK and NleB families have a different conformational behavior of the lid-domain.

Figure 19 Donor substrate-mediated conformational changes.

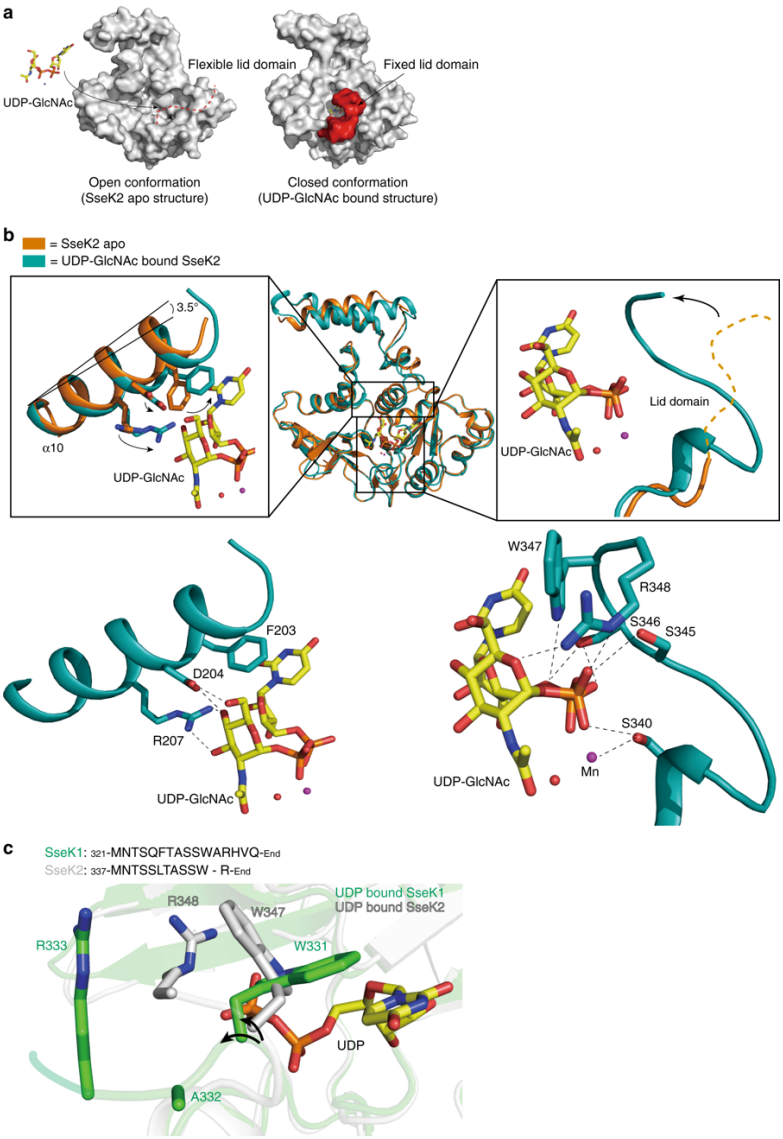

a Comparison of surface structures between apo form and UDP-GlcNAc bound SseK2. The flexible C-terminus creates an open conformation for access of UDP-GlcNAc and after binding of the UDP-GlcNAc, the C-terminal lid domain (red color) interacts with UDP-GlcNAc and is fixed in closed conformation. Yellow stick represents UDP-GlcNAc. **b** After the donor-substrate binds to the active site, the α10 helix tilts about 3.5 degrees and the flexible C-terminal lid domain is fixed towards the UDP-GlcNAc. Due to hydrogen bonding at Arg207, Asp204, and aromatic stacking at Phe203, the α10 helix is able to tilt. The flexible C-terminal lid domain can be fixed by hydrogen bonding of Ser340, Ser345, Ser346, Arg348, and Trp347. Orange and blue-green colors represent SseK2 apo and UDP-GlcNAc bound SseK2 structure, respectively. Black dashed lines represent hydrogen bonds. **c** Direction of the lid-

domain is different between the SseK1 (in green) and SseK2 (in white) structures. Curved arrows (in black) each correspond to the direction of the backbone of the lid-domain.

Figure 20 Binding of short FADD, TRADD and GAPDH peptides to SseK1.

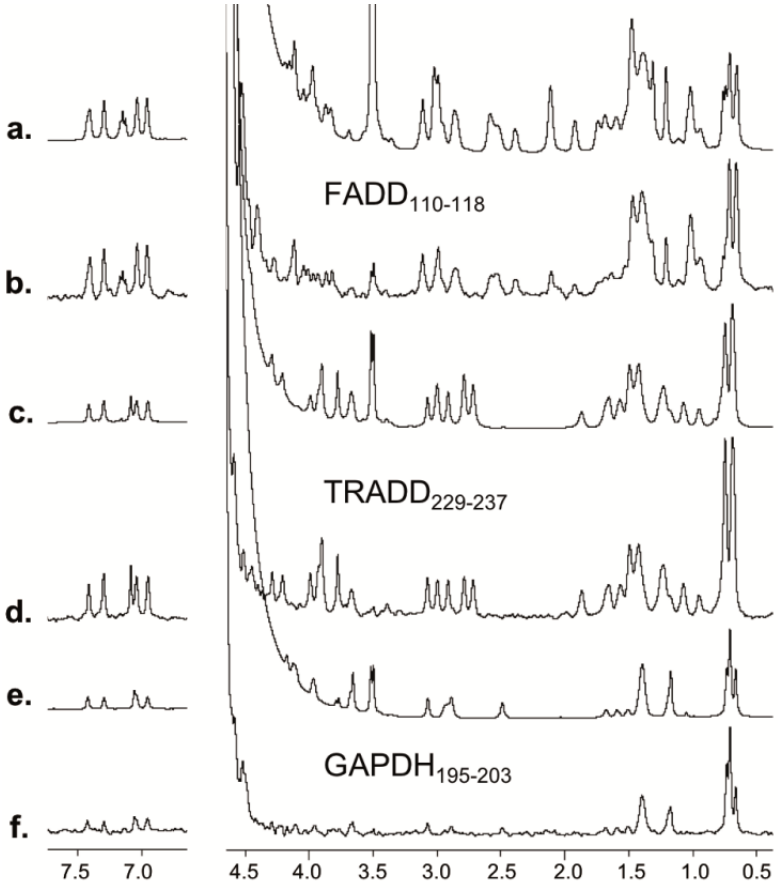

Reference and STD NMR difference spectra of peptides in the presence of 25 μM SseK1, 25 μM $MnSO_4$, 25 μM UDP, and 25 mM Tris-d_{11} pH 7.4 in D_2O at 288 K (800 MHz). STD NMR difference spectra magnified 20x. **a**, **b** Reference and STD NMR difference spectra of 1 mM $FADD_{110-118}$ respectively. **c**, **d** Reference and STD NMR difference spectra of 1 mM $TRADD_{229-237}$ respectively. **e**, **f** Reference and STD NMR difference spectra of 1 mM $GAPDH_{195-203}$ respectively.

Figure 21 Binding of FADD, TRADD and GAPDH peptides to SseK2**.**

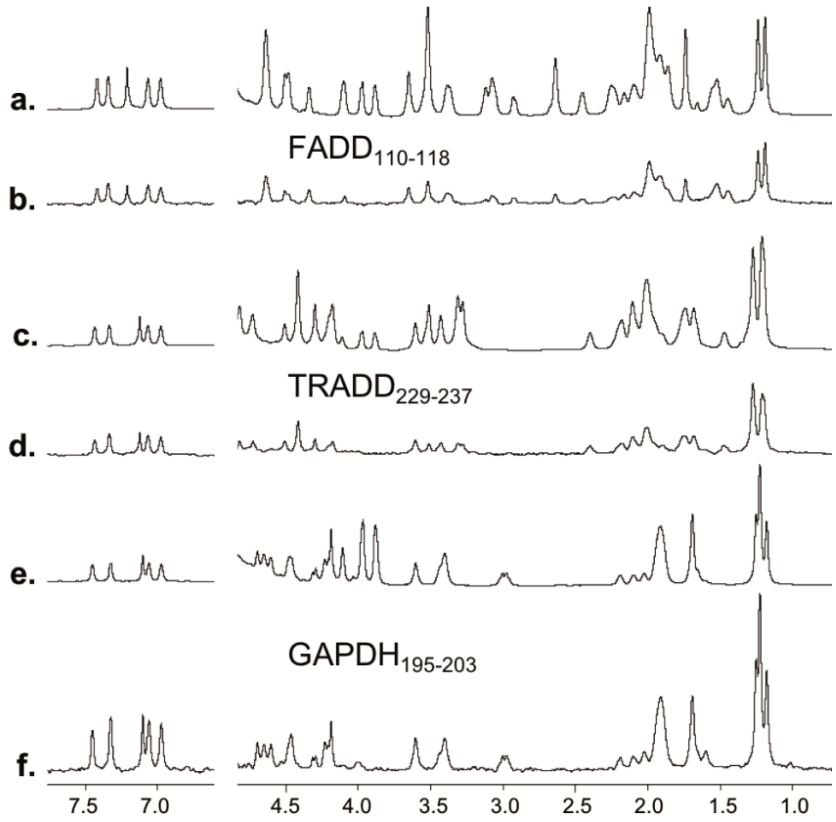

Reference and STD NMR difference spectra of peptides in the presence of 25 μM SseK1, 25 μM $MnSO_4$, 25 μM UDP, and 25 mM Tris-d_{11} pH 7.4 in D_2O at 288 K (800 MHz). STD NMR difference spectra magnified 20x. **a**, **b** Reference and STD NMR difference spectra of 1 mM $FADD_{110-118}$ respectively. **c**, **d** Reference and STD NMR difference spectra of 1 mM $TRADD_{229-237}$ respectively. **e**, **f** Reference and STD NMR difference spectra of 1 mM $GAPDH_{195-203}$ respectively.

Figure 22 Binding modes of short peptide substrates.

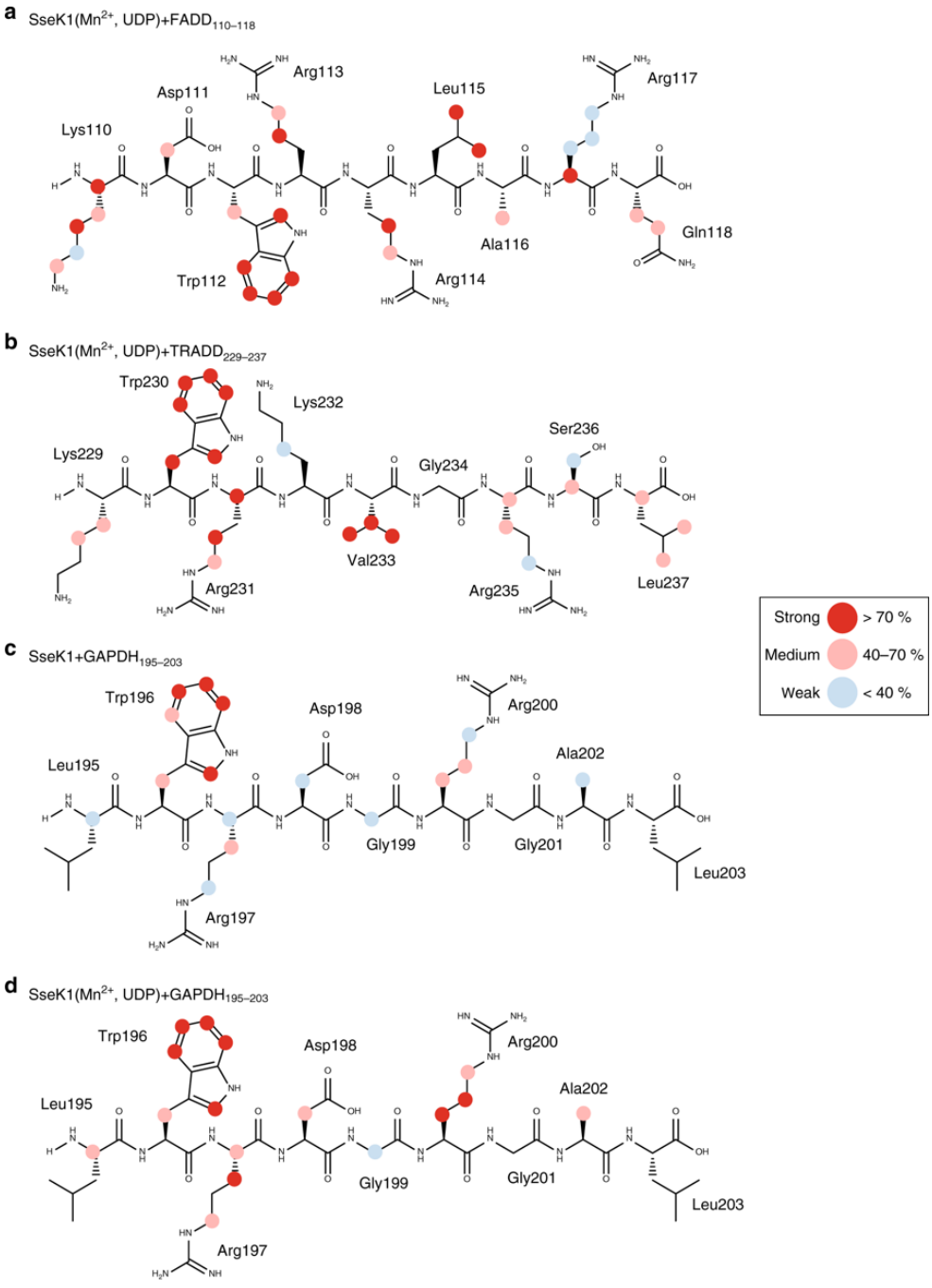

Binding epitope mappings of **a** $FADD_{110-118}$ **b**$TRADD_{229-237}$ and **c**, **d** $GAPDH_{195-203}$ peptides in the presence of 25 μM SseK1. Samples in **a**, **b** and **d** contained 25 μM Mn^{2+}, and 25 μM UDP. All STD intensities normalized against Hζ2 of the tryptophan. Colored circles represent magnitude of normalized intensities (blue:< 40%, pink: 40–70%, red:> 70%). Comparison of $GAPDH_{195–203}$ binding to SseK1, **c** in the absence, and, **d** in the presence of Mn^{2+} and UDP, reveals a significant change in the binding mode of

the substrate peptide upon addition of the cofactor and the nucleotide diphosphate. For STD NMR study of binding to SseK2 see **Figure 23**

Figure 23 Binding modes of short FADD, TRADD, and GAPDH substrate peptides to SseK2 from STD NMR.

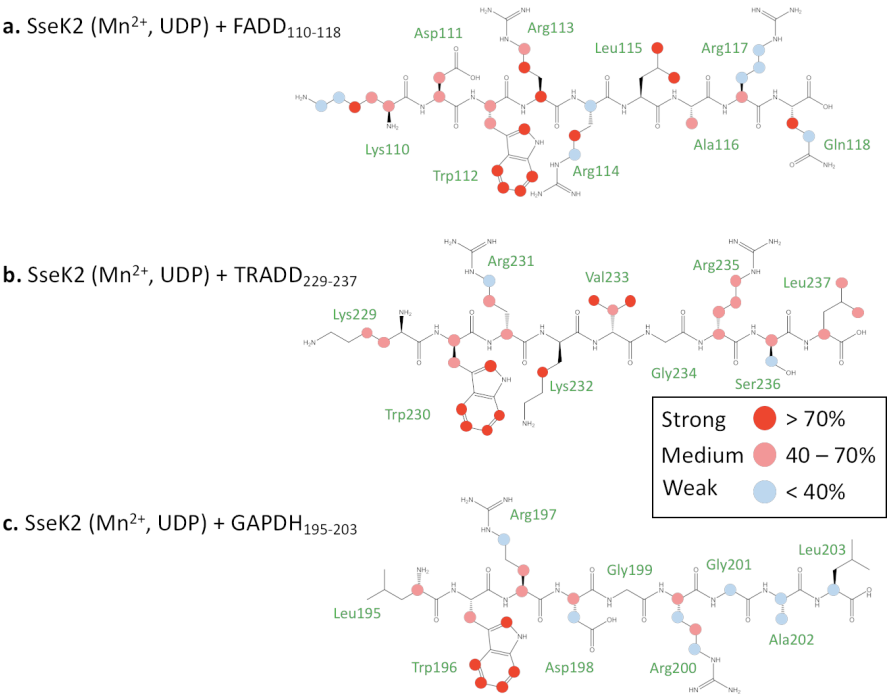

Binding epitope mappings of **a** $FADD_{110-118}$ **b** $TRADD_{229-237}$ and **c** $GAPDH_{195-203}$ peptides in the presence of 25 μM SseK2. Samples contained 25 μM Mn^{2+}, and 25 μM UDP. All STD intensities were normalized against the Hζ2 of the tryptophan. Colored circles represent magnitude of normalized intensities (blue: < 40%, pink: 40-70%, red: >70%).

Peptide substrate recognition by SseK1 and SseK2. To obtain structural information on the molecular recognition of the substrates, we performed saturation transfer difference (STD) NMR experiments using short peptides from FADD, TRADD, and GAPDH. Standard homo- and heteronuclear 2D NMR techniques were used to obtain the chemical shift assignments of $GAPDH_{195-203}$, $FADD_{110-118}$, and $TRADD_{229-237}$ (**Table 9–11**). For each peptide, four different

enzyme systems were prepared: apo-SseK1, apo-SseK2, holo-SseK1, and holo-SseK2, where apo and holo stand for the enzyme without and with Mn^{2+} and UDP, respectively. We observed that all three peptides bound to both SseK1 and SseK2, irrespectively of the forms used in the experiments (**Figure 20, 21**). These data imply that binding of the short peptide ligands occurs independently of enzymatic activity and can also take place in the absence of the sugar nucleotide. In STD NMR experiments, strong signal intensities from different hydrogen atoms of the ligand permit identification of the main contacts of the peptides with the enzyme in the bound state (Mayer & Meyer, 1999, 2001). After intensity normalization, binding epitope maps of the peptides were obtained (**Figure 22, 23**). In all cases, high STD signals, indicating close contacts, were observed for the conserved Trp and Arg side chains. The results support the concept that a WR-motif (W112/R113 in FADD, W230/R231 in TRADD, and W196/R197 in GAPDH) appears to be central for recognition. For $TRADD_{229-237}$, although rather similar binding modes to SseK1 and SseK2 were observed, the binding epitope was spread across the entire molecule when bound to SseK1 but was more concentrated around the WR-motif for SseK2. The epitopes of $FADD_{110-118}$ are comparable when bound to either SseK1 or SseK2. For $GAPDH_{195-203}$, differences in binding to both enzymes were observed. For the binding of $GAPDH_{195-203}$ to SseK1, the data support a significant conformational rearrangement of the peptide ligand upon addition of Mn^{2+} and UDP. This was evidenced by a significant change in the binding epitope mapping, particularly a large increase in STD intensities for the arginine side-chains (**Figure 22c, d**). However, for all other peptides, and for $GAPDH_{195-203}$ binding to SseK2, no such rearrangement occurs (**Figure 24**).

Figure 24 Binding modes of short FADD, TRADD, and GAPDH substrate peptides to SseK1 and SseK2 in the absence of Mn^{2+} and UDP from STD NMR.

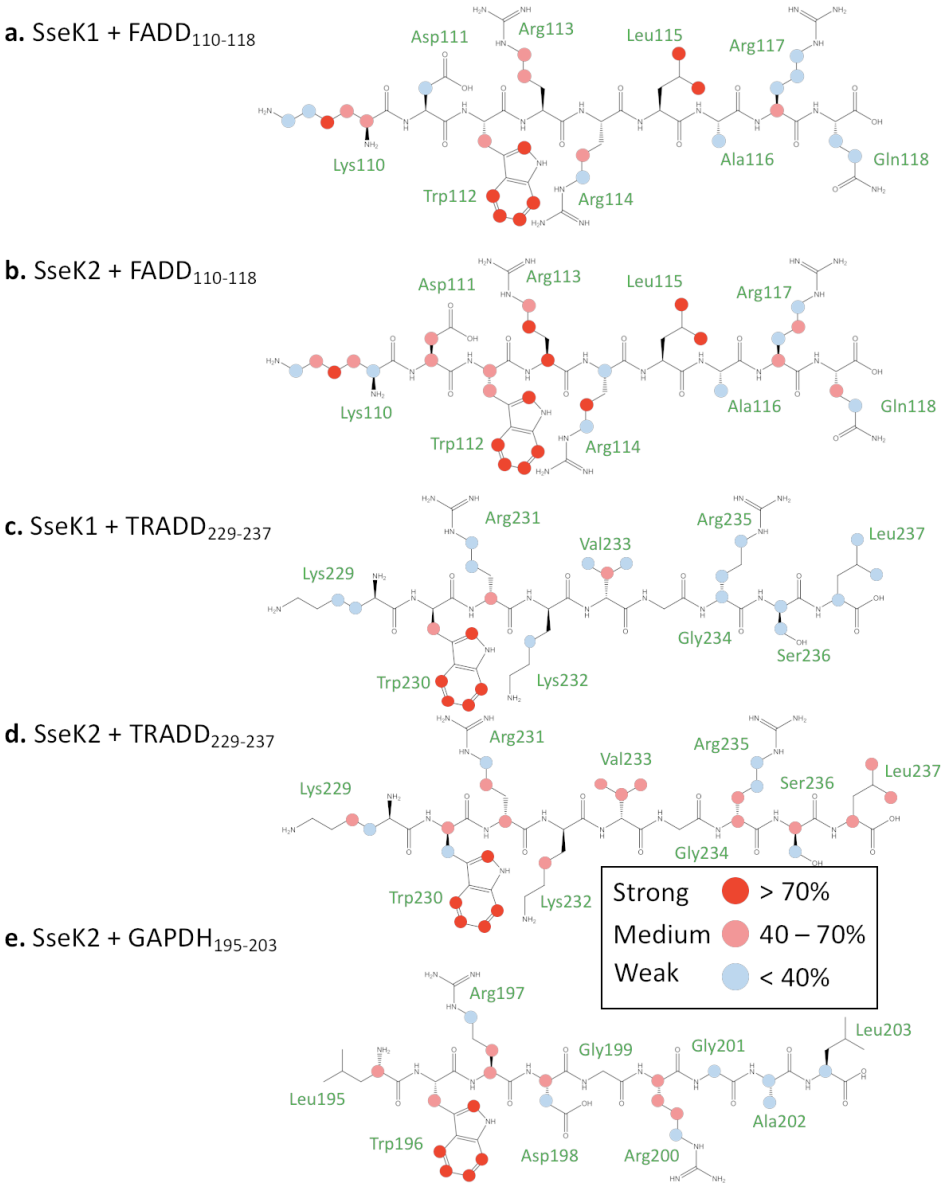

Binding epitope mappings of **a** $FADD_{110-118}$ binding to SseK1 **b** $FADD_{110-118}$ binding to SseK2, **c** $TRADD_{229-237}$ binding to SseK1, **d** $TRADD_{229-237}$ binding to SseK2, **e**, $GAPDH_{195-203}$ binding to SseK2. The binding epitope of $GAPDH_{195-203}$ binding to SseK1 in the absence of UDP is in **Figure 22c**. Samples contained 25 μM SseK1 or SseK2 and 25 μM Mn^{2+}. All STD intensities were normalized against the Hζ2 of the tryptophan. Colored circles represent magnitude of normalized intensities (blue: < 40%, pink: 40-70%, red: >70%). Except for $GAPDH_{195-203}$ binding to SseK1, all the peptides show similar binding modes in the presence or the absence of Mn^{2+} and UDP.

Figure 25 Long Gaussian accelerated MD simulations predict significant differences in the dynamics of HLH domain between SseK1 and SseK2.

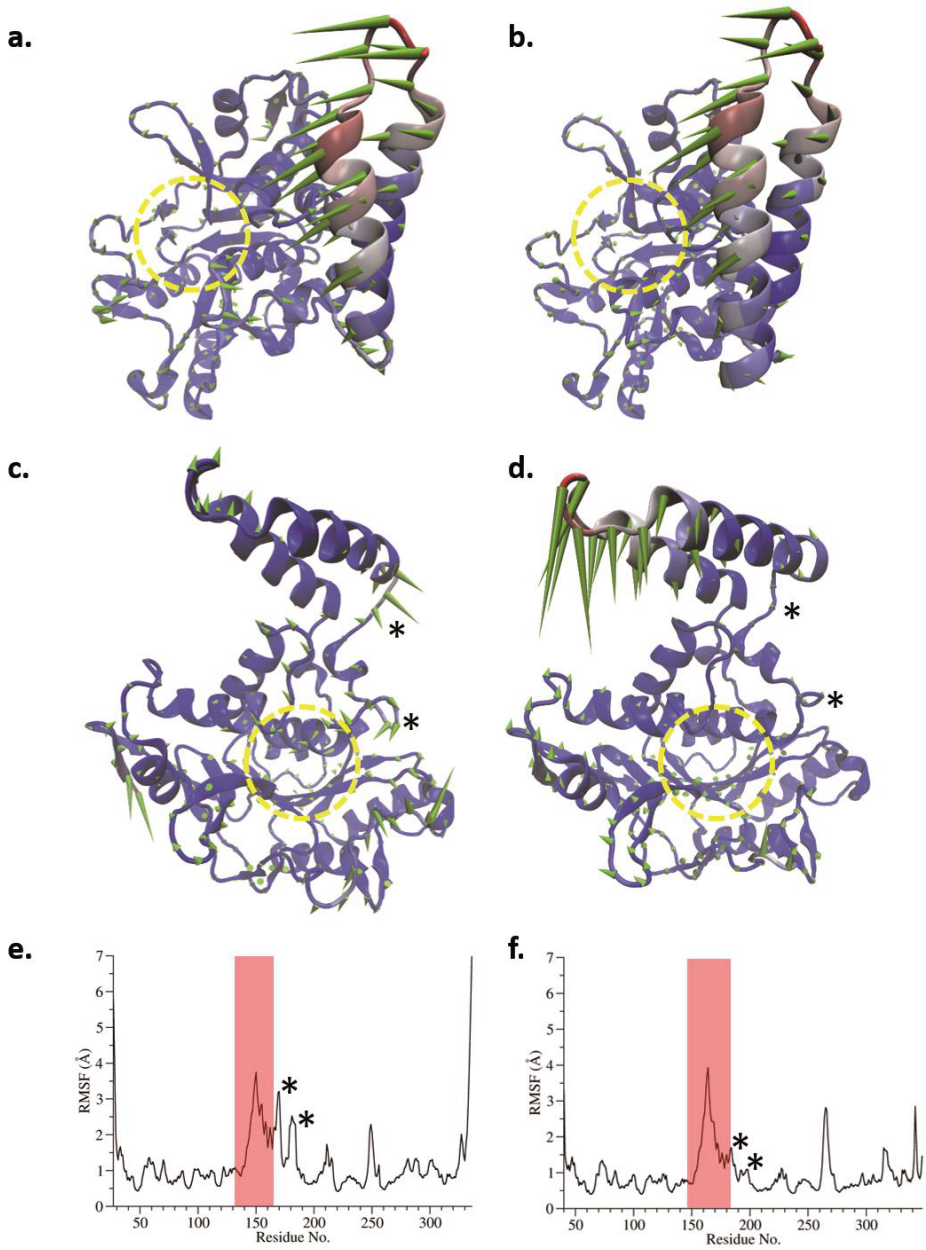

a, **b** Cartoon representation of SseK1 (left) and SseK2 (right), showing the first eigenvector from principal component analysis. Green cones indicate the direction of motion. The magnitude of motion is represented both by cone length and by cartoon color scheme (high (red) –low (blue)). The UDP-binding site is highlighted by a dashed yellow circle. **c**, **d** Cartoon representation of SseK1 (left) and SseK2 (right), showing the second eigenvector from principal component analysis. Green cones indicate direction of motion. Magnitude of motion represented both by cone length and by cartoon color scheme (high (red) –low (blue)). UDP-binding site highlighted by dashed yellow circle. Asterisks show regions with significant differences in motional fluctuations between SseK1 and SseK2, as determined from

backbone RMSF. **e**, **f** Backbone RMSF for each residue of SseK1 (left) and SseK2 (right). Red box shows HLH region. Asterisks highlight regions with significant differences between SseK1 and SseK2.

To elucidate the specific role of the WR-motif, we measured the kinetics of SseK1 to four $GAPDH_{187-203}$-derived synthetic peptides (designated as WT, W196A, R197A, and W196A/R197A). Each of the W196A, R197A, and W196A/R197A mutant forms decreased the catalytic efficiency of about 40.5%, 47.4%, and 17.3%, respectively as compared to WT $GAPDH_{187-203}$ peptide (**Figure 25b**). In particular, the double mutant form (W196A/R197A) synergistically decreased enzyme catalysis, supporting our STD-NMR experiments that suggested that the WR-motif of the peptides is of utmost importance for binding to these enzymes.

Table 9 Chemical shift assignment of $GAPDH_{195-203}$(*).

$GAPDH_{195-203}$ Assignment			
Residue	**Proton ID**	**^{1}H (ppm)**	**^{13}C (ppm)**
Leu-195	HA	3.80	51.50
	HD	0.74	21.46
	HD	0.70	20.84
	HG	1.47	39.78
Trp-196	HA	4.49	55.01
	HB	3.06	26.73
	HD	7.04	124.17
	HE3	7.41	117.87
	HH2	6.93	119.06
	HZ2	7.28	111.61
	HZ3	7.02	121.70
Arg-197	HA	3.92	52.98
	HB	1.48	28.03
	HD	2.86	40.38
	HG	1.16	23.93
Asp-198	HA	4.16	51.23
	HB	2.48	37.75
Arg-200	HD	2.92	40.38

	HB	1.66	27.58
	HG	1.38	24.02
Gly-199/201	HA	3.75	42.63
	HA	3.64	42.42
Ala-202	HA	4.10	49.30
	HB	1.15	16.46
Leu-203	HA	3.97	53.63
	HB	1.37	40.24
	HB	1.42	23.81
	HD	0.69	22.19
	HD	0.64	20.57
	HG	0.71	20.59
	HA	3.80	51.50
	HD	0.74	21.46
	HD	0.70	20.84
	HG	1.47	39.78

(*) Due to strong overlapping some assignments are missing.

Table 10 Chemical shift assignment of $FADD_{110-118}$(*).

$FADD_{110-118}$ Assignment			
Residue	**Proton ID**	**^{1}H (ppm)**	**^{13}C (ppm)**
Lys-110	HA	3.71	52.57
	HB	1.54	30.03
	HG	0.98	20.99
	HD	1.30	26.09
	HE	2.54	38.70
Asp-111	HA	4.52	50.59
	HB	2.57	37.62
Trp-112	HA	4.37	54.69
	HB	3.12	26.50
	HD1	7.02	121.65
	HE3	7.40	117.94
	HZ2	7.29	111.62
	HZ3	7.14	124.56
	HH2	6.94	119.01
Arg-113	HA	3.87	53.49
	HB	1.40	27.49

	HD	2.87	40.20
	HG	1.06	23.66
Arg-114	HA	3.98	53.27
	HB	1.43	24.03
	HD	2.99	40.20
	HG	1.36	24.21
Leu-115	HA	4.12	51.98
	HB	1.43	24.03
	HG	0.71	21.90
	HG	0.65	20.30
Ala-116	HA	4.09	49.75
	HB	1.19	16.20
Arg-117	HA	4.00	53.67
	HB	1.94	27.20
	HD	2.12	31.20
	HG	1.74	27.12
Gln-118	HA	4.10	53.26
	HB	1.59	27.61
	HG	2.99	40.20

(*) Due to strong overlapping some assignments are missing.

Table 11 Chemical shift assignment of $TRADD_{229-237}$(*).

$TRADD_{229-237}$ Assignment			
Residue	**Proton ID**	**^{1}H (ppm)**	**^{13}C (ppm)**
Lys-229	HA	3.78	52.76
	HB	1.67	-
	HD	1.48	-
	HE	2.77	39.09
	HG	1.21	-
Trp-230	HA	4.43	55.08
	HB	3.05	26.78
	HD	7.06	124.27
	HE3	7.38	117.91
	HH2	6.94	119.25
	HZ2	7.29	111.73
	HZ3	7.04	121.62

Arg-231	HA	3.95	52.45
	HB	1.40	-
	HD	2.89	40.46
	HG	1.26	-
Lys-232	HA	3.85	53.51
	HB	1.49	-
	HD	1.49	-
	HE	2.77	39.09
	HG	1.16	-
Val-233	HA	3.89	59.45
	HB	1.88	30.08
	HG	0.72	17.85
Gly-234	HA	3.77	42.02
Arg-235	HA	4.18	53.21
	HB	1.58	-
	HD	2.99	40.44
	HG	1.44	-
Ser-236	HA	4.24	55.52
	HB	3.66	60.93
Leu-237	HA	4.01	53.72
	HB	1.40	40.14
	HD1	0.70	22.22
	HD2	0.66	20.54
	HG	1.41	24.19

(*) Due to strong overlapping some assignments are missing.

To investigate the relevance of the WR-motif for binding, we also carried out STD NMR experiments focused on analyzing the impact of single and double mutations on the affinity of the molecular recognition of the synthetic peptide $TRADD_{229-237}$. As we were interested only in analyzing the impact on binding, we ran competition experiments for the interactions of the $TRADD_{229-237}$-derived peptides with SseK1. Five synthetic peptides (designated as WT, W230A, R231A, W230A/R231A, and R235A) were analyzed. All of them bound to SseK1, as detected by STD NMR, yet their affinities were different, as reflected in their differences in average STD

NMR intensities (e.g., the most intense alpha proton showed 14%, 9%, 6%, 4%, and 10% for WT, W230A, R231A, W230A/R231A, R235A, respectively). This result indicates that the highest affinity for SseK1 is achieved when the full WR-motif is present. Again, the results were compatible with the double mutant showing the lowest binding affinity. We then confirmed the differences in affinity compared to the WT peptide by performing competition STD NMR experiments. In binary samples containing SseK1 and equimolar concentrations of the $TRADD_{229-237}$ and one of the mutant TRADD peptides, none of the mutants was able to significantly displace the WT peptide, which demonstrates that modifications at the WR-motif impact negatively the affinity of the peptide for the enzyme (**Figure 26, 27**)

STD NMR data revealed that all the peptide ligands were recognized in solution. Hence, it is clear that differences in glycosylation of full-length FADD, TRADD, and GAPDH substrates by SseK1 and SseK2 are not due to differences in binding modes of their death domain sequences, but instead due to differences outside the binding site. In agreement with the similarity of binding modes of the short peptides detected by STD NMR, most of the sequence differences of SseK1 and SseK2 are likely in regions away from the binding site, including the HLH domain. Hence, differences in glycosylation specificity may be attributed to differences in the internal dynamics between the two enzymes at those distinct regions.

Figure 26 STD NMR competition experiments of $TRADD_{229-237}$ wild-typeand mutants.

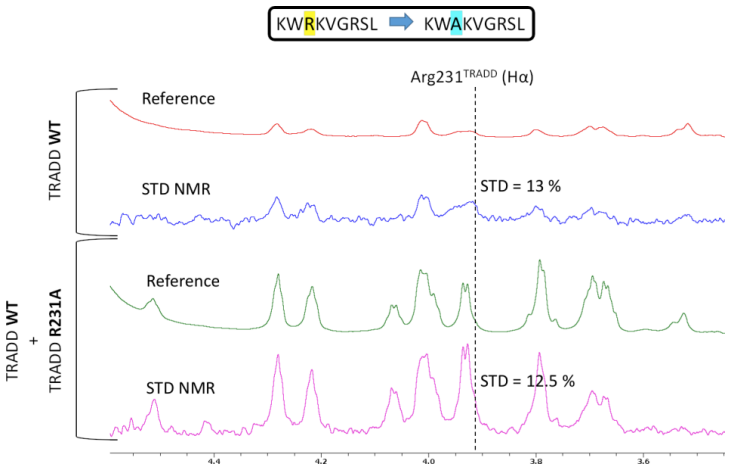

a Competition of TRADD WT with single mutant TRADD W230A. Top: reference and STD NMR spectrum of TRADD WT in the presence of SseK1; Bottom: reference and STD NMR spectrum of the same sample after addition of an equimolar concentration of the mutant TRADD W230A. **b** Competition of TRADD WT with single mutant TRADD R231A. Top: reference and STD NMR spectrum of TRADD WT in the presence of SseK1; Bottom: reference and STD NMR spectrum of the same sample after addition of an equimolar concentration of the mutant TRADD R231A. Within the experimental error, the STD intensities of TRADD WT are not affected by the addition of the mutants. This means that the affinity of the WT peptide is significantly higher than those of the mutants.

Figure 27: STD NMR competition experiments of TRADD229-237wild-type and mutants.

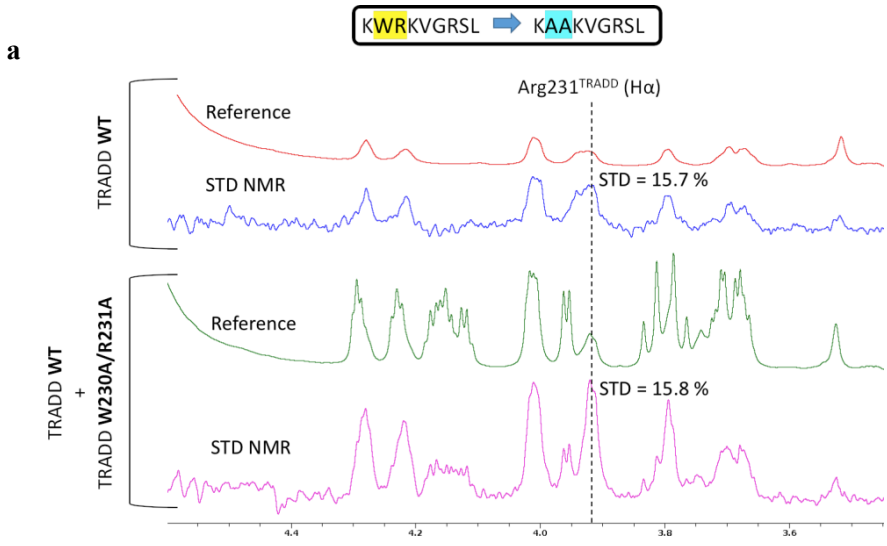

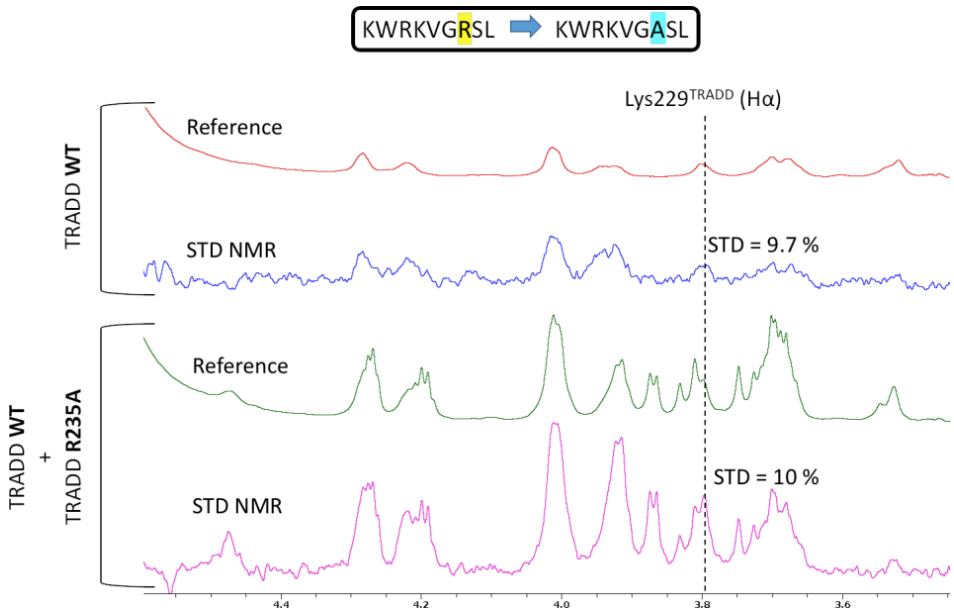

a Competition of TRADD WT with double mutant TRADD W230A/R231A. Top: reference and STD NMR spectrum of TRADD WT in the presence of SseK1; Bottom: reference and STD NMR spectrum of the same sample after addition of an equimolar concentration of the mutant TRADD W230A. **b** Competition of TRADD WT with single mutant TRADD R235A. Top: reference and STD NMR spectrum of TRADD WT in the presence of SseK1; Bottom: reference and STD NMR spectrum of the same sample after addition of an equimolar concentration of the mutant TRADD R231A. Within the experimental error, the STD intensities of TRADD WT are not affected by the addition of the mutants. This means that the affinity of the WT peptide is significantly higher than those of the mutants.

To test that hypothesis, we ran long (800 ns) Gaussian accelerated molecular dynamics (GaMD) simulations of SseK1 and SseK2 (Y. Miao, Feher, & McCammon, 2015). Principal component analysis (PCA) showed that, in both cases, the motions of largest amplitude are indeed present around the HLH domain **(Figure 28e, f)**, primarily due to rotation of the HLH towards the binding site **(Figure 28a, b)**. Noticeably, the simulations showed that SseK1 is significantly more flexible than SseK2 in the loop region connecting the HLH **(Figure 28e, f)**. Additionally,

significant differences were observed at the tip of the HLH, as SseK2 exhibited a substantial tilting motion towards the binding site **(Figure 28c, d)**. These data reveal that there exist significant differences in the dynamics of the HLH domain between SseK1 and SseK2 that affect the HLH domain approach towards the substrate binding pocket, which could explain the differences in substrate specificity of these two enzymes and in turn, glycosylation.

Figure 28 Long Gaussian accelerated MD simulations predict significant differences in the dynamics of HLH domain between SseK1 and SseK2.

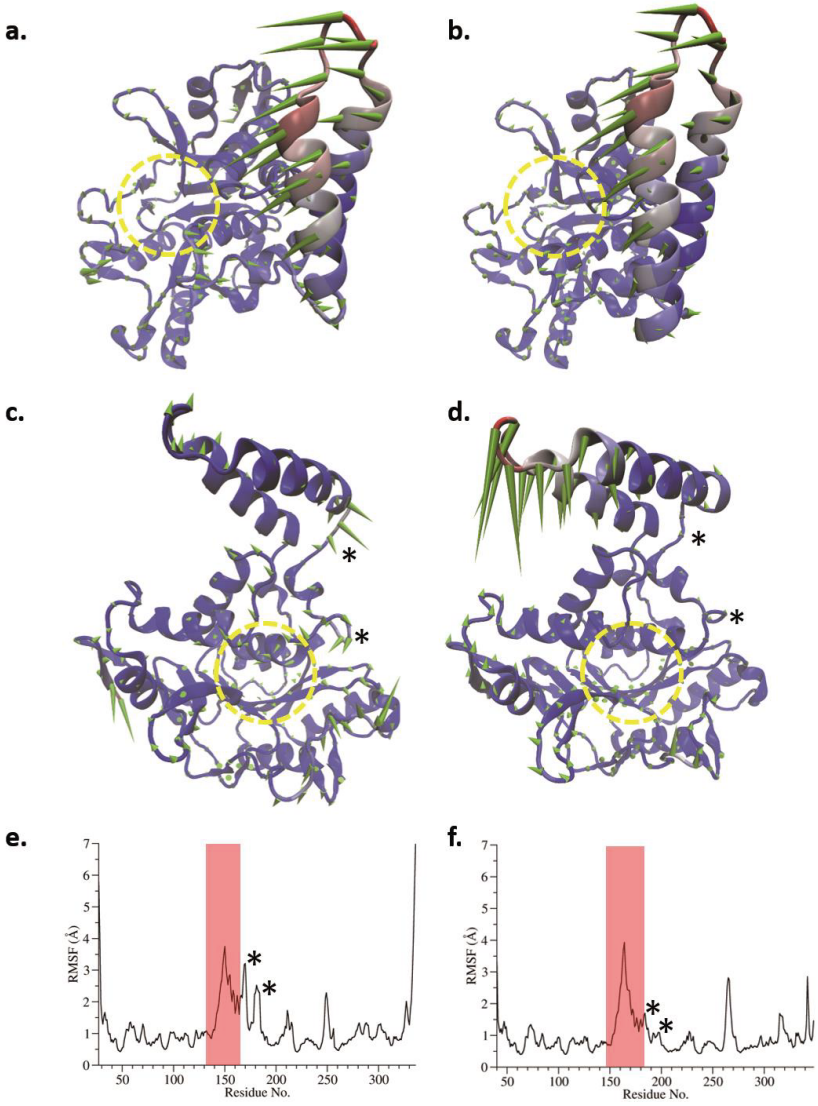

a, **b** Cartoon representation of SseK1 (left) and SseK2 (right), showing the first eigenvector from principal component analysis. Green cones indicate the direction of motion. The magnitude of motion is

represented both by cone length and by cartoon color scheme (high (red) –low (blue)). The UDP-binding site is highlighted by a dashed yellow circle. **c**, **d** Cartoon representation of SseK1 (left) and SseK2 (right), showing the second eigenvector from principal component analysis. Green cones indicate direction of motion. Magnitude of motion represented both by cone length and by cartoon color scheme (high (red) –low (blue)). UDP-binding site highlighted by dashed yellow circle. Asterisks show regions with significant differences in motional fluctuations between SseK1 and SseK2, as determined from backbone RMSF. **e**,**f** Backbone RMSF for each residue of SseK1 (left) and SseK2 (right). Red box shows HLH region. Asterisks highlight regions with significant differences between SseK1 and SseK2.

Figure 29 $FADD_{110-118}$ remains in solution in its native helical conformation, as predicted from NMR chemical shift indexing.

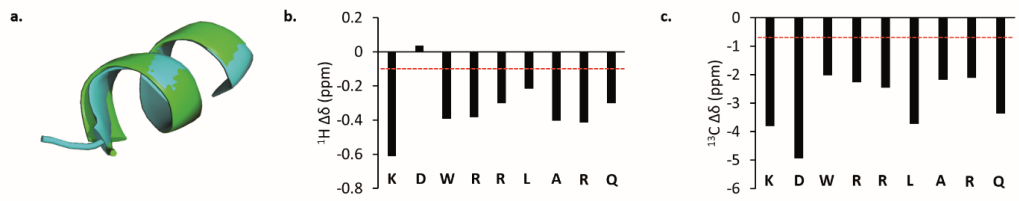

a Overlaid structures of $FADD_{110-118}$ as predicted by PEPFOLD3[1](green) and the equivalent region from the crystal structure of FADD (cyan; PDB 3EZQ). **b**, **c** Difference between random coil and observed **b**,^{1}H and **c**,^{13}C chemical shifts for $FADD_{110-118}$. Random coil shifts are corrected for neighbors (Gloster, 2014), temperature and pH (H. Zhang et al., 2014). Threshold for helicity shown as red dotted line (Lairson et al., 2008; Pearson et al., 2013).

To understand further the molecular basis of substrate peptide recognition we generated a ternary SseK2: UDP-GlcNAc: $FADD_{110-118}$complex using an induced fit molecular docking protocol. Since this ternary complex was not accessible experimentally neither by X-ray crystallography nor by NMR spectroscopy, molecular modeling provides the only insight into the structure of the full complex in the presence of both the donor sugar nucleotide and the acceptor. Peptide structure prediction and NMR chemical shift indexing indicated that the

peptide remained in its native helical conformation **(Figure 29)**. Docking of $FADD_{110-118}$ was only possible using the SseK2 structure with the C-terminal lid in the open conformation, since the closed lid precludes access to the binding site. The resulting model was in good agreement with STD NMR data, with $Trp112^{FADD}$ and $Arg113^{FADD}$ in close proximity to the protein surface **(Figure 30a, b)**. In addition, the sidechain of $Arg113^{FADD}$ was also found in close proximity to His260, Glu271, and Asn338, as observed in the docking of the acceptor Arg to the SseK2-UDP-GlcNAc crystal structure **(Figure 30c** and see below**)**.

Figure 30 Induced fit docking 3D molecular model, in agreement with STD NMR data, of the complex of SseK2 with UDP-GlcNAc and $FADD_{110-118}$.

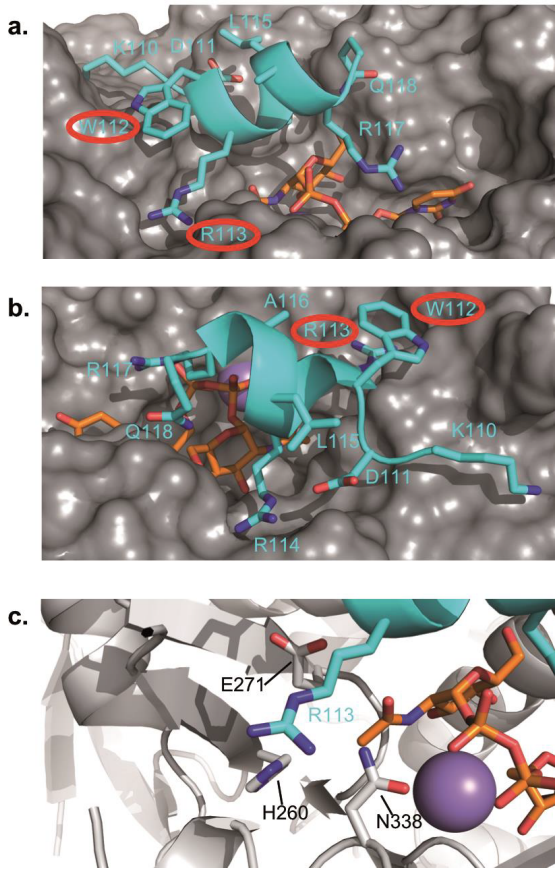

a, **b**, **c** Different views of the 3D molecular model of the complex between SseK2 (grey surface) and FADD110-118(blue cartoon/sticks). UDP-GlcNAc shown as orange sticks. In **a** and **b** red circles indicate the WR motif that shows strongest STD signals. Hydrogen atoms omitted for clarity.

Furthermore, it was possible to graft the published 3D structure of the full-length FADD protein (PDB 3EZQ) into our SseK2: UDP-GlcNAc: $FADD_{110-118}$ model complex without any significant atomic overlap (**Figure 31**). We wanted to investigate whether the presence of the GlcNAc ring in the donor substrate might have an impact on the acceptor binding mode, and to analyze the dynamics of the full ternary SseK2: UDP-GlcNAc: FADD. We subjected this complex to a 500 ns Gaussian GaMD simulation. PCA showed that the most significant motions involved rotation and translation (**Figure 32a, b**) of both the SseK2 HLH and the FADD C-terminal α-helix towards one another. A distinct energy minimum was observed at short inter-helical distances (**Figure 32c**). At this minimum, a clear intermolecular complementarity was observed. In particular, electrostatic interactions were observed between $Lys176^{SseK2}$ and $Asp175^{FADD}$, and between $Asp180^{SseK2}$ and $Arg166^{FADD}$ (**Figure 33a**). $Leu172^{FADD}$ interacts with a hydrophobic patch defined by $Val169^{SseK2}$ and $Leu170^{SseK2}$. The α3-helix of FADD is highly negatively charged and interacts closely with Lys264, Arg348, and the manganese ion of SseK2 (**Figure 33b**). Our simulation suggests that Asp123 of FADD directly coordinates the manganese ion. Finally, along the 500 ns of the GaMD simulations, significant conformational rearrangements of the arginine side chains in the $FADD_{110-118}$ region were observed (**Figure 34a-d**). On average, Arg117 of FADD is the residue from FADD showing the shortest distance to the C_1anomeric carbon of UDP-GlcNAc, and is the only one simultaneously establishing close contacts with His260, Glu271, and the beta-phosphate of UDP-GlcNAc.

Figure 31 3D molecular model of the complex of SseK2 with UDP-GlcNAc and full FADD.

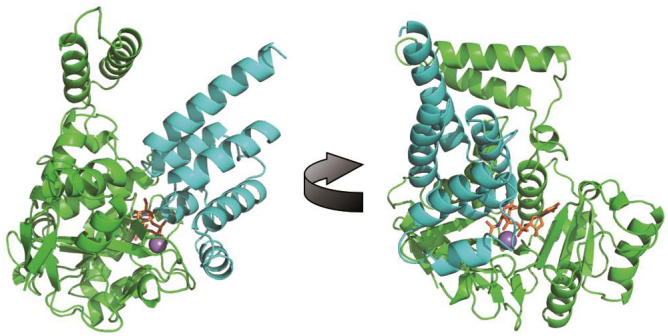

Cartoon representation of the 3D model of the SseK2: UDP-GlcNAc: FADD complex generated by grafting the FADD crystal structure (3EZQ) onto the previously docked $FADD_{110\text{-}118}$ structure. SseK2 shown in green, FADD in blue, Mn^{2+}as a purple sphere, and UDP-GlcNAc as orange sticks. Hydrogen atoms omitted for clarity.

Figure 32 Molecular dynamics of the 3D molecular modelof the complex of SseK2 with UDP-GlcNAc and full FADD.

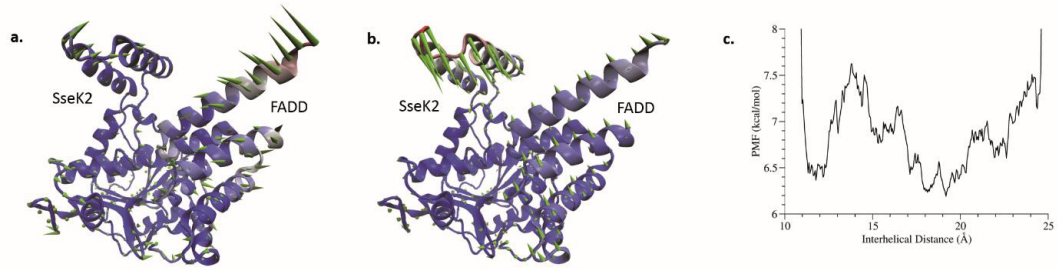

Cartoon representation of the SseK2: UDP-GlcNAc: FADD complex, showing **a** the first and **b** second eigenvectors from principal component analysis. Green cones indicate direction of motion. Magnitude of motion represented both by cone length and by carton color scheme (high (red) –low (blue)). **c** Potential of mean force calculated as a function of interhelical distance by reweighting boost potentials from Gaussian aMD simulations. Reweighting was calculated by cumulant expansion to the second order. Interhelical distance defined as distance between the center of mass of the backbone heavy atoms of $SseK2_{168\text{-}177}$ and $FADD_{170\text{-}177}$.

Figure 33 Molecular dynamics of the 3D molecular model of the complex of SseK2 with UDP-GlcNAc and FADD.

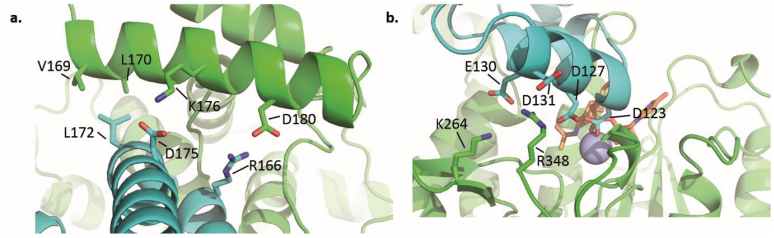

a and **b** Representative structure of the SseK2: UDP-GlcNAc: FADD complex from GaMD simulations, showing close helical contact between the two proteins. Cartoon representation of SseK2 (cyan) and FADD (green) backbone, key sidechains shown as sticks, UDP as orange sticks, and Mn^{2+}as purple sphere. Hydrogen atoms are omitted for clarity.

Figure 34 Molecular dynamics of the docking model of the ternary SseK2:UDP-GlcNAc:FADD complex show significant conformational rearrangements of Arg113, Arg114, and Arg117 of FADD, orienting Arg117 for a front face attack to GlcNAc, and support the relevance of Glu271 and His260 in acceptor FADD substrate binding.

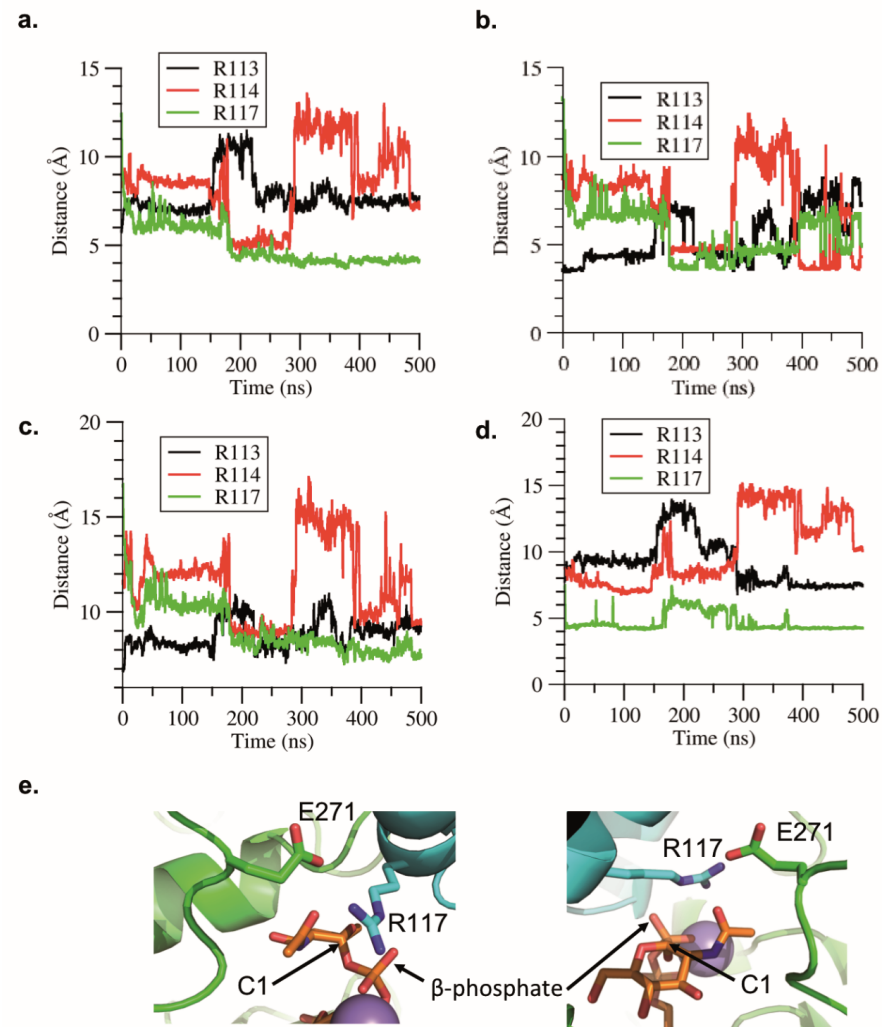

Representative distances (Å) for contacts between the center of mass of the guanidinium groups of Arg113 (black lines), Arg114 (red lines), and Arg117 (green lines) of FADD and **a** the anomeric carbon of GlcNAc of UDP-GlcNAc, **b** the center of mass of the carboxylate group of Glu271 of SseK2, **c** the center of mass of the imidazole group of His260 of SseK2, **d** the center of mass of the beta-phosphate of UDP-GlcNAc. On average, Arg117 of FADD is the residue from FADD closest to the anomeric carbon of GlcNAc and is the only residue establishing close contacts with His260, Glu271, and the beta-

phosphate of UDP-GlcNAc. **e** Representative structure of the ternary complex of SseK2 (green), FADD (cyan) and UDP-GlcNAc (orange) from GaMD simulations, showing that Arg117 is properly oriented for a front face attack with close contact with the anomeric carbon of the UDP-GlcNAc donor substrate. Manganese is shown as a purple sphere and hydrogen atoms are omitted for clarity.

Together, these data provide evidence for specific recognition of FADD by SseK2 via interactions far from the active site, which may provide insight into differences in substrate glycosylation specificity of SseK1 and SseK2. These data also suggest that Arg117 is the best oriented residue from FADD for accepting the transferred glycosyl from the donor UDP-GlcNAc, in keeping with the role of this residue as the only acceptor site in FADD (S. Li et al., 2013; Pearson et al., 2013).

Catalytic importance of HEN motif. In the SseK2-UDP-GlcNAc crystal structure (chain D), Asn272 (corresponding to $Asn256^{SseK1}$) is closer to the C_1 anomeric carbon of UDP-GlcNAc (5.1 Å) as compared to Glu271 (5.6 Å). These data indicate that the Asn272 may play an important role in binding and catalysis. In addition, Glu271 is located at the entrance of the putative acceptor arginine-binding site. To obtain insight into the importance of these residues in substrate recognition, we conducted in-silico docking of the acceptor Arg to the SseK2-UDP crystal structure. It was observed that a closed conformation of SseK2 structure possesses a putative acceptor substrate binding site pocket that is connected to the anomeric carbon of GlcNAc. We used a closed conformation of SseK2 with a putative acceptor substrate binding site pocket connected to the anomeric carbon of GlcNAc for automated computational docking (Discovery Studio, Accelrys). As a result, the negatively charged pocket of the concave active site interacts with the positively charged guanidine group. In particular, Glu271, the β-phosphate

of UDP, and His260 were located in a position suitable for hydrogen bonding (**Figure 35a**). All of these residues are highly conserved in the SseK and NleB families (**Figure 18**).

Figure 35 Docking structure of acceptor substrate binding mode.

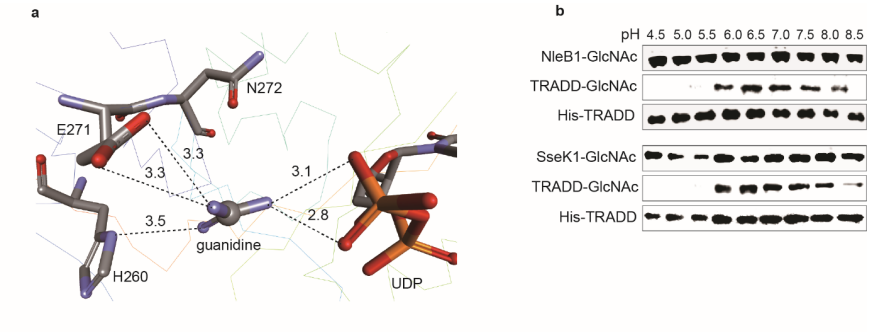

a Guanidine docking at the active site of the UDP boundSseK2 crystal structure. His260, Glu271, and the β-phosphate of UDP interact with guanidine via hydrogen bonding. Dashed lines represent hydrogen bonds. **b** pH-dependency of NleB1 and SseK1.Glycosylated TRADD was detected using a GlcNAc-arginine specific antibody.

In the docking structure of SseK2, a single negatively charged residue ($Glu271^{SseK2}$) and an additional β-phosphate from UDP are in close contact to the guanidinium group of the acceptor Arg. The $Glu271^{SseK2}$corresponds to the $Glu253^{NleB1}$ whose mutation to Ala did not inhibit NF-κB signaling (S. Li et al., 2013), in agreement with the importance of this residue in glycosylation of the acceptor Arg. Further studies are required to determine its precise role either in catalysis or binding (see below).

In addition, $His260^{SseK2}$ is located near the guanidinium group of the acceptor Arg. A pH activity profile for both SseK1 and NleB1 revealed that NleB1 and SseK1 have an optimal pH between 6.0 ~ 8.0 and 6.0 ~ 8.5, respectively (**Figure 35b**). This highlights the potential role of histidine as a catalytic base because the pK_a value of histidine is ~ 6.0. To test the role of these residues in substrate recognition and catalysis, we mutated His260, Glu271, and Asn272, which

together form the 'HEN' motif. This motif is highly conserved at both the primary sequence and tertiary structure levels (**Figure 36**). Wild-type (WT) SseK1 and the HEN motif single mutants were overexpressed with TRADD in HEK293T cells. WT SseK1 inhibited cPARP production (**Figure 37a**). As expected, the DxD-AxA double mutant, resulted in an increase in cPARP level. The HEN motif single mutants (His260, Glu271, and Asn272 in SseK2) led to an increase in the cPARP levels, a similar outcome to the DxD-AxA double mutant. When we observed the oligomerization form in a non-reducing gel, TRADD oligomer was detected in the mutant forms, suggesting that each mutant loses its glycosylation activity and fails to inhibit TRADD oligomerization.

Figure 36 Structural conservation of the HEN motif.

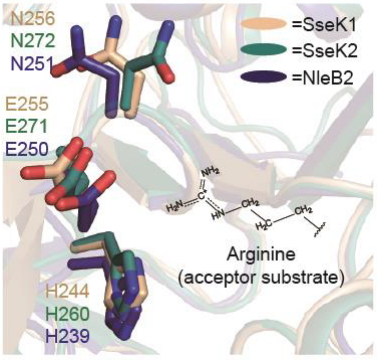

Superimposition of SseK1, SseK2, and NleB2 based on the C-αand each HEN motif is shown in stick shape. Acceptor substrate (arginine) was sketched in the putative binding site based on the docking model. The three structures are expressed in different colors.

NF-κB activity data in A549 cells correlated highly with the results from the PARP cleavage assay (**Figure 37b**). Surprisingly, NF-κB levels increased more in H244A, E255A, and N256A than in the AxA mutant. Furthermore, we also investigated enzyme kinetics using the L-arginine substrate and the purified recombinant SseK1 and SseK2 (**Figure 37c, 38a**). The catalytic activities of the mutants (H244A/H260A, E255A/E271A, and N256A/N272A in SseK1/SseK2) decreased significantly compared to WT, though they were not essential for activity. The

H244A/H260A and N256A/N272A mutants showed lower catalytic activity than the DxD-AxA double mutant.

We also studied the glycosylation activity of WT and HEN mutant enzymes in vitro, in cell culture, and in mouse infection experiments using *C. rodentium*. We first incubated NleB1, NleB2, SseK1, or SseK2 with FADD, TRADD, or GAPDH. We observed that, consistent with previous studies (El Qaidi et al., 2017; X. F. Gao et al., 2013), WT NleB1, SseK1, and SseK2 glycosylated FADD (**Figure 37d**). None of the point mutations in the HEN motif of any of the enzymes retained the ability to glycosylate FADD (**Figure 37d**). Similar data were observed in studies of TRADD and GAPDH glycosylation (**Figure 37e, f**). We also noticed that NleB1 and SseK1 are self-glycosylated, though the functional importance of this modification is unknown. We also measured the ability of NleB1 and SseK1 to glycosylate TRADD and GAPDH when co-transfected into HEK 293T cells. We immunoprecipitated TRADD or GAPDH using an anti-FLAG antibody and then performed Western blotting for Arg-GlcNAc. Similar to our *in vitro* studies, we failed to observe any glycosylation of host substrates by any HEN mutation (**Figure 37g, h**).

To extend these data, we conducted a series of mouse challenge experiments with *Citrobacter rodentium*. *C. rodentium* has only 1 copy of NleB, which functions similarly to EHEC NleB1 (El Qaidi et al., 2017). To evaluate whether the HEN motif of NleB is important to *C. rodentium* virulence, we deleted the *C. rodentium nleB* gene and then complemented this mutant with different EHEC *nleB1* and *nleB2* expression plasmids. We infected mice with *C. rodentium* Δ*nleB* strains expressing either WT NleB1 (Δ*nleB*/p*nleB1*) or the HEN mutants H242A, E253A, and N254A. Mice infected with Δ*nleB C. rodentium* showed an approximately 100-fold reduction in colonization magnitude after 14 days, as compared with WT *C. rodentium*,

in support of previous findings (X. F. Gao et al., 2013) (**Figure 37i**). While this mutant was fully complemented by expressing WT EHEC NleB1, none of the HEN mutants complemented the colonization defect (**Figure 37i**). Additionally, neither WT EHEC NleB2 nor an NleB2 mutant in which all HEN amino acids were mutated to alanines complemented the colonization defect. These data demonstrate that the HEN motif is highly important for enzymatic activity and virulence.

Figure 37 HEN motif plays a key role in NleB/SseK enzyme activity.

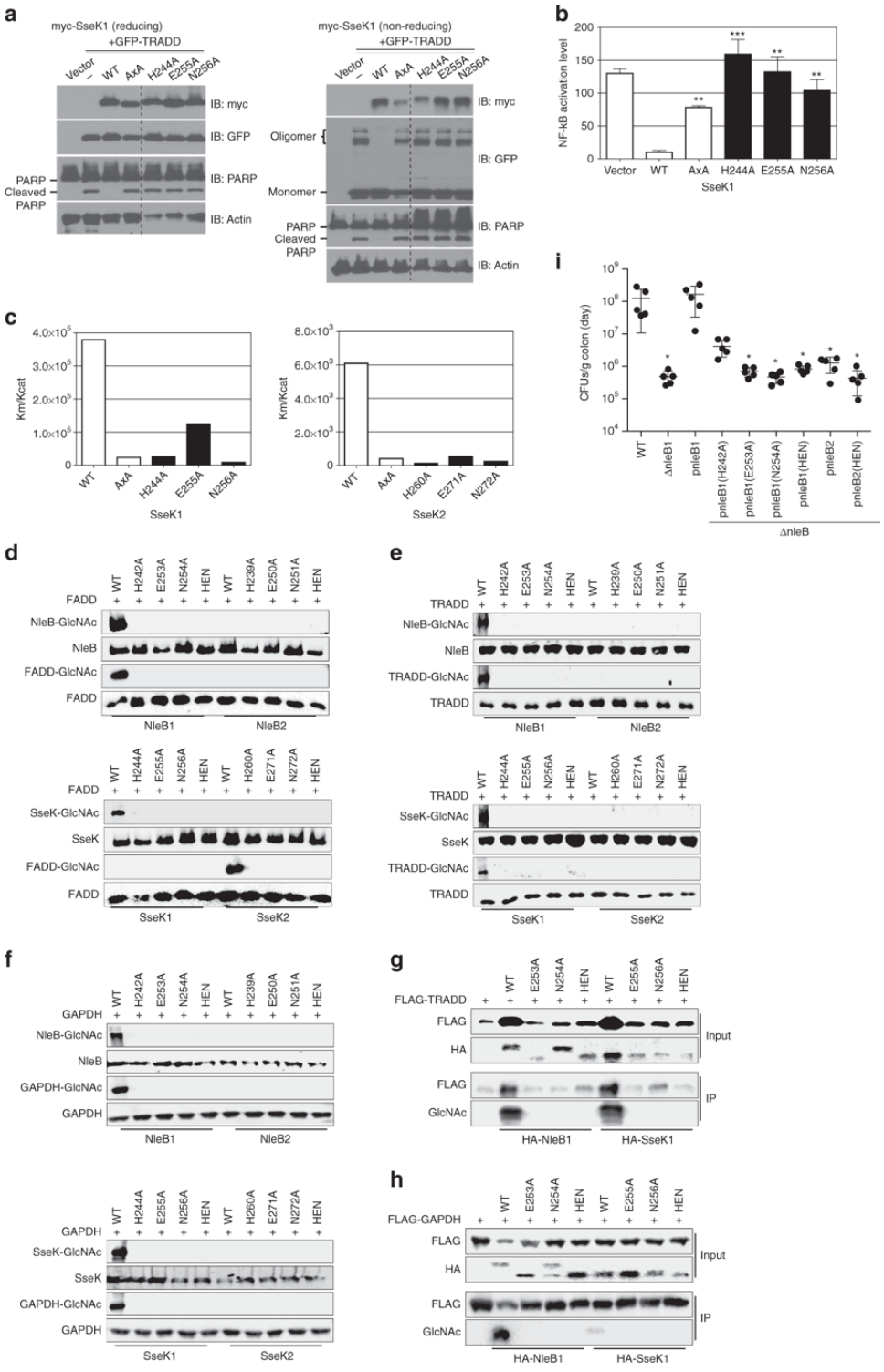

a SseK1 mutants were generated and the cellular function in HEK293T cells was investigated. A non-reducing gel (right panel) was used to confirm the presence of the TRADD oligomer. Mutants in red represent mutations of residues proposed to be catalytically important. Data represent at least three

repetitions. **b** The NF-κB level in A549-NF-κB luc cells was measured to check the enzymatic functions. Data represent the mean and standard deviation in triplicate. Multiple comparisons perform by one-way ANOVA followed by Turkey's Multiple Comparison Test (**$P < 0.01$, ***$P < 0.001$ compare to WT). **c** Enzyme kinetic assays of SseK1 and SseK2, respectively. **d** *In vitro* glycosylation of FADD by NleB1, NleB2 (top panel) and SseK1 and SseK2 HEN mutants (bottom panel). **e** *In vitro* glycosylation of TRADD by NleB1, NleB2 (top panel) and SseK1 and SseK2 HEN mutants (bottom panel). **f** *In vitro* glycosylation of GAPDH by NleB1, NleB2 (top panel) and SseK1 and SseK2 HEN mutants (bottom panel). **g** Glycosylation of TRADD after co-transfection with either NleB1 or SseK1 (WT and HEN mutants) in HEK293T cells. FLAG-TRADD was immunoprecipitated and then immunoblotted using an anti-Arg-GlcNAc antibody. **h** Glycosylation of GAPDH after co-transfection with either NleB1 or SseK1 (WT and HEN mutants) in HEK293T cells. FLAG-TRADD was immunoprecipitated and then immunoblotted using an anti-Arg-GlcNAc antibody. **i** Colonization (log10 CFUs/g colon) of indicated *C. rodentium* strains (14 days post-gavage) in C57BL/6 J mice ($n = 6$). Asterisks indicate significantly different colonization magnitude as compared to WT; Kruskal-Wallis test. Uncropped blots are shown in **Figure 39, 40**.

Figure 38 Enzyme kinetics assay using recombinant proteins.

a

SseK1	Km (uM-1) *P-Value	Kcat (s-1) *P-Value	Kcat/Km (uM-1/s-1)	Relative catalytic efficacies (%)
WT	0.06 ± 0.01 *0.0629	23466 ± 666.7 *<0.0001	379279.10	
DxD	0.19 ± 0.06 0.0019	4551 ± 230.67 *<0.0001	23398.46	6.17
H244A	0.27 ± 0.05 0.0216	7104 ± 221.27 *<0.0001	26676.68	7.03
E255A	0.13 ± 0.004 0.0379	16416 ± 188.8 *<0.0001	124741.60	32.89
N256A	0.48 ± 0.06 0.0049	4148 ± 168.88 *<0.0001	8674.20	2.29

SseK2	Km (uM-1) *P-Value	Kcat (s-1) *P-Value	Kcat/Km (uM-1/s-1)	Relative catalytic efficacies (%)
WT	0.33 ± 0.07 *0.0072	2026 ± 57.71 *0.0002	6093.23	
DxD	1.76 ± 0.56 *<0.0001	713.9 ± 69.60 *0.0044	405.63	6.66
H260A	1.75 ± 0.27 *0.0002	219.5 ± 48.28 *0.0561	125.64	2.06
E271A	0.91 ± 0.16 *0.0006	494.2 ± 64.28 *0.0404	544.57	8.94
N272A	1.69 ± 0.28 *0.0003	400.4 ± 88.79 *0.1146	237.63	3.90

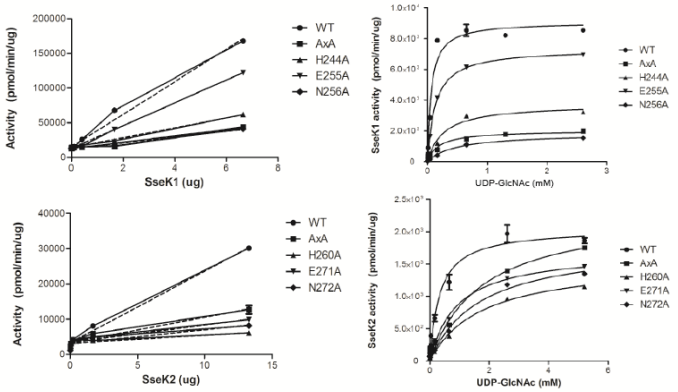

b

	SseK1			
GAPDH	Km (uM) *P-Value	Kcat (s-1) *P-Value	Kcat/Km (uM/s-1)	Relative catalytic efficacies (%)
WT	2.36 ± 0.74 *0.1273	101.00 ± 3.51 *<0.0001	42.83	
WA	3.19 ± 0.53 *0.0589	55.25 ± 3.74 *0.0001	17.34	40.49
RA	2.88 ± 0.73 *0.0913	58.44 ± 2.43 *0.0007	20.28	47.35
AA	4.97 ± 0.72 *0.0144	36.75 ± 2.27 *0.0005	7.40	17.28

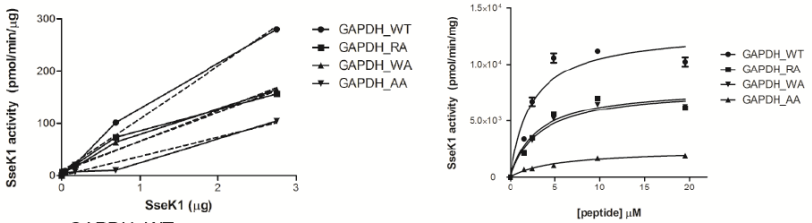

GAPDH_WT: TVDGPSGKLWRDGRGAL
GAPDH_WA (W196A): TVDGPSGKLARDGRGAL
GAPDH_RA (R197A): TVDGPSGKLWADGRGAL
GAPDH_AA (W196A, R197A): TVDGPSGKLAADGRGAL

a Point mutant constructs were generated by PCR based point-mutagenesis and purified by Ni-NTA and size-exclusion chromatography. UDP-Glo™ Glycosyltransferase Assay kit (Promega, #V6961) was

carried out as per manufacturer's instructions. L-arginine (>98.5% purity, Duchefa BIOCHEMIE) was used as an acceptor substrate. **b** SseK1 enzyme kinetics assay data for $GAPDH_{187-203}$ synthetic peptide and mutant forms of the WR motif. Plates were read using a VICTOR5 (PerkinElmer) device. Graph generation and calculation of each K_m and K_{cat} values are automatically calculated using the *GraphPad Prism* 5 software program. The data represent at least two repetitions. The final specific activity of the transfer reaction was corrected considering the hydrolysis reaction, which was performed using SseK1/SseK2, UDP-GlcNAc and $MnCl_2$. Plus-minus values are mean ± SE.

Figure 39 Uncropped images of **Figure 37a** blots.

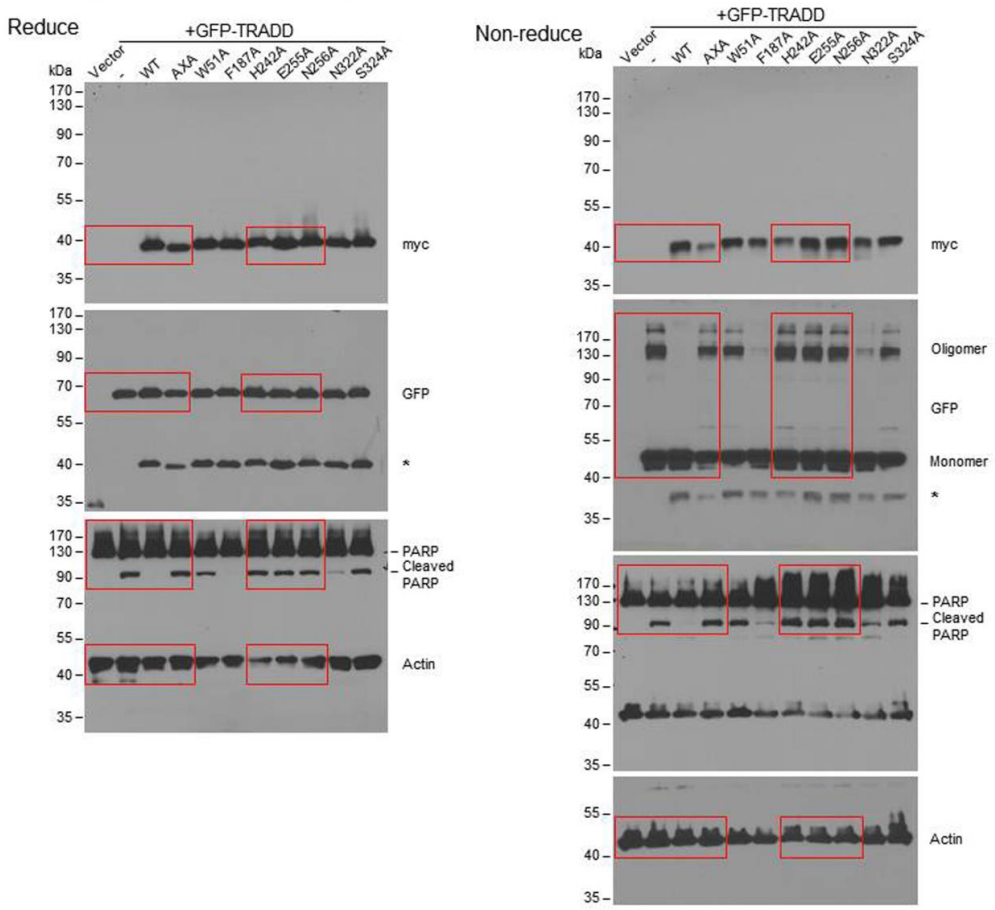

Figure 40 Uncropped images of **Figure 37d-h** and **Figure 35b** blots

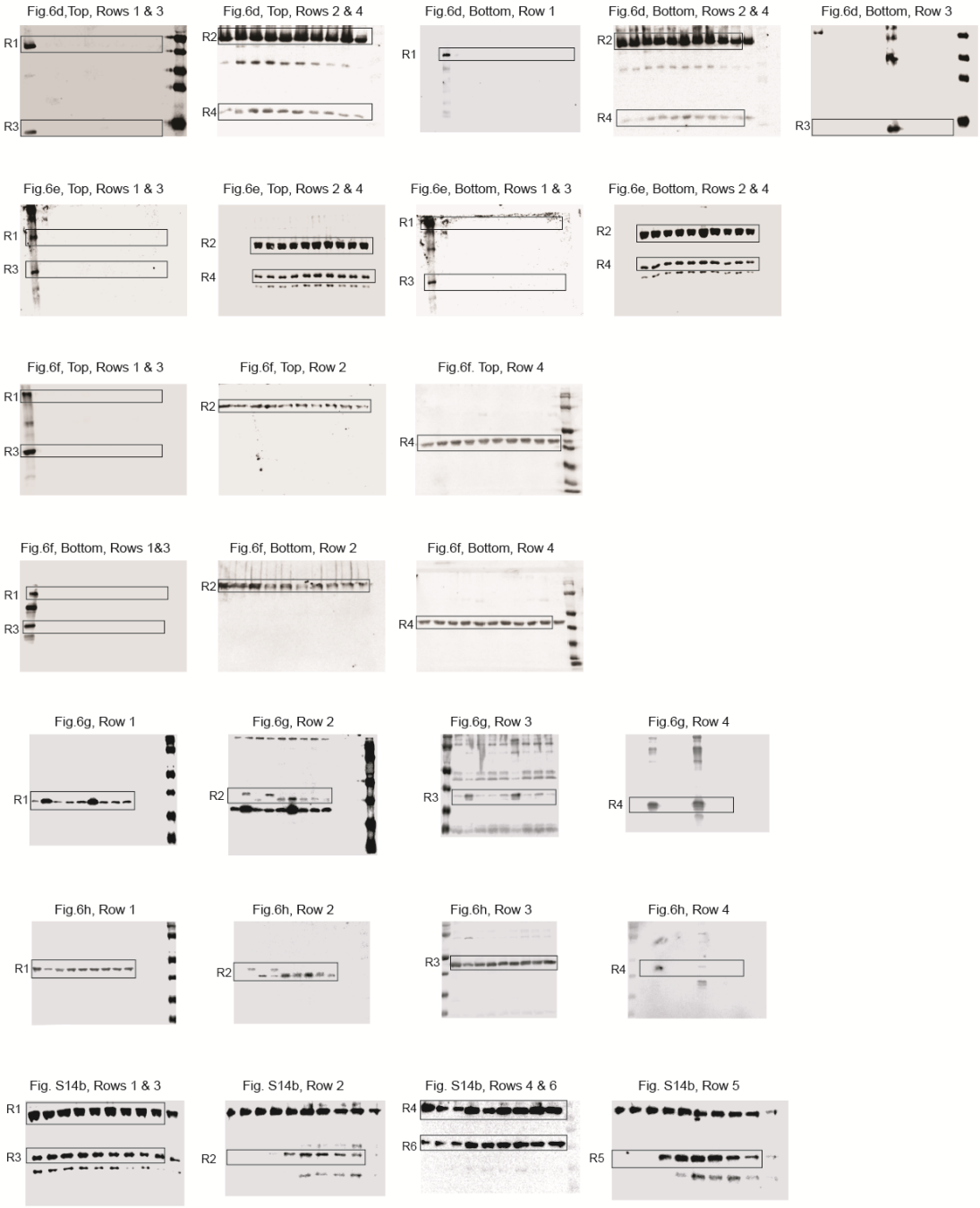

Discussion

The overall crystal structures of SseK1 and SseK2 from *S. typhimurium* as well as NleB2 from enteropathogenic *E. coli* are similar, revealing high identities between the amino acids at the

active binding site level. These enzymes glycosylate the guanidinium moiety of Arg residues, which are residues with poor nucleophilic character because electrons on this moiety are partially delocalized. In addition, we identified several characteristics in the active site that are compatible with an S_Ni mechanism and with the role of HEN motif residues in catalysis: (a) we experimentally demonstrate by NMR that these enzymes are retaining GTs; (b) donor-substrate-mediated fixation of the C-terminal lid could shield the active site from the hydrophilic environment, avoiding unwanted hydrolysis of UDP-GlcNAc, -a behavior reported in other retaining GT-A fold GTs such as *Legionella pneumophila* glucosyltransferase (Hurtado-Guerrero et al., 2010) and the toxin B; (Reinert, Jank, Aktories, & Schulz, 2005) (c) mutations of the HEN motif lead to a significant reduction in glycosylation both at in vitro and in vivo levels, implying that these residues affect enzyme catalysis. Based upon our kinetic, structural, and computational studies, we suggest that His and Glu might improve the poor nucleophile character of the acceptor Arg guanidinium moiety to facilitate catalysis; and (d) based on our MD simulations, the acceptor Arg is facing the anomeric carbon, which is compatible with a front face mechanism for glycosyl transfer with retention of anomeric configuration.

Each HEN residue of SseK3 is on the β-strand, but in the case of SseK1, SseK2, and NleB2, the HEN residues are located on the loop structure. This has implications for the differences in the activity of the enzymes due to the HEN motif because the loop structure is more flexible than the β-strand. In addition, there are differences in the regulation of the C-terminal lid domain between SseK1, SseK2, and SseK3. The arginine on the C-terminus participates in an interaction with UDP-GlcNAc in SseK2 and SseK3, but not in SseK1. Based on this result, the departure of the leaving group is likely to be easier, due to a weaker enzyme-substrate interaction network in

SseK1, than in SseK2 and SesK3. We suggest that this may also be a reason for the differences in enzyme activity in the SseK family.

Although the tertiary structure of NleB1 is likely similar to NleB2, SseK1, and SseK2, a previous study has reported that NleB2 has a lower activity than NleB1 on the same target (TRADD) (S. Li et al., 2013). In this study, we also demonstrate that the enzymatic activity of SseK1 is ~ 62 times higher than that of SseK2 based on enzyme kinetic assays. The substrate specificities of the NleB/SseK family of *C. rodentium*, *Escherichia coli* and *Salmonella enterica* are different (El Qaidi et al., 2017). Based on these differences, we can infer from the crystal structures that these discrepancies between orthologs of this family might be attributed partially to the HLH domain, which is a structural feature not present in other GTs (**Figure 41a**). The amino acids of this domain are not conserved and are structurally flexible (**Figure 41b**), as confirmed by the long GaMD simulations (**Figure 28**). The flexible HLH domain is close to the active site, which indicates this domain may be involved in the recognition of the acceptor protein substrates containing death domains. In fact, GaMD simulations of the grafted SseK2: UDP-GlcNAc: FADD complex show that the HLH domain interacts directly with FADD C-terminal α-helix through side chain complementarity (**Figure 33**). These data support the role of the HLH domain in the recognition of the acceptor protein substrates containing death domains.

STD NMR spectroscopy revealed that, in contrast to their enzymatic activity profile, both SseK1 and SseK2 interact with all short peptides from FADD, TRADD, and GAPDH (**Figure 22, 23**). Each of these peptides contains a conserved WR-motif, which forms a key structural requirement for binding to the enzymes, as revealed by STD NMR spectroscopy and molecular modeling. Therefore, it appears that recognition of death domains may be due to complementarity with the active site, whilst distinction between different death domain-containing proteins is mediated

through interactions far from the active site. Overall our data provide compelling evidence of the molecular basis for Arg glycosylation, the differences in substrate specificity among orthologs, and will provide a framework for the design of pan-NleB/SseK inhibitors targeting enteric pathogens.

Figure 41 Flexible structure of the HLH domain.

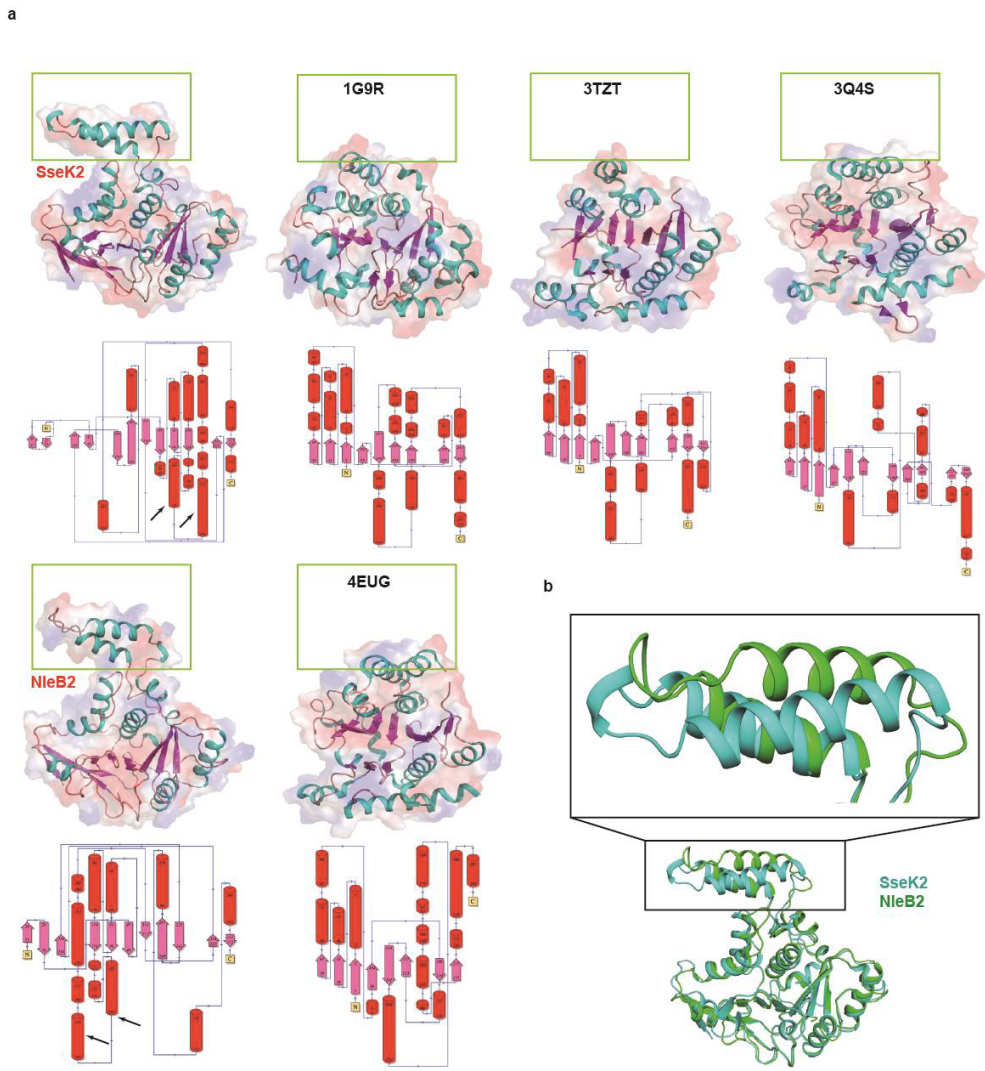

SseK and NleB have a protruding helix-loop-helix (HLH) domain. **a** Protein structures were arranged based on beta-sheet (purple color) similarity and the HLH region is shown as a yellowish green quadrangle (each upper panel). Protein structure topology is also shown in the lower panel using the *PDBSUM* website. The HLH domains are indicated by black arrows. The four letters in the yellow-green

rectangles indicate the PDB access codes. **b** Superimposition between SseK1, SseK2, and NleB2 based on the amino acid backbone C-αcarbons.

Chapter 5 - Conclusions

To survive and multiply in a host, microbial pathogens evolve strategies to deliver arsenals of effectors, disrupt host homeostasis, and subvert host innate immune responses.

In this thesis work, we characterized bacterial T3SS effectors and their interactions with the host NF-κB signaling pathway.

In the first project of this thesis (Chapter 2), we identified a new T3SS effector that impacts RPS3/NF-κB activities in the host nucleus and elucidated the mechanism. Our work demonstrated that SseL targets the RPS3/NF-κB pathway and decreases nuclear RPS3. Human RPS3 contains twenty lysine residues that are potential ubiquitination sites (Danielsen et al., 2011; Wagner et al., 2011). Our work and previous findings (Jung et al., 2017; Simms et al., 2017; Sundaramoorthy et al., 2017) indicate that RPS3 can be ubiquitinated and regulatory RPS3 ubiquitination plays an important role in regulating mammalian ribosome-associated quality control pathways. In addition, non-ribosomal RPS3 is protected from ubiquitnation and proteasome-dependent degradation to help retain ribosome function and biogenesis (T. S. Kim et al., 2006). SseL is a deubiquitinase (Pruneda et al., 2016). We performed pulldown and co-immunoprecipitation assays to provide in vivo and in vitro evidence to show a direct interaction between RPS3 and SseL, and this phenotype was dependent upon SseL DUB activity. Our work provides evidence that SseL deubiquitinates RPS3 in mammalian cells, while the SseL C262A mutant did not alter RPS3 nuclear translocation and lost the ability to deubiquitinate RPS3. Our work might provide a potential target for the development of anti-inflammatory agents targeting NF-κB signaling. For the future work, efforts can be made to first determine the specific E3

ligase for nuclear RPS3 ubiquitination and what residue of RPS3 is ubiquitinated that contributes to RPS3 translocation.

In Chapter 3, we identified a cofactor functioning between the host kinase protein IKKβ and the bacterial virulence effector NleH1. By employing mass spectrometry, we determined that Hsp90 interacts with both NleH1 and IKKβ. A previous study had shown that Hsp90 binds directly to RPS3 and inhibition of Hsp90 activity induces the degradation of free forms of RPS3 (T. S. Kim et al., 2006). Our work further determined that inhibition of Hsp90 activity blocks TNF-mediated RPS3 nuclear translocation and p65 nuclear translocation, and we also identified a direct interaction between NleH1 and IKKβ, suggesting that Hsp90 is an important cofactor. In addition, the absence of NleH1 abolished the reduction in EHEC adherence in the context of Hsp90 inhibition, which suggests interaction between NleH1 and Hsp90 is crucial for bacterial virulence. As IKKβ has many important roles in normal cellular function, developing multiple mechanisms that selectively target IKKβ signaling could be a very interesting prospect. For the future direction, it is necessary to better understand the mechanism on the interaction between NleH1 and Hsp90.

In Chapter 4, we determined differences within the SseK/NleB family on recognition of the sugar nucleotide and peptide substrates and found some common features governing substrate recognition. Our work showed that *Salmonella* SseK1 and SseK2, and *E. coli* NleB1 are orthologs that behave as NleB1-like glycosyltransferases. They are retaining glycosyltransferases and comprises three domains including helix-loop-helix (HLH), lid, and catalytic domains. The HLH domain plays an important role in the recognition of the acceptor protein substrates containing death domains. His-Glu-Asn (HEN) motif in the active site is essential for enzyme catalysis. Our work provides compelling evidence of the molecular basis for Arg glycosylation,

the differences in substrate specificity among orthologs, and will provide a framework for the design of pan-NleB/SseK inhibitors targeting enteric pathogens.

References

Alkalay, I., Yaron, A., Hatzubai, A., Orian, A., Ciechanover, A., & Ben-Neriah, Y. (1995). Stimulation-dependent I kappa B alpha phosphorylation marks the NF-kappa B inhibitor for degradation via the ubiquitin-proteasome pathway. *Proc Natl Acad Sci U S A, 92*(23), 10599-10603.

Bakshi, C. S., Singh, V. P., Wood, M. W., Jones, P. W., Wallis, T. S., & Galyov, E. E. (2000). Identification of SopE2, a Salmonella secreted protein which is highly homologous to SopE and involved in bacterial invasion of epithelial cells. *J Bacteriol, 182*(8), 2341-2344.

Baruch, K., Gur-Arie, L., Nadler, C., Koby, S., Yerushalmi, G., Ben-Neriah, Y., . . . Rosenshine, I. (2011). Metalloprotease type III effectors that specifically cleave JNK and NF-kappa B. *Embo Journal, 30*(1), 221-231.

Batchelor, M., Prasannan, S., Daniell, S., Reece, S., Connerton, I., Bloomberg, G., . . . Matthews, S. (2000). Structural basis for recognition of the translocated intimin receptor (Tir) by intimin from enteropathogenic Escherichia coli. *EMBO J, 19*(11), 2452-2464. doi:10.1093/emboj/19.11.2452

Battye, T. G., Kontogiannis, L., Johnson, O., Powell, H. R., & Leslie, A. G. (2011). iMOSFLM: a new graphical interface for diffraction-image processing with MOSFLM. *Acta Crystallogr D Biol Crystallogr, 67*(Pt 4), 271-281. doi:10.1107/S0907444910048675

Bayer-Santos, E., Durkin, C. H., Rigano, L. A., Kupz, A., Alix, E., Cerny, O., . . . Holden, D. W. (2016). The Salmonella Effector SteD Mediates MARCH8-Dependent Ubiquitination of MHC II Molecules and Inhibits T Cell Activation. *Cell Host & Microbe, 20*(5), 584-595.

Bernal-Bayard, J., Cardenal-Munoz, E., & Ramos-Morales, F. (2010). The Salmonella Type III Secretion Effector, Salmonella Leucine-rich Repeat Protein (SlrP), Targets the Human Chaperone ERdj3. *Journal of Biological Chemistry, 285*(21), 16360-16368.

Bernal-Bayard, J., & Ramos-Morales, F. (2009). Salmonella Type III Secretion Effector SlrP Is an E3 Ubiquitin Ligase for Mammalian Thioredoxin. *Journal of Biological Chemistry, 284*(40), 27587-27595.

Beverly, L. J., Lockwood, W. W., Shah, P. P., Erdjument-Bromage, H., & Varmus, H. (2012). Ubiquitination, localization, and stability of an anti-apoptotic BCL2-like protein, BCL2L10/BCLb, are regulated by Ubiquilin1. *Proc Natl Acad Sci U S A, 109*(3), E119-126. doi:10.1073/pnas.1119167109

Bhavsar, A. P., Brown, N. F., Stoepel, J., Wiermer, M., Martin, D. D. O., Hsu, K. J., . . . Finlay, B. B. (2013). The Salmonella Type III Effector SspH2 Specifically Exploits the NLR Co-chaperone Activity of SGT1 to Subvert Immunity. *Plos Pathogens, 9*(7).

Biemans-Oldehinkel, E., Sal-Man, N., Deng, W., Foster, L. J., & Finlay, B. B. (2011). Quantitative proteomic analysis reveals formation of an EscL-EscQ-EscN type III complex in enteropathogenic Escherichia coli. *J Bacteriol, 193*(19), 5514-5519. doi:10.1128/JB.05235-11

Blasche, S., Mortl, M., Steuber, H., Siszler, G., Nisa, S., Schwarz, F., . . . Koegl, M. (2013). The E. coli Effector Protein NleF Is a Caspase Inhibitor. *PLoS One, 8*(3).

Blocker, A., Jouihri, N., Larquet, E., Gounon, P., Ebel, F., Parsot, C., . . . Allaoui, A. (2001). Structure and composition of the Shigella flexneri "needle complex", a part of its type III secreton. *Mol Microbiol, 39*(3), 652-663.

Broemer, M., Krappmann, D., & Scheidereit, C. (2004). Requirement of Hsp90 activity for I kappa B kinase (IKK) biosynthesis and for constitutive and inducible IKK and NF-kappa B activation. *Oncogene, 23*(31), 5378-5386.

Brown, N. F., Coombes, B. K., Bishop, J. L., Wickham, M. E., Lowden, M. J., Gal-Mor, O., . . . Finlay, B. B. (2011). Salmonella phage ST64B encodes a member of the SseK/NleB effector family. *PLoS One, 6*(3), e17824. doi:10.1371/journal.pone.0017824

Bruno, V. M., Hannemann, S., Lara-Tejero, M., Flavell, R. A., Kleinstein, S. H., & Galan, J. E. (2009). Salmonella Typhimurium type III secretion effectors stimulate innate immune responses in cultured epithelial cells. *PLoS Pathog, 5*(8), e1000538. doi:10.1371/journal.ppat.1000538

Calderwood, S. K. (2015). Cdc37 as a co-chaperone to Hsp90. *Subcell Biochem, 78*, 103-112. doi:10.1007/978-3-319-11731-7_5

Caldwell, A. L., & Gulig, P. A. (1991). The Salmonella-Typhimurium Virulence Plasmid Encodes a Positive Regulator of a Plasmid-Encoded Virulence Gene. *Journal of Bacteriology, 173*(22), 7176-7185.

Campos, M., Cisneros, D. A., Nivaskumar, M., & Francetic, O. (2013). The type II secretion system - a dynamic fiber assembly nanomachine. *Res Microbiol, 164*(6), 545-555. doi:10.1016/j.resmic.2013.03.013

Castanar, L., Sistare, E., Virgili, A., Williamson, R. T., & Parella, T. (2015). Suppression of phase and amplitude J(HH) modulations in HSQC experiments. *Magn Reson Chem, 53*(2), 115-119. doi:10.1002/mrc.4149

Chaikuad, A., Froese, D. S., Berridge, G., von Delft, F., Oppermann, U., & Yue, W. W. (2011). Conformational plasticity of glycogenin and its maltosaccharide substrate during glycogen biogenesis. *Proc Natl Acad Sci U S A, 108*(52), 21028-21033. doi:10.1073/pnas.1113921108

Chen, G., Cao, P., & Goeddel, D. V. (2002). TNF-induced recruitment and activation of the IKK complex require Cdc37 and Hsp90. *Mol Cell, 9*(2), 401-410.

Cheong, M. S., Kirik, A., Kim, J. G., Frame, K., Kirik, V., & Mudgett, M. B. (2014). AvrBsT Acetylates Arabidopsis ACIP1, a Protein that Associates with Microtubules and Is Required for Immunity. *Plos Pathogens, 10*(2).

Clarke, S. C., Haigh, R. D., Freestone, P. P., & Williams, P. H. (2002). Enteropathogenic Escherichia coli infection: history and clinical aspects. *Br J Biomed Sci, 59*(2), 123-127.

Collier-Hyams, L. S., Zeng, H., Sun, J., Tomlinson, A. D., Bao, Z. Q., Chen, H., . . . Neish, A. S. (2002). Salmonella AvrA effector inhibits the key proinflammatory, anti-apoptotic NF-kappa B pathway. *Journal of Immunology, 169*(6), 2846-2850.

Collins, J. W., Keeney, K. M., Crepin, V. F., Rathinam, V. A., Fitzgerald, K. A., Finlay, B. B., & Frankel, G. (2014). Citrobacter rodentium: infection, inflammation and the microbiota. *Nat Rev Microbiol, 12*(9), 612-623. doi:10.1038/nrmicro3315

Coombes, B. K., Wickham, M. E., Brown, N. F., Lemire, S., Bossi, L., Hsiao, W. W., . . . Finlay, B. B. (2005). Genetic and molecular analysis of GogB, a phage-encoded type III-secreted substrate in Salmonella enterica serovar typhimurium with autonomous expression from its associated phage. *J Mol Biol, 348*(4), 817-830. doi:10.1016/j.jmb.2005.03.024

Coynault, C., Robbesaule, V., Popoff, M. Y., & Norel, F. (1992). Growth-Phase and Spvr Regulation of Transcription of Salmonella-Typhimurium Spvabc Virulence Genes. *Microbial Pathogenesis, 13*(2), 133-143.

Creasey, E. A., Delahay, R. M., Bishop, A. A., Shaw, R. K., Kenny, B., Knutton, S., & Frankel, G. (2003). CesT is a bivalent enteropathogenic Escherichia coli chaperone required for translocation of both Tir and Map. *Molecular Microbiology, 47*(1), 209-221.

Creasey, E. A., Delahay, R. M., Daniell, S. J., & Frankel, G. (2003). Yeast two-hybrid system survey of interactions between LEE-encoded proteins of enteropathogenic Escherichia coli. *Microbiology, 149*(Pt 8), 2093-2106. doi:10.1099/mic.0.26355-0

Crepin, V. F., Shaw, R., Abe, C. M., Knutton, S., & Frankel, G. (2005). Polarity of enteropathogenic Escherichia coli EspA filament assembly and protein secretion. *J Bacteriol, 187*(8), 2881-2889. doi:10.1128/JB.187.8.2881-2889.2005

Creuzburg, K., Giogha, C., Wong Fok Lung, T., Scott, N. E., Muhlen, S., Hartland, E. L., & Pearson, J. S. (2017). The Type III Effector NleD from Enteropathogenic Escherichia coli Differentiates between Host Substrates p38 and JNK. *Infect Immun, 85*(2). doi:10.1128/IAI.00620-16

Csermely, P., Schnaider, T., Soti, C., Prohaszka, Z., & Nardai, G. (1998). The 90-kDa molecular chaperone family: Structure, function, and clinical applications. A comprehensive review. *Pharmacology & Therapeutics, 79*(2), 129-168.

Daniell, S. J., Takahashi, N., Wilson, R., Friedberg, D., Rosenshine, I., Booy, F. P., . . . Aizawa, S. (2001). The filamentous type III secretion translocon of enteropathogenic Escherichia coli. *Cell Microbiol, 3*(12), 865-871.

Danielsen, J. M., Sylvestersen, K. B., Bekker-Jensen, S., Szklarczyk, D., Poulsen, J. W., Horn, H., . . . Nielsen, M. L. (2011). Mass spectrometric analysis of lysine ubiquitylation reveals promiscuity at site level. *Mol Cell Proteomics, 10*(3), M110 003590. doi:10.1074/mcp.M110.003590

Delahay, R. M., Knutton, S., Shaw, R. K., Hartland, E. L., Pallen, M. J., & Frankel, G. (1999). The coiled-coil domain of EspA is essential for the assembly of the type III secretion translocon on the surface of enteropathogenic Escherichia coli. *Journal of Biological Chemistry, 274*(50), 35969-35974.

Delepelaire, P. (2004). Type I secretion in gram-negative bacteria. *Biochim Biophys Acta, 1694*(1-3), 149-161. doi:10.1016/j.bbamcr.2004.05.001

Deng, W., Puente, J. L., Gruenheid, S., Li, Y., Vallance, B. A., Vazquez, A., . . . Finlay, B. B. (2004). Dissecting virulence: systematic and functional analyses of a pathogenicity island. *Proc Natl Acad Sci U S A, 101*(10), 3597-3602. doi:10.1073/pnas.0400326101

Desvaux, M., Hebraud, M., Talon, R., & Henderson, I. R. (2009). Secretion and subcellular localizations of bacterial proteins: a semantic awareness issue. *Trends Microbiol, 17*(4), 139-145. doi:10.1016/j.tim.2009.01.004

Diepold, A., Wiesand, U., & Cornelis, G. R. (2011). The assembly of the export apparatus (YscR,S,T,U,V) of the Yersinia type III secretion apparatus occurs independently of other structural components and involves the formation of an YscV oligomer. *Mol Microbiol, 82*(2), 502-514. doi:10.1111/j.1365-2958.2011.07830.x

Dohlich, K., Zumsteg, A. B., Goosmann, C., & Kolbe, M. (2014). A Substrate-Fusion Protein Is Trapped inside the Type III Secretion System Channel in Shigella flexneri. *Plos Pathogens, 10*(1).

Du, F. Y., & Galan, J. E. (2009). Selective Inhibition of Type III Secretion Activated Signaling by the Salmonella Effector AvrA. *Plos Pathogens, 5*(9).

Echtenkamp, F., Deng, W., Wickham, M. E., Vazquez, A., Puente, J. L., Thanabalasuriar, A., . . . Hardwidge, P. R. (2008). Characterization of the NleF effector protein from attaching and

effacing bacterial pathogens. *FEMS Microbiol Lett, 281*(1), 98-107. doi:10.1111/j.1574-6968.2008.01088.x

El Qaidi, S., Chen, K., Halim, A., Siukstaite, L., Rueter, C., Hurtado-Guerrero, R., . . . Hardwidge, P. R. (2017). NleB/SseK effectors from Citrobacter rodentium, Escherichia coli, and Salmonella enterica display distinct differences in host substrate specificity. *J Biol Chem, 292*(27), 11423-11430. doi:10.1074/jbc.M117.790675

El Qaidi, S., Wu, M., Zhu, C., & Hardwidge, P. R. (2018). Salmonella, E. coli, and Citrobacter Type III Secretion System Effector Proteins that Alter Host Innate Immunity. *Adv Exp Med Biol*. doi:10.1007/5584_2018_289

Elliott, S. J., Wainwright, L. A., McDaniel, T. K., Jarvis, K. G., Deng, Y. K., Lai, L. C., . . . Kaper, J. B. (1998). The complete sequence of the locus of enterocyte effacement (LEE) from enteropathogenic Escherichia coli E2348/69. *Mol Microbiol, 28*(1), 1-4.

Esposito, D., Gunster, R. A., Martino, L., El Omari, K., Wagner, A., Thurston, T. L. M., & Rittinger, K. (2018). Structural basis for the glycosyltransferase activity of the Salmonella effector SseK3. *J Biol Chem, 293*(14), 5064-5078. doi:10.1074/jbc.RA118.001796

Eulalio, A., Frohlich, K. S., Mano, M., Giacca, M., & Vogel, J. (2011). A Candidate Approach Implicates the Secreted Salmonella Effector Protein SpvB in P-Body Disassembly. *PLoS One, 6*(3).

Evaristo, C., Spranger, S., Barnes, S. E., Miller, M. L., Molinero, L. L., Locke, F. L., . . . Alegre, M. L. (2016). Cutting Edge: Engineering Active IKK beta in T Cells Drives Tumor Rejection. *Journal of Immunology, 196*(7), 2933-2938.

Figueiredo, J. F., Lawhon, S. D., Gokulan, K., Khare, S., Raffatellu, M., Tsolis, R. M., . . . Adams, L. G. (2009). Salmonella enterica Typhimurium SipA induces CXC-chemokine expression through p38MAPK and JUN pathways. *Microbes and Infection, 11*(2), 302-310.

Fitzhenry, R. J., Pickard, D. J., Hartland, E. L., Reece, S., Dougan, G., Phillips, A. D., & Frankel, G. (2002). Intimin type influences the site of human intestinal mucosal colonisation by enterohaemorrhagic Escherichia coli O157:H7. *Gut, 50*(2), 180-185.

Frankel, G., Phillips, A. D., Trabulsi, L. R., Knutton, S., Dougan, G., & Matthews, S. (2001). Intimin and the host cell--is it bound to end in Tir(s)? *Trends Microbiol, 9*(5), 214-218.

Friesner, R. A., Banks, J. L., Murphy, R. B., Halgren, T. A., Klicic, J. J., Mainz, D. T., . . . Shenkin, P. S. (2004). Glide: a new approach for rapid, accurate docking and scoring. 1. Method and assessment of docking accuracy. *J Med Chem, 47*(7), 1739-1749. doi:10.1021/jm0306430

Fronzes, R., Remaut, H., & Waksman, G. (2008). Architectures and biogenesis of non-flagellar protein appendages in Gram-negative bacteria. *EMBO J, 27*(17), 2271-2280. doi:10.1038/emboj.2008.155

Fujii, T., Cheung, M., Blanco, A., Kato, T., Blocker, A. J., & Namba, K. (2012). Structure of a type III secretion needle at 7-angstrom resolution provides insights into its assembly and signaling mechanisms. *Proceedings of the National Academy of Sciences of the United States of America, 109*(12), 4461-4466.

Galan, J. E., Lara-Tejero, M., Marlovits, T. C., & Wagner, S. (2014). Bacterial type III secretion systems: specialized nanomachines for protein delivery into target cells. *Annu Rev Microbiol, 68*, 415-438. doi:10.1146/annurev-micro-092412-155725

Gao, X., Pham, T. H., Feuerbacher, L. A., Chen, K., Hays, M. P., Singh, G., . . . Hardwidge, P. R. (2016). Citrobacter rodentium NleB Protein Inhibits Tumor Necrosis Factor (TNF) Receptor-associated Factor 3 (TRAF3) Ubiquitination to Reduce Host Type I Interferon Production. *J Biol Chem, 291*(35), 18232-18238. doi:10.1074/jbc.M116.738278

Gao, X., Wan, F., Mateo, K., Callegari, E., Wang, D., Deng, W., . . . Hardwidge, P. R. (2009). Bacterial effector binding to ribosomal protein s3 subverts NF-kappaB function. *PLoS Pathog, 5*(12), e1000708. doi:10.1371/journal.ppat.1000708

Gao, X. F., Wang, X. G., Pham, T. H., Feuerbacher, L. A., Lubos, M. L., Huang, M. Z., . . . Hardwidge, P. R. (2013). NleB, a Bacterial Effector with Glycosyltransferase Activity, Targets GAPDH Function to Inhibit NF-kappa B Activation (vol 13, pg 87, 2013). *Cell Host & Microbe, 13*(3), 371-372.

Garmendia, J., Frankel, G., & Crepin, V. F. (2005). Enteropathogenic and enterohemorrhagic Escherichia coli infections: translocation, translocation, translocation. *Infect Immun, 73*(5), 2573-2585. doi:10.1128/IAI.73.5.2573-2585.2005

Ghosh, P. (2004). Process of protein transport by the type III secretion system. *Microbiol Mol Biol Rev, 68*(4), 771-795. doi:10.1128/MMBR.68.4.771-795.2004

Giogha, C., Lung, T. W. F., Muhlen, S., Pearson, J. S., & Hartland, E. L. (2015). Substrate recognition by the zinc metalloprotease effector NleC from enteropathogenic Escherichia coli. *Cellular Microbiology, 17*(12), 1766-1778.

Gloster, T. M. (2014). Advances in understanding glycosyltransferases from a structural perspective. *Curr Opin Struct Biol, 28*, 131-141. doi:10.1016/j.sbi.2014.08.012

Goetz, M. P., Toft, D. O., Ames, M. M., & Erlichman, C. (2003). The Hsp90 chaperone complex as a novel target for cancer therapy. *Ann Oncol, 14*(8), 1169-1176.

Grabe, G. J., Zhang, Y., Przydacz, M., Rolhion, N., Yang, Y., Pruneda, J. N., . . . Hare, S. A. (2016). The Salmonella Effector SpvD Is a Cysteine Hydrolase with a Serovar-specific Polymorphism Influencing Catalytic Activity, Suppression of Immune Responses, and Bacterial Virulence. *Journal of Biological Chemistry, 291*(50), 25853-25863.

Gregory, R. C., Taniguchi, T., & D'Andrea, A. D. (2003). Regulation of the Fanconi anemia pathway by monoubiquitination. *Semin Cancer Biol, 13*(1), 77-82.

Greten, F. R., Eckmann, L., Greten, T. F., Park, J. M., Li, Z. W., Egan, L. J., . . . Karin, M. (2004). IKK beta links inflammation and tumorigenesis in a mouse model of colitis-associated cancer. *Cell, 118*(3), 285-296.

Grishin, A. M., Cherney, M., Anderson, D. H., Phanse, S., Babu, M., & Cygler, M. (2014). NleH defines a new family of bacterial effector kinases. *Structure, 22*(2), 250-259. doi:10.1016/j.str.2013.11.006

Guiney, D. G., & Lesnick, M. (2005). Targeting of the actin cytoskeleton during infection by Salmonella strains. *Clinical Immunology, 114*(3), 248-255.

Gunster, R. A., Matthews, S. A., Holden, D. W., & Thurston, T. L. (2017). SseK1 and SseK3 Type III Secretion System Effectors Inhibit NF-kappaB Signaling and Necroptotic Cell Death in Salmonella-Infected Macrophages. *Infect Immun, 85*(3). doi:10.1128/IAI.00010-17

Hakansson, S., Schesser, K., Persson, C., Galyov, E. E., Rosqvist, R., Homble, F., & WolfWatz, H. (1996). The YopB protein of Yersinia pseudotuberculosis is essential for the translocation of Yop effector proteins across the target cell plasma membrane and displays a contact-dependent membrane disrupting activity. *Embo Journal, 15*(21), 5812-5823.

Halgren, T. A., Murphy, R. B., Friesner, R. A., Beard, H. S., Frye, L. L., Pollard, W. T., & Banks, J. L. (2004). Glide: a new approach for rapid, accurate docking and scoring. 2. Enrichment factors in database screening. *J Med Chem, 47*(7), 1750-1759. doi:10.1021/jm030644s

Haltiwanger, R. S., & Lowe, J. B. (2004). Role of glycosylation in development. *Annu Rev Biochem, 73*, 491-537. doi:10.1146/annurev.biochem.73.011303.074043

Han, J., Zhong, C. Q., & Zhang, D. W. (2011). Programmed necrosis: backup to and competitor with apoptosis in the immune system. *Nature Immunology, 12*(12), 1143-1149. doi:10.1038/ni.2159

Haneda, T., Ishii, Y., Shimizu, H., Ohshima, K., Iida, N., Danbara, H., & Okada, N. (2012). Salmonella type III effector SpvC, a phosphothreonine lyase, contributes to reduction in inflammatory response during intestinal phase of infection. *Cellular Microbiology, 14*(4), 485-499.

Haraga, A., & Miller, S. I. (2006). A Salmonella type III secretion effector interacts with the mammalian serine/threonine protein kinase PKN1. *Cellular Microbiology, 8*(5), 837-846.

Harder, E., Damm, W., Maple, J., Wu, C., Reboul, M., Xiang, J. Y., . . . Friesner, R. A. (2016). OPLS3: A Force Field Providing Broad Coverage of Drug-like Small Molecules and Proteins. *J Chem Theory Comput, 12*(1), 281-296. doi:10.1021/acs.jctc.5b00864

Hardt, W. D., & Galan, J. E. (1997). A secreted Salmonella protein with homology to an avirulence determinant of plant pathogenic bacteria. *Proc Natl Acad Sci U S A, 94*(18), 9887-9892.

Hauser, A. R. (2009). The type III secretion system of Pseudomonas aeruginosa: infection by injection. *Nat Rev Microbiol, 7*(9), 654-665. doi:10.1038/nrmicro2199

Hegde, V., Yadavilli, S., & Deutsch, W. A. (2007). Knockdown of ribosomal protein S3 protects human cells from genotoxic stress. *DNA Repair (Amst), 6*(1), 94-99. doi:10.1016/j.dnarep.2006.09.004

Heiskanen, P., Taira, S., & Rhen, M. (1994). Role of Rpos in the Regulation of Salmonella Plasmid Virulence (Spv) Genes. *Fems Microbiology Letters, 123*(1-2), 125-130.

Higgins, R., Gendron, J. M., Rising, L., Mak, R., Webb, K., Kaiser, S. E., . . . Bennett, E. J. (2015). The Unfolded Protein Response Triggers Site-Specific Regulatory Ubiquitylation of 40S Ribosomal Proteins. *Mol Cell, 59*(1), 35-49. doi:10.1016/j.molcel.2015.04.026

Hinz, M., Broemer, M., Arslan, S. C., Otto, A., Mueller, E. C., Dettmer, R., & Scheidereit, C. (2007). Signal responsiveness of IkappaB kinases is determined by Cdc37-assisted transient interaction with Hsp90. *J Biol Chem, 282*(44), 32311-32319. doi:10.1074/jbc.M705785200

Hochmann, H., Pust, S., von Figura, G., Aktories, K., & Barth, H. (2006). Salmonella enterica SpvB ADP-ribosylates actin at position arginine-177-characterization of the catalytic domain within the SpvB protein and a comparison to binary clostridial actin-ADP-ribosylating toxins. *Biochemistry, 45*(4), 1271-1277.

Hodgkinson, J. L., Horsley, A., Stabat, D., Simon, M., Johnson, S., da Fonseca, P. C., . . . Blocker, A. J. (2009). Three-dimensional reconstruction of the Shigella T3SS transmembrane regions reveals 12-fold symmetry and novel features throughout. *Nat Struct Mol Biol, 16*(5), 477-485. doi:10.1038/nsmb.1599

Hodgson, A., Wier, E. M., Fu, K., Sun, X., Yu, H. B., Zheng, W. X., . . . Wan, F. Y. (2015). Metalloprotease NleC Suppresses Host NF-kappa B/Inflammatory Responses by Cleaving p65 and Interfering with the p65/RPS3 Interaction. *Plos Pathogens, 11*(3).

Holm, L., & Laakso, L. M. (2016). Dali server update. *Nucleic Acids Res, 44*(W1), W351-355. doi:10.1093/nar/gkw357

Hu, B., Morado, D. R., Margolin, W., Rohde, J. R., Arizmendi, O., Picking, W. L., . . . Liu, J. (2015). Visualization of the type III secretion sorting platform of Shigella flexneri. *Proc Natl Acad Sci U S A, 112*(4), 1047-1052. doi:10.1073/pnas.1411610112

Hu, J., & Torres, A. G. (2015). Enteropathogenic Escherichia coli: foe or innocent bystander? *Clin Microbiol Infect, 21*(8), 729-734. doi:10.1016/j.cmi.2015.01.015

Hurtado-Guerrero, R., Zusman, T., Pathak, S., Ibrahim, A. F., Shepherd, S., Prescott, A., . . . van Aalten, D. M. (2010). Molecular mechanism of elongation factor 1A inhibition by a Legionella pneumophila glycosyltransferase. *Biochem J, 426*(3), 281-292. doi:10.1042/BJ20091351

Ide, T., Laarmann, S., Greune, L., Schillers, H., Oberleithner, H., & Schmidt, M. A. (2001). Characterization of translocation pores inserted into plasma membranes by type III-secreted Esp proteins of enteropathogenic Escherichia coli. *Cellular Microbiology, 3*(10), 669-679.

Jackson, B. R., Griffin, P. M., Cole, D., Walsh, K. A., & Chai, S. J. (2013). Outbreak-associated Salmonella enterica serotypes and food Commodities, United States, 1998-2008. *Emerg Infect Dis, 19*(8), 1239-1244. doi:10.3201/eid1908.121511

Jacobson, M. P., Pincus, D. L., Rapp, C. S., Day, T. J., Honig, B., Shaw, D. E., & Friesner, R. A. (2004). A hierarchical approach to all-atom protein loop prediction. *Proteins, 55*(2), 351-367. doi:10.1002/prot.10613

Jones, R. M., Wu, H. X., Wentworth, C., Luo, L. P., Collier-Hyams, L., & Neish, A. S. (2008). Salmonella AvrA coordinates suppression of host immune and apoptotic defenses via JNK pathway blockade. *Cell Host & Microbe, 3*(4), 233-244.

Jung, Y., Kim, H. D., Yang, H. W., Kim, H. J., Jang, C. Y., & Kim, J. (2017). Modulating cellular balance of Rps3 mono-ubiquitination by both Hel2 E3 ligase and Ubp3 deubiquitinase regulates protein quality control. *Exp Mol Med, 49*(11), e390. doi:10.1038/emm.2017.128

Kaniga, K., Trollinger, D., & Galan, J. E. (1995). Identification of two targets of the type III protein secretion system encoded by the inv and spa loci of Salmonella typhimurium that have homology to the Shigella IpaD and IpaA proteins. *J Bacteriol, 177*(24), 7078-7085.

Kaniga, K., Uralil, J., Bliska, J. B., & Galan, J. E. (1996). A secreted protein tyrosine phosphatase with modular effector domains in the bacterial pathogen Salmonella typhimurium. *Mol Microbiol, 21*(3), 633-641.

Kaper, J. B., Nataro, J. P., & Mobley, H. L. (2004). Pathogenic Escherichia coli. *Nat Rev Microbiol, 2*(2), 123-140. doi:10.1038/nrmicro818

Karmali, M. A. (1989). Infection by verocytotoxin-producing Escherichia coli. *Clin Microbiol Rev, 2*(1), 15-38.

Keestra, A. M., Winter, M. G., Klein-Douwel, D., Xavier, M. N., Winter, S. E., Kim, A., . . . Baumler, A. J. (2011). A Salmonella Virulence Factor Activates the NOD1/NOD2 Signaling Pathway. *Mbio, 2*(6).

Kelly, M., Hart, E., Mundy, R., Marches, O., Wiles, S., Badea, L., . . . Hartland, E. L. (2006). Essential role of the type III secretion system effector NleB in colonization of mice by Citrobacter rodentium. *Infect Immun, 74*(4), 2328-2337. doi:10.1128/IAI.74.4.2328-2337.2006

Kenny, B., DeVinney, R., Stein, M., Reinscheid, D. J., Frey, E. A., & Finlay, B. B. (1997). Enteropathogenic E-coli (EPEC) transfers its receptor for intimate adherence into mammalian cells. *Cell, 91*(4), 511-520.

Keszei, A. F. A., Tang, X. J., McCormick, C., Zeqiraj, E., Rohde, J. R., Tyers, M., & Sicheri, F. (2014). Structure of an SspH1-PKN1 Complex Reveals the Basis for Host Substrate Recognition and Mechanism of Activation for a Bacterial E3 Ubiquitin Ligase. *Molecular and Cellular Biology, 34*(3), 362-373.

Kim, J., Thanabalasuriar, A., Chaworth-Musters, T., Fromme, J. C., Frey, E. A., Lario, P. I., . . . Gruenheid, S. (2007). The bacterial virulence factor NleA inhibits cellular protein secretion by disrupting mammalian COPII function. *Cell Host Microbe, 2*(3), 160-171. doi:10.1016/j.chom.2007.07.010

Kim, T. S., Jang, C. Y., Kim, H. D., Lee, J. Y., Ahn, B. Y., & Kim, J. (2006). Interaction of Hsp90 with ribosomal proteins protects from ubiquitination and proteasome-dependent degradation. *Mol Biol Cell, 17*(2), 824-833. doi:10.1091/mbc.e05-08-0713

Kim, T. S., Kim, H. D., & Kim, J. (2009). PKCdelta-dependent functional switch of rpS3 between translation and DNA repair. *Biochim Biophys Acta, 1793*(2), 395-405. doi:10.1016/j.bbamcr.2008.10.017

Kim, W., Youn, H., Lee, S., Kim, E., Kim, D., Sub Lee, J., . . . Youn, B. (2018). RNF138-mediated ubiquitination of rpS3 is required for resistance of glioblastoma cells to radiation-induced apoptosis. *Exp Mol Med, 50*(1), e434. doi:10.1038/emm.2017.247

Kirschner, K. N., Yongye, A. B., Tschampel, S. M., Gonzalez-Outeirino, J., Daniels, C. R., Foley, B. L., & Woods, R. J. (2008). GLYCAM06: a generalizable biomolecular force field. Carbohydrates. *J Comput Chem, 29*(4), 622-655. doi:10.1002/jcc.20820

Knodler, L. A., Celli, J., Hardt, W. D., Vallance, B. A., Yip, C., & Finlay, B. B. (2002). Salmonella effectors within a single pathogenicity island are differentially expressed and translocated by separate type III secretion systems. *Molecular Microbiology, 43*(5), 1089-1103.

Koronakis, V., Hughes, C., & Koronakis, E. (1991). Energetically distinct early and late stages of HlyB/HlyD-dependent secretion across both Escherichia coli membranes. *EMBO J, 10*(11), 3263-3272.

Koronakis, V., Sharff, A., Koronakis, E., Luisi, B., & Hughes, C. (2000). Crystal structure of the bacterial membrane protein TolC central to multidrug efflux and protein export. *Nature, 405*(6789), 914-919. doi:10.1038/35016007

Korotkov, K. V., Sandkvist, M., & Hol, W. G. (2012). The type II secretion system: biogenesis, molecular architecture and mechanism. *Nat Rev Microbiol, 10*(5), 336-351. doi:10.1038/nrmicro2762

Kujat Choy, S. L., Boyle, E. C., Gal-Mor, O., Goode, D. L., Valdez, Y., Vallance, B. A., & Finlay, B. B. (2004). SseK1 and SseK2 are novel translocated proteins of Salmonella enterica serovar typhimurium. *Infect Immun, 72*(9), 5115-5125. doi:10.1128/IAI.72.9.5115-5125.2004

Lairson, L. L., Henrissat, B., Davies, G. J., & Withers, S. G. (2008). Glycosyltransferases: structures, functions, and mechanisms. *Annu Rev Biochem, 77*, 521-555. doi:10.1146/annurev.biochem.76.061005.092322

Lara-Tejero, M., Kato, J., Wagner, S., Liu, X. Y., & Galan, J. E. (2011). A Sorting Platform Determines the Order of Protein Secretion in Bacterial Type III Systems. *Science, 331*(6021), 1188-1191.

Le Negrate, G. (2012). Subversion of innate immune responses by bacterial hindrance of NF-kappaB pathway. *Cell Microbiol, 14*(2), 155-167. doi:10.1111/j.1462-5822.2011.01719.x

Le Negrate, G., Faustin, B., Welsh, K., Loeffler, M., Krajewska, M., Hasegawa, P., . . . Reed, J. C. (2008). Salmonella secreted factor L deubiquitinase of Salmonella typhimurium inhibits NF-kappaB, suppresses IkappaBalpha ubiquitination and modulates innate immune responses. *J Immunol, 180*(7), 5045-5056.

Lee, M., Jun, S. Y., Yoon, B. Y., Song, S., Lee, K., & Ha, N. C. (2012). Membrane fusion proteins of type I secretion system and tripartite efflux pumps share a binding motif for TolC in gram-negative bacteria. *PLoS One, 7*(7), e40460. doi:10.1371/journal.pone.0040460

Lee, S. B., Kwon, I. S., Park, J., Lee, K. H., Ahn, Y., Lee, C., . . . Ahn, J. Y. (2010). Ribosomal protein S3, a new substrate of Akt, serves as a signal mediator between neuronal apoptosis and DNA repair. *J Biol Chem, 285*(38), 29457-29468. doi:10.1074/jbc.M110.131367

Lenders, M. H., Weidtkamp-Peters, S., Kleinschrodt, D., Jaeger, K. E., Smits, S. H., & Schmitt, L. (2015). Directionality of substrate translocation of the hemolysin A Type I secretion system. *Sci Rep, 5*, 12470. doi:10.1038/srep12470

Lewis, J., Devin, A., Miller, A., Lin, Y., Rodriguez, Y., Neckers, L., & Liu, Z. G. (2000). Disruption of hsp90 function results in degradation of the death domain kinase, receptor-interacting protein (RIP), and blockage of tumor necrosis factor-induced nuclear factor-kappaB activation. *J Biol Chem, 275*(14), 10519-10526.

Li, S., Zhang, L., Yao, Q., Li, L., Dong, N., Rong, J., . . . Shao, F. (2013). Pathogen blocks host death receptor signalling by arginine GlcNAcylation of death domains. *Nature, 501*(7466), 242-+.

Li, W., Liu, Y., Sheng, X., Yin, P., Hu, F., Liu, Y., . . . Wang, J. (2014). Structure and mechanism of a type III secretion protease, NleC. *Acta Crystallogr D Biol Crystallogr, 70*(Pt 1), 40-47. doi:10.1107/S1399004713024619

Lin, S. L., Le, T. X., & Cowen, D. S. (2003). SptP, a Salmonella typhimurium type III-secreted protein, inhibits the mitogen-activated protein kinase pathway by inhibiting Raf activation. *Cell Microbiol, 5*(4), 267-275.

Lira-Navarrete, E., de Las Rivas, M., Companon, I., Pallares, M. C., Kong, Y., Iglesias-Fernandez, J., . . . Hurtado-Guerrero, R. (2015). Dynamic interplay between catalytic and lectin domains of GalNAc-transferases modulates protein O-glycosylation. *Nat Commun, 6*, 6937. doi:10.1038/ncomms7937

Liu, T., Zhang, L., Joo, D., & Sun, S. C. (2017). NF-kappaB signaling in inflammation. *Signal Transduct Target Ther, 2*. doi:10.1038/sigtrans.2017.23

Liu, X. Y., Lu, R., Wu, S. P., & Sun, J. (2010). Salmonella regulation of intestinal stem cells through the Wnt/beta-catenin pathway. *Febs Letters, 584*(5), 911-916.

Loquet, A., Sgourakis, N. G., Gupta, R., Giller, K., Riedel, D., Goosmann, C., . . . Lange, A. (2012). Atomic model of the type III secretion system needle. *Nature, 486*(7402), 276-279. doi:10.1038/nature11079

Lossi, N. S., Manoli, E., Forster, A., Dajani, R., Pape, T., Freemont, P., & Filloux, A. (2013). The HsiB1C1 (TssB-TssC) complex of the Pseudomonas aeruginosa type VI secretion system forms a bacteriophage tail sheathlike structure. *J Biol Chem, 288*(11), 7536-7548. doi:10.1074/jbc.M112.439273

Luperchio, S. A., Newman, J. V., Dangler, C. A., Schrenzel, M. D., Brenner, D. J., Steigerwalt, A. G., & Schauer, D. B. (2000). Citrobacter rodentium, the causative agent of transmissible murine colonic hyperplasia, exhibits clonality: synonymy of C. rodentium and mouse-pathogenic Escherichia coli. *J Clin Microbiol, 38*(12), 4343-4350.

Ma, K. W., & Ma, W. B. (2016). YopJ Family Effectors Promote Bacterial Infection through a Unique Acetyltransferase Activity. *Microbiology and Molecular Biology Reviews, 80*(4).

Marcus, S. L., Brumell, J. H., Pfeifer, C. G., & Finlay, B. B. (2000). Salmonella pathogenicity islands: big virulence in small packages. *Microbes Infect, 2*(2), 145-156.

Mayer, M., & Meyer, B. (1999). Characterization of Ligand Binding by Saturation Transfer Difference NMR Spectroscopy. *Angew Chem Int Ed Engl, 38*(12), 1784-1788. doi:10.1002/(SICI)1521-3773(19990614)38:12<1784::AID-ANIE1784>3.0.CO;2-Q

Mayer, M., & Meyer, B. (2001). Group epitope mapping by saturation transfer difference NMR to identify segments of a ligand in direct contact with a protein receptor. *J Am Chem Soc, 123*(25), 6108-6117.

Mazaira, G. I., Zgajnar, N. R., Lotufo, C. M., Daneri-Becerra, C., Sivils, J. C., Soto, O. B., . . . Galigniana, M. D. (2018). The Nuclear Receptor Field: A Historical Overview and Future Challenges. *Nucl Receptor Res, 5*. doi:10.11131/2018/101320

Mazurkiewicz, P., Thomas, J., Thompson, J. A., Liu, M., Arbibe, L., Sansonetti, P., & Holden, D. W. (2008). SpvC is a Salmonella effector with phosphothreonine lyase activity on host mitogen-activated protein kinases. *Molecular Microbiology, 67*(6), 1371-1383.

McClelland, M., Sanderson, K. E., Spieth, J., Clifton, S. W., Latreille, P., Courtney, L., . . . Wilson, R. K. (2001). Complete genome sequence of Salmonella enterica serovar Typhimurium LT2. *Nature, 413*(6858), 852-856. doi:10.1038/35101614

McDaniel, T. K., Jarvis, K. G., Donnenberg, M. S., & Kaper, J. B. (1995). A genetic locus of enterocyte effacement conserved among diverse enterobacterial pathogens. *Proc Natl Acad Sci U S A, 92*(5), 1664-1668.

Medzhitov, R., & Janeway, C. A., Jr. (1997). Innate immunity: the virtues of a nonclonal system of recognition. *Cell, 91*(3), 295-298.

Miao, E. A., & Miller, S. I. (2000). A conserved amino acid sequence directing intracellular type III secretion by Salmonella typhimurium. *Proceedings of the National Academy of Sciences of the United States of America, 97*(13), 7539-7544.

Miao, Y., Feher, V. A., & McCammon, J. A. (2015). Gaussian Accelerated Molecular Dynamics: Unconstrained Enhanced Sampling and Free Energy Calculation. *J Chem Theory Comput, 11*(8), 3584-3595. doi:10.1021/acs.jctc.5b00436

Mills, E., Baruch, K., Charpentier, X., Kobi, S., & Rosenshine, I. (2008). Real-time analysis of effector translocation by the type III secretion system of enteropathogenic Escherichia coli. *Cell Host Microbe, 3*(2), 104-113. doi:10.1016/j.chom.2007.11.007

Minamino, T., & MacNab, R. M. (2000). FliH, a soluble component of the type III flagellar export apparatus of Salmonella, forms a complex with FliI and inhibits its ATPase activity. *Mol Microbiol, 37*(6), 1494-1503.

Minamino, T., Shimada, M., Okabe, M., Saijo-Hamano, Y., Imada, K., Kihara, M., & Namba, K. (2010). Role of the C-terminal cytoplasmic domain of FlhA in bacterial flagellar type III protein export. *J Bacteriol, 192*(7), 1929-1936. doi:10.1128/JB.01328-09

Monjaras Feria, J., Garcia-Gomez, E., Espinosa, N., Minamino, T., Namba, K., & Gonzalez-Pedrajo, B. (2012). Role of EscP (Orf16) in injectisome biogenesis and regulation of type

III protein secretion in enteropathogenic Escherichia coli. *J Bacteriol, 194*(22), 6029-6045. doi:10.1128/JB.01215-12

Mundy, R., MacDonald, T. T., Dougan, G., Frankel, G., & Wiles, S. (2005). Citrobacter rodentium of mice and man. *Cell Microbiol, 7*(12), 1697-1706. doi:10.1111/j.1462-5822.2005.00625.x

Murli, S., Watson, R. O., & Galan, J. E. (2001). Role of tyrosine kinases and the tyrosine phosphatase SptP in the interaction of Salmonella with host cells. *Cell Microbiol, 3*(12), 795-810.

Murphy, S. H., Suzuki, K., Downes, M., Welch, G. L., De Jesus, P., Miraglia, L. J., . . . Verma, I. M. (2011). Tumor suppressor protein (p)53, is a regulator of NF-kappaB repression by the glucocorticoid receptor. *Proc Natl Acad Sci U S A, 108*(41), 17117-17122. doi:10.1073/pnas.1114420108

Newell, D. G., & La Ragione, R. M. (2018). Enterohaemorrhagic and other Shiga toxin-producing Escherichia coli (STEC): Where are we now regarding diagnostics and control strategies? *Transbound Emerg Dis, 65 Suppl 1*, 49-71. doi:10.1111/tbed.12789

Newton, H. J., Pearson, J. S., Badea, L., Kelly, M., Lucas, M., Holloway, G., . . . Hartland, E. L. (2010). The type III effectors NleE and NleB from enteropathogenic E. coli and OspZ from Shigella block nuclear translocation of NF-kappaB p65. *PLoS Pathog, 6*(5), e1000898. doi:10.1371/journal.ppat.1000898

Nicaud, J. M., Mackman, N., Gray, L., & Holland, I. B. (1985). Regulation of haemolysin synthesis in E. coli determined by HLY genes of human origin. *Mol Gen Genet, 199*(1), 111-116.

Norris, F. A., Wilson, M. P., Wallis, T. S., Galyov, E. E., & Majerus, P. W. (1998). SopB, a protein required for virulence of Salmonella dublin, is an inositol phosphate phosphatase. *Proc Natl Acad Sci U S A, 95*(24), 14057-14059.

Ochman, H., Soncini, F. C., Solomon, F., & Groisman, E. A. (1996). Identification of a pathogenicity island required for Salmonella survival in host cells. *Proc Natl Acad Sci U S A, 93*(15), 7800-7804.

Odendall, C., Rolhion, N., Forster, A., Poh, J., Lamont, D. J., Liu, M., . . . Holden, D. W. (2012). The Salmonella Kinase SteC Targets the MAP Kinase MEK to Regulate the Host Actin Cytoskeleton. *Cell Host & Microbe, 12*(5), 657-668.

Ogino, T., Ohno, R., Sekiya, K., Kuwae, A., Matsuzawa, T., Nonaka, T., . . . Abe, A. (2006). Assembly of the type III secretion apparatus of enteropathogenic Escherichia coli. *Journal of Bacteriology, 188*(8), 2801-2811.

Olsson, M. H., Sondergaard, C. R., Rostkowski, M., & Jensen, J. H. (2011). PROPKA3: Consistent Treatment of Internal and Surface Residues in Empirical pKa Predictions. *J Chem Theory Comput, 7*(2), 525-537. doi:10.1021/ct100578z

Pallett, M. A., Berger, C. N., Pearson, J. S., Hartland, E. L., & Frankel, G. (2014). The Type III Secretion Effector NleF of Enteropathogenic Escherichia coli Activates NF-kappa B Early during Infection. *Infection and Immunity, 82*(11), 4878-4888.

Pan, M., Li, S., Li, X., Shao, F., Liu, L., & Hu, H. G. (2014). Synthesis of and specific antibody generation for glycopeptides with arginine N-GlcNAcylation. *Angew Chem Int Ed Engl, 53*(52), 14517-14521. doi:10.1002/anie.201407824

Park, H. H., Lo, Y. C., Lin, S. C., Wang, L., Yang, J. K., & Wu, H. (2007). The death domain superfamily in intracellular signaling of apoptosis and inflammation. *Annu Rev Immunol, 25*, 561-586. doi:10.1146/annurev.immunol.25.022106.141656

Park, J. B., Kim, Y. H., Yoo, Y., Kim, J., Jun, S. H., Cho, J. W., . . . Cho, H. S. (2018). Structural basis for arginine glycosylation of host substrates by bacterial effector proteins. *Nat Commun, 9*(1), 4283. doi:10.1038/s41467-018-06680-6

Patel, J. C., & Galan, J. E. (2005). Manipulation of the host actin cytoskeleton by Salmonella--all in the name of entry. *Curr Opin Microbiol, 8*(1), 10-15. doi:10.1016/j.mib.2004.09.001

Patel, J. C., & Galan, J. E. (2006). Differential activation and function of Rho GTPases during Salmonella-host cell interactions. *J Cell Biol, 175*(3), 453-463. doi:10.1083/jcb.200605144

Pearl, L. H. (2016). Review: The HSP90 molecular chaperone-an enigmatic ATPase. *Biopolymers, 105*(8), 594-607. doi:10.1002/bip.22835

Pearson, J. S., Giogha, C., Muehlen, S., Nachbur, U., Pham, C. L. L., Zhang, Y., . . . Hartland, E. L. (2017). EspL is a bacterial cysteine protease effector that cleaves RHIM proteins to block necroptosis and inflammation (vol 2, 16258, 2017). *Nature Microbiology, 2*(4).

Pearson, J. S., Giogha, C., Ong, S. Y., Kennedy, C. L., Kelly, M., Robinson, K. S., . . . Hartland, E. L. (2013). A type III effector antagonizes death receptor signalling during bacterial gut infection. *Nature, 501*(7466), 247-+.

Pearson, J. S., Zhang, Y., Newton, H. J., & Hartland, E. L. (2015). Post-modern pathogens: surprising activities of translocated effectors from E. coli and Legionella. *Curr Opin Microbiol, 23*, 73-79. doi:10.1016/j.mib.2014.11.005

Petty, N. K., Bulgin, R., Crepin, V. F., Cerdeno-Tarraga, A. M., Schroeder, G. N., Quail, M. A., . . . Thomson, N. R. (2010). The Citrobacter rodentium genome sequence reveals convergent evolution with human pathogenic Escherichia coli. *J Bacteriol, 192*(2), 525-538. doi:10.1128/JB.01144-09

Pham, T. H., Gao, X. F., Singh, G., & Hardwidge, P. R. (2013). Escherichia coli Virulence Protein NleH1 Interaction with the v-Crk Sarcoma Virus CT10 Oncogene-like Protein (CRKL) Governs NleH1 Inhibition of the Ribosomal Protein 53 (RPS3)/Nuclear Factor kappa B (NF-kappa B) Pathway. *Journal of Biological Chemistry, 288*(48), 34567-34574.

Pham, T. H., Gao, X. F., Tsai, K., Olsen, R., Wan, F. Y., & Hardwidge, P. R. (2012). Functional Differences and Interactions between the Escherichia coli Type III Secretion System Effectors NleH1 and NleH2. *Infection and Immunity, 80*(6), 2133-2140.

Phillips, A. D., Navabpour, S., Hicks, S., Dougan, G., Wallis, T., & Frankel, G. (2000). Enterohaemorrhagic Escherichia coli O157:H7 target Peyer's patches in humans and cause attaching/effacing lesions in both human and bovine intestine. *Gut, 47*(3), 377-381.

Pilar, A. V. C., Reid-Yu, S. A., Cooper, C. A., Mulder, D. T., & Coombes, B. K. (2012). GogB Is an Anti-Inflammatory Effector that Limits Tissue Damage during Salmonella Infection through Interaction with Human FBXO22 and Skp1. *Plos Pathogens, 8*(6).

Poh, J., Odendall, C., Spanos, A., Boyle, C., Liu, M., Freemont, P., & Holden, D. W. (2008). SteC is a Salmonella kinase required for SPI-2-dependent F-actin remodelling. *Cellular Microbiology, 10*(1), 20-30.

Pollock, G. L., Oates, C. V. L., Giogha, C., Lung, T. W. F., Ong, S. Y., Pearson, J. S., & Hartland, E. L. (2017). Distinct Roles of the Antiapoptotic Effectors NleB and NleF from Enteropathogenic Escherichia coli. *Infection and Immunity, 85*(4).

Portaliou, A. G., Tsolis, K. C., Loos, M. S., Zorzini, V., & Economou, A. (2016). Type III Secretion: Building and Operating a Remarkable Nanomachine. *Trends Biochem Sci, 41*(2), 175-189. doi:10.1016/j.tibs.2015.09.005

Pruneda, J. N., Durkin, C. H., Geurink, P. P., Ovaa, H., Santhanam, B., Holden, D. W., & Komander, D. (2016). The Molecular Basis for Ubiquitin and Ubiquitin-like Specificities in Bacterial Effector Proteases. *Mol Cell, 63*(2), 261-276. doi:10.1016/j.molcel.2016.06.015

Quezada, C. M., Hicks, S. W., Galan, J. E., & Stebbins, C. E. (2009). A family of Salmonella virulence factors functions as a distinct class of autoregulated E3 ubiquitin ligases. *Proceedings of the National Academy of Sciences of the United States of America, 106*(12), 4864-4869.

Radics, J., Konigsmaier, L., & Marlovits, T. C. (2014). Structure of a pathogenic type 3 secretion system in action. *Nature Structural & Molecular Biology, 21*(1), 82-+.

Reinert, D. J., Jank, T., Aktories, K., & Schulz, G. E. (2005). Structural basis for the function of Clostridium difficile toxin B. *J Mol Biol, 351*(5), 973-981. doi:10.1016/j.jmb.2005.06.071

Rolhion, N., Furniss, R. C. D., Grabe, G., Ryan, A., Liu, M., Matthews, S. A., & Holden, D. W. (2016). Inhibition of Nuclear Transport of NF-kappa B p65 by the Salmonella Type III Secretion System Effector SpvD. *Plos Pathogens, 12*(5).

Romo-Castillo, M., Andrade, A., Espinosa, N., Monjaras Feria, J., Soto, E., Diaz-Guerrero, M., & Gonzalez-Pedrajo, B. (2014). EscO, a functional and structural analog of the flagellar FliJ protein, is a positive regulator of EscN ATPase activity of the enteropathogenic Escherichia coli injectisome. *J Bacteriol, 196*(12), 2227-2241. doi:10.1128/JB.01551-14

Royan, S. V., Jones, R. M., Koutsouris, A., Roxas, J. L., Falzari, K., Weflen, A. W., . . . Hecht, G. A. (2010). Enteropathogenic E. coli non-LEE encoded effectors NleH1 and NleH2 attenuate NF-kappaB activation. *Mol Microbiol, 78*(5), 1232-1245. doi:10.1111/j.1365-2958.2010.07400.x

Ruchaud-Sparagano, M. H., Muhlen, S., Dean, P., & Kenny, B. (2011). The Enteropathogenic E. coli (EPEC) Tir Effector Inhibits NF-kappa B Activity by Targeting TNF alpha Receptor-Associated Factors. *Plos Pathogens, 7*(12).

Russo, A., Saide, A., Cagliani, R., Cantile, M., Botti, G., & Russo, G. (2016). rpL3 promotes the apoptosis of p53 mutated lung cancer cells by down-regulating CBS and NFkappaB upon 5-FU treatment. *Sci Rep, 6*, 38369. doi:10.1038/srep38369

Rust, H. L., Zurita-Lopez, C. I., Clarke, S., & Thompson, P. R. (2011). Mechanistic studies on transcriptional coactivator protein arginine methyltransferase 1. *Biochemistry, 50*(16), 3332-3345. doi:10.1021/bi102022e

Ruter, C., & Hardwidge, P. R. (2014). 'Drugs from Bugs': bacterial effector proteins as promising biological (immune-) therapeutics. *Fems Microbiology Letters, 351*(2), 126-132.

Rytkonen, A., Poh, J., Garmendia, J., Boyle, C., Thompson, A., Liu, M., . . . Holden, D. W. (2007). SseL, a Salmonella deubiquitinase required for macrophage killing and virulence. *Proc Natl Acad Sci U S A, 104*(9), 3502-3507. doi:10.1073/pnas.0610095104

Sal-Man, N., Biemans-Oldehinkel, E., Sharon, D., Croxen, M. A., Scholz, R., Foster, L. J., & Finlay, B. B. (2012). EscA Is a Crucial Component of the Type III Secretion System of Enteropathogenic Escherichia coli. *Journal of Bacteriology, 194*(11), 2819-2828.

Sal-Man, N., Deng, W., & Finlay, B. B. (2012). EscI: a crucial component of the type III secretion system forms the inner rod structure in enteropathogenic Escherichia coli. *Biochem J, 442*(1), 119-125. doi:10.1042/BJ20111620

Sandkvist, M. (2001). Type II secretion and pathogenesis. *Infect Immun, 69*(6), 3523-3535. doi:10.1128/IAI.69.6.3523-3535.2001

Sastry, G. M., Adzhigirey, M., Day, T., Annabhimoju, R., & Sherman, W. (2013). Protein and ligand preparation: parameters, protocols, and influence on virtual screening enrichments. *J Comput Aided Mol Des, 27*(3), 221-234. doi:10.1007/s10822-013-9644-8

Scallan, E., Hoekstra, R. M., Angulo, F. J., Tauxe, R. V., Widdowson, M. A., Roy, S. L., . . . Griffin, P. M. (2011). Foodborne illness acquired in the United States--major pathogens. *Emerg Infect Dis, 17*(1), 7-15. doi:10.3201/eid1701.P11101

10.3201/eid1701.091101p1

Schraidt, O., Lefebre, M. D., Brunner, M. J., Schmied, W. H., Schmidt, A., Radics, J., . . . Marlovits, T. C. (2010). Topology and organization of the Salmonella typhimurium type III secretion needle complex components. *PLoS Pathog, 6*(4), e1000824. doi:10.1371/journal.ppat.1000824

Schraidt, O., & Marlovits, T. C. (2011). Three-dimensional model of Salmonella's needle complex at subnanometer resolution. *Science, 331*(6021), 1192-1195. doi:10.1126/science.1199358

Scott, N. E., Giogha, C., Pollock, G. L., Kennedy, C. L., Webb, A. I., Williamson, N. A., . . . Hartland, E. L. (2017). The bacterial arginine glycosyltransferase effector NleB preferentially modifies Fas-associated death domain protein (FADD). *Journal of Biological Chemistry, 292*(42), 17337-17350.

Sen, N., Paul, B. D., Gadalla, M. M., Mustafa, A. K., Sen, T., Xu, R., . . . Snyder, S. H. (2012). Hydrogen sulfide-linked sulfhydration of NF-kappaB mediates its antiapoptotic actions. *Mol Cell, 45*(1), 13-24. doi:10.1016/j.molcel.2011.10.021

Sengoku, T., Suzuki, T., Dohmae, N., Watanabe, C., Honma, T., Hikida, Y., . . . Yanagisawa, T. (2018). Structural basis of protein arginine rhamnosylation by glycosyltransferase EarP. *Nat Chem Biol, 14*(4), 368-374. doi:10.1038/s41589-018-0002-y

Shaw, R. K., Daniell, S., Ebel, F., Frankel, G., & Knutton, S. (2001). EspA filament-mediated protein translocation into red blood cells. *Cellular Microbiology, 3*(4), 213-222.

Shi, Y., Chan, D. W., Jung, S. Y., Malovannaya, A., Wang, Y., & Qin, J. (2011). A data set of human endogenous protein ubiquitination sites. *Mol Cell Proteomics, 10*(5), M110 002089. doi:10.1074/mcp.M110.002089

Shneider, M. M., Buth, S. A., Ho, B. T., Basler, M., Mekalanos, J. J., & Leiman, P. G. (2013). PAAR-repeat proteins sharpen and diversify the type VI secretion system spike. *Nature, 500*(7462), 350-353. doi:10.1038/nature12453

Silberger, D. J., Zindl, C. L., & Weaver, C. T. (2017). Citrobacter rodentium: a model enteropathogen for understanding the interplay of innate and adaptive components of type 3 immunity. *Mucosal Immunol, 10*(5), 1108-1117. doi:10.1038/mi.2017.47

Simms, C. L., Yan, L. L., & Zaher, H. S. (2017). Ribosome Collision Is Critical for Quality Control during No-Go Decay. *Mol Cell, 68*(2), 361-373 e365. doi:10.1016/j.molcel.2017.08.019

Song, T., Li, K., Zhou, W., Zhou, J., Jin, Y., Dai, H., . . . Liang, L. (2017). A Type III Effector NleF from EHEC Inhibits Epithelial Inflammatory Cell Death by Targeting Caspase-4. *Biomed Res Int, 2017*, 4101745. doi:10.1155/2017/4101745

Stender, S., Friebel, A., Linder, S., Rohde, M., Mirold, S., & Hardt, W. D. (2000). Identification of SopE2 from Salmonella typhimurium, a conserved guanine nucleotide exchange factor for Cdc42 of the host cell. *Mol Microbiol, 36*(6), 1206-1221.

Sun, H., Kamanova, J., Lara-Tejero, M., & Galan, J. E. (2016). A Family of Salmonella Type III Secretion Effector Proteins Selectively Targets the NF-kappa B Signaling Pathway to Preserve Host Homeostasis. *Plos Pathogens, 12*(3).

Sun, J., Hobert, M. E., Rao, A. S., Neish, A. S., & Madara, J. L. (2004). Bacterial activation of beta-catenin signaling in human epithelia. *American Journal of Physiology-Gastrointestinal and Liver Physiology, 287*(1), G220-G227.

Sun, S. C., Chang, J. H., & Jin, J. (2013). Regulation of nuclear factor-kappa B in autoimmunity. *Trends in Immunology, 34*(6), 282-289.

Sundaramoorthy, E., Leonard, M., Mak, R., Liao, J., Fulzele, A., & Bennett, E. J. (2017). ZNF598 and RACK1 Regulate Mammalian Ribosome-Associated Quality Control Function by Mediating Regulatory 40S Ribosomal Ubiquitylation. *Mol Cell, 65*(4), 751-760 e754. doi:10.1016/j.molcel.2016.12.026

Suresh, R., & Mosser, D. M. (2013). Pattern recognition receptors in innate immunity, host defense, and immunopathology. *Adv Physiol Educ, 37*(4), 284-291. doi:10.1152/advan.00058.2013

Taipale, M., Krykbaeva, I., Koeva, M., Kayatekin, C., Westover, K. D., Karras, G. I., & Lindquist, S. (2012). Quantitative analysis of HSP90-client interactions reveals principles of substrate recognition. *Cell, 150*(5), 987-1001. doi:10.1016/j.cell.2012.06.047

Tauschek, M., Gorrell, R. J., Strugnell, R. A., & Robins-Browne, R. M. (2002). Identification of a protein secretory pathway for the secretion of heat-labile enterotoxin by an enterotoxigenic strain of Escherichia coli. *Proc Natl Acad Sci U S A, 99*(10), 7066-7071. doi:10.1073/pnas.092152899

Thomas, N. A., Deng, W., Baker, N., Puente, J., & Finlay, B. B. (2007). Hierarchical delivery of an essential host colonization factor in enteropathogenic Escherichia coli. *J Biol Chem, 282*(40), 29634-29645. doi:10.1074/jbc.M706019200

Thomas, S., Holland, I. B., & Schmitt, L. (2014). The Type 1 secretion pathway - the hemolysin system and beyond. *Biochim Biophys Acta, 1843*(8), 1629-1641. doi:10.1016/j.bbamcr.2013.09.017

Thomassin, J. L., He, X., & Thomas, N. A. (2011). Role of EscU auto-cleavage in promoting type III effector translocation into host cells by enteropathogenic Escherichia coli. *BMC Microbiol, 11*, 205. doi:10.1186/1471-2180-11-205

Vanquelef, E., Simon, S., Marquant, G., Garcia, E., Klimerak, G., Delepine, J. C., . . . Dupradeau, F. Y. (2011). R.E.D. Server: a web service for deriving RESP and ESP charges and building force field libraries for new molecules and molecular fragments. *Nucleic Acids Res, 39*(Web Server issue), W511-517. doi:10.1093/nar/gkr288

Voulhoux, R., Ball, G., Ize, B., Vasil, M. L., Lazdunski, A., Wu, L. F., & Filloux, A. (2001). Involvement of the twin-arginine translocation system in protein secretion via the type II pathway. *EMBO J, 20*(23), 6735-6741. doi:10.1093/emboj/20.23.6735

Wagner, S. A., Beli, P., Weinert, B. T., Nielsen, M. L., Cox, J., Mann, M., & Choudhary, C. (2011). A proteome-wide, quantitative survey of in vivo ubiquitylation sites reveals widespread regulatory roles. *Mol Cell Proteomics, 10*(10), M111 013284. doi:10.1074/mcp.M111.013284

Wan, F., Anderson, D. E., Barnitz, R. A., Snow, A., Bidere, N., Zheng, L., . . . Lenardo, M. J. (2007). Ribosomal protein S3: a KH domain subunit in NF-kappaB complexes that mediates selective gene regulation. *Cell, 131*(5), 927-939. doi:10.1016/j.cell.2007.10.009

Wan, F., & Lenardo, M. J. (2009). Specification of DNA binding activity of NF-kappaB proteins. *Cold Spring Harb Perspect Biol, 1*(4), a000067. doi:10.1101/cshperspect.a000067

Wan, F. Y., Weaver, A., Gao, X. F., Bern, M., Hardwidge, P. R., & Lenardo, M. J. (2011). IKK beta phosphorylation regulates RPS3 nuclear translocation and NF-kappa B function during infection with Escherichia coli strain O157:H7. *Nature Immunology, 12*(4), 335-U119.

Wang, G., Geisbrecht, B. V., Rueter, C., & Hardwidge, P. R. (2017). Enterotoxigenic Escherichia coli Flagellin Inhibits TNF-Induced NF-kappaB Activation in Intestinal Epithelial Cells. *Pathogens, 6*(2). doi:10.3390/pathogens6020018

Wang, P. Y., Chang, K. T., Lin, Y. M., Kuo, T. Y., & Wang, G. S. (2018). Ubiquitination of MBNL1 Is Required for Its Cytoplasmic Localization and Function in Promoting Neurite Outgrowth. *Cell Rep, 22*(9), 2294-2306. doi:10.1016/j.celrep.2018.02.025

Warawa, J., Finlay, B. B., & Kenny, B. (1999). Type III secretion-dependent hemolytic activity of enteropathogenic Escherichia coli. *Infect Immun, 67*(10), 5538-5540.

Wier, E. M., Neighoff, J., Sun, X., Fu, K., & Wan, F. (2012). Identification of an N-terminal truncation of the NF-kappaB p65 subunit that specifically modulates ribosomal protein S3-dependent NF-kappaB gene expression. *J Biol Chem, 287*(51), 43019-43029. doi:10.1074/jbc.M112.388694

Wiggins, C. A., & Munro, S. (1998). Activity of the yeast MNN1 alpha-1,3-mannosyltransferase requires a motif conserved in many other families of glycosyltransferases. *Proc Natl Acad Sci U S A, 95*(14), 7945-7950.

Wilson, R. K., Shaw, R. K., Daniell, S., Knutton, S., & Frankel, G. (2001). Role of EscF, a putative needle complex protein, in the type III protein translocation system of enteropathogenic Escherichia coli. *Cell Microbiol, 3*(11), 753-762.

Wu, M., El Qaidi, S., & Hardwidge, P. R. (2018). SseL Deubiquitinates RPS3 to Inhibit Its Nuclear Translocation. *Pathogens, 7*(4). doi:10.3390/pathogens7040086

Wu, M., & Hardwidge, P. R. (2018). Hsp90 Interacts with the Bacterial Effector NleH1. *Pathogens, 7*(4). doi:10.3390/pathogens7040087

Wu, S. P., Ye, Z. D., Liu, X. Y., Zhao, Y., Xia, Y. L., Steiner, A., . . . Sun, J. (2010). Salmonella typhimurium infection increases p53 acetylation in intestinal epithelial cells. *American Journal of Physiology-Gastrointestinal and Liver Physiology, 298*(5), G784-G794.

Xu, X., & Hensel, M. (2010). Systematic analysis of the SsrAB virulon of Salmonella enterica. *Infect Immun, 78*(1), 49-58. doi:10.1128/IAI.00931-09

Yadavilli, S., Mayo, L. D., Higgins, M., Lain, S., Hegde, V., & Deutsch, W. A. (2009). Ribosomal protein S3: A multi-functional protein that interacts with both p53 and MDM2 through its KH domain. *DNA Repair (Amst), 8*(10), 1215-1224. doi:10.1016/j.dnarep.2009.07.003

Yang, Z., Soderholm, A., Lung, T. W., Giogha, C., Hill, M. M., Brown, N. F., . . . Teasdale, R. D. (2015). SseK3 Is a Salmonella Effector That Binds TRIM32 and Modulates the Host's NF-kappaB Signalling Activity. *PLoS One, 10*(9), e0138529. doi:10.1371/journal.pone.0138529

Yao, Q., Zhang, L., Wan, X. B., Chen, J., Hu, L. Y., Ding, X. J., . . . Shao, F. (2014). Structure and Specificity of the Bacterial Cysteine Methyltransferase Effector NleE Suggests a Novel Substrate in Human DNA Repair Pathway. *Plos Pathogens, 10*(11).

Ye, Z. D., Petrof, E. O., Boone, D., Claud, E. C., & Sun, J. (2007). Salmonella effector AvrA regulation of colonic epithelial cell inflammation by deubiquitination. *American Journal of Pathology, 171*(3), 882-892.

Yen, H., Karino, M., & Tobe, T. (2016). Modulation of the Inflammasome Signaling Pathway by Enteropathogenic and Enterohemorrhagic Escherichia coli. *Front Cell Infect Microbiol, 6*, 89. doi:10.3389/fcimb.2016.00089

Yen, H., Sugimoto, N., & Tobe, T. (2015). Enteropathogenic Escherichia coli Uses NleA to Inhibit NLRP3 Inflammasome Activation. *PLoS Pathog, 11*(9), e1005121. doi:10.1371/journal.ppat.1005121

Yen, H. L., Ooka, T., Iguchi, A., Hayashi, T., Sugimoto, N., & Tobe, T. (2010). NleC, a Type III Secretion Protease, Compromises NF-kappa B Activation by Targeting p65/RelA. *Plos Pathogens, 6*(12).

Yombi, J. C., Martins, L., Vandercam, B., Rodriguez-Villalobos, H., & Robert, A. (2015). Clinical features and outcome of typhoid fever and invasive non-typhoidal salmonellosis in a tertiary hospital in Belgium: analysis and review of the literature. *Acta Clin Belg, 70*(4), 265-271. doi:10.1179/2295333715Y.0000000016

Zanetti M, T. Z., Dalcanton F, de Mello MMJ, de Oliveira D, Araujo PHH, Riella HG and Fiori MA. (2015). Microbiological Characterization of Pure Geraniol and Comparison with Bactericidal Activity of the Cinnamic Acid in Gram-Positive and Gram-Negative Bacteria. *Journal of Microbial & Biochemical Technology, 7*(4), 186-193.

Zarivach, R., Vuckovic, M., Deng, W., Finlay, B. B., & Strynadka, N. C. (2007). Structural analysis of a prototypical ATPase from the type III secretion system. *Nat Struct Mol Biol, 14*(2), 131-137. doi:10.1038/nsmb1196

Zhang, H., Zhu, F., Yang, T., Ding, L., Zhou, M., Li, J., . . . Wu, H. (2014). The highly conserved domain of unknown function 1792 has a distinct glycosyltransferase fold. *Nat Commun, 5*, 4339. doi:10.1038/ncomms5339

Zhang, L., Ding, X. J., Cui, J., Xu, H., Chen, J., Gong, Y. N., . . . Shao, F. (2012). Cysteine methylation disrupts ubiquitin-chain sensing in NF-kappa B activation. *Nature, 481*(7380), 204-+.

Zhang, X., Zhou, L., & Cheng, X. (2000). Crystal structure of the conserved core of protein arginine methyltransferase PRMT3. *EMBO J, 19*(14), 3509-3519. doi:10.1093/emboj/19.14.3509

Zhou, D., Mooseker, M. S., & Galan, J. E. (1999). Role of the S. typhimurium actin-binding protein SipA in bacterial internalization. *Science, 283*(5410), 2092-2095.

Zhou, D. G. (2001). A Salmonella inositol polyphosphatase acts in conjunction with other bacterial effectors to promote host cell actin cytoskeleton rearrangements and bacterial internalization (vol 39, pg 248, 2001). *Molecular Microbiology, 40*(6), 1461-1461.